Thermal, hydrological and geochemical dynamics of the active layer at a continuous permafrost site, Taymyr Peninsula, Siberia

Julia Boike

Ber. Polarforsch. 242 (1997)
ISSN 0176 - 5027

Julia Boike
Alfred-Wegener-Institut für Polar- und Meeresforschung
Forschungsstelle Potsdam
Telegrafenberg A 43
D-14473 Potsdam

Die vorliegende Arbeit ist die unveränderte Druckfasssung einer Dissertation, die im Februar 1997 im Fachbereich Geowissenschaften an der Universität Potsdam eingereicht wurde

Acknowledgements

During the past years, many people and organizations have contributed to realize the research project presented in this dissertation.

Research funds were provided by the German Federal Ministry of Education and Research. Additional support in form of a Horton Research Grant was made available by the American Geophysical Union.

I would like to express my sincere thanks to my professors Dr. Hans-Wolfgang Hubberten, Dr. Kurt Roth and Dr. Roland Oberhänsli for their guidance, support and, most importantly, for leaving me the intellectual and financial space to develop and realize my own ideas. Especially the scientific exchange with Kurt, his patience and welcoming of a newcomer in his 'Soil Physics' group at Hohenheim made this research so much fun. Thanks, Kurt, for teaching me so much and for challenging my intellectual curiosity.

The Arctic demands of its researchers a natural love for the North and sometimes great endurance, especially when living for months in a snowy, rainy, isolated part of the northern hemisphere in a leaking tent is required. However, we are being remunerated by the beauty of the natural world and the friends and colleagues we meet along the way. Through three expeditions to Siberia, I did not only get to know a beautiful landscape, I also learned about a different country and its people. In our Russian partners, I am grateful to have gained, not only scientific partners, but also respected friends. I would like to express my thanks to the members of the 1994 and 1995 expeditions from the Arctic and Antarctic Research Institute, St. Petersburg, who put a great amount of energy and patience into coordinating these expeditions. Especially with Dr. Dima Bolshiyanov, Misha Anisimov, Andre Ivanov and Victor Meshcheryakov, I shared the wonderful experience of the Arctic and some very special parties. Thanks, for sharing one of the most beautiful spots of the earth with me!

The following people provided their enthusiasm and hard work, sometime under most adverse Arctic weather conditions: Misha Anisimova, Dima Bolshiyanov, Holger Becker, Dr. Dorothea Gintz, Birgit Hagedorn, Andre Ivanov, Thomas Müller-Lupp, Victor Meshcheryakov and Pier Paul Overduin. It was fun to work with you and sharing some of the most beautiful times in the Siberian Arctic.

The German Weather Service in Hamburg (Dr. Däke, DWD) generously lend equipment to the expedition. Stable isotope analysis was carried out in the laboratories of Prof. Friedrichsen, FU Berlin, and Dr. Mackensen, AWI Bremerhaven. Dr. Timo Heimovaara generously provided programs and technical support for analyzing TDR waveforms.

Special thanks go to the staff of AWI Potsdam, especially to Conrad Kopsch (engineering), Ingeborg Sass (library), Eduard Claudius (computers) and Helga Henschel (just everything), who always supported this work most professionally. Dr.

Peter von der Gathen supported me by giving late night rides home, helpful comments and partial proofreading of the thesis.

During the early stages, this research benefited from scientific discussions with Dr. Wilko van Loon and the great hospitality of his and his family in Arnhem, Holland.

Valuable discussion on stable isotopes were guided by Drs. Hedi Oberhänsli, Wolf-Dieter Hermichen and Birgit Hagedorn. Discussions on permafrost throughout this thesis were granted by Christine Siegert who always had an open ear for me (and something to eat). Especially Christine's enthusiasm, bottomless well of knowledge of Russian research helped me a great deal in defining and coordinating this research.

Also deserving of mention are the destructive comments on my lack of intelligence generously cast my way by my office colleagues Thomas Kulbe and Markus Schwab, without which I surely would have thought I was omnipotent. Thanks, guys!

I acknowledge the support and encouragement of my friends and family in Germany and Canada and their special efforts not to lose me to the 'exciting world of research'. Completion of this thesis would have been unthinkable without the valuable help during the last stages provided by Regina Pác.

Last and most special thanks go to my friend and partner Pier Paul Overduin who provided constant scientific and mental support all the way and proofread the entire thesis. Maybe it sometimes did not give the impression - but you were always most important to me!

Table of contents

Chapter 4

Thermal and hydrological dynamics of the active layer at a continuous permafrost site (Taymyr Peninsula, Siberia)

Chapter 5

Climatological and hydrological influences on stable hydrogen and oxygen isotopes of active layer waters, Levinson-Lessing Lake area, Taymyr Peninsula

Chapter 6

Summary and conclusions

Abstract

About 65 % of Russia is underlain by permafrost. In these regions, the upper ground, the active layer, seasonally freezes and thaws. The overall goal of this thesis was to improve our understanding on the coupled thermal, hydrological and geochemical regime of this layer in a continuous permafrost setting from field experiments. These experiments were conducted in the Levinson-Lessing Lake catchment on the Taymyr Peninsula, northern Siberia (74° 32'N; 98° 35'E) from July to September 1994 and May to October 1995. The objectives were to quantify the seasonal fluxes of water and heat in the active layer from spring thaw to fall freeze-back and to identify the sources of active layer water using the stable isotope ratios $\delta^{18}O$ and δD.

Time domain reflectometry (TDR) is evaluated as a field technique for measuring volumetric water content θ and bulk electrical conductivity σ_b in arctic soils. Calibration measurements of θ and σ_b were carried out on three different slopes that were characteristic for this catchment. Comparison of θ calculated from TDR using two different approaches and gravimetrically determined water contents show a close correlation. For the calculation of the soil water electrical conductivity σ_w from TDR determined σ_b two theoretical models based on the pore geometry were tested using independent σ_w of soil solutions obtained with suction cups. Unacceptable high deviations of predicted σ_w resulted in the development of a new model. Best results for σ_w are obtained using this regression model, with highest precision when probe specific calibration is carried out. Therefore TDR can be applied to obtain quantitative estimates of θ and σ_w in the active layer for a range of arctic field soils in this permafrost setting. However, the application of TDR determined σ_b in different permafrost soils to infer σ_w requires additional calibration. Based on these results, TDR is recommended as an *in situ* technique for studying the temporal dynamics of soil water and solutes in the active layer.

Using TDR, liquid water was found to be present in frozen soil at temperatures down to -12 °C and its volumetric fraction increased with temperature until ground melting started. The ground thermal regime during spring thaw and fall freeze-back is dominated by the heat of fusion which stabilizes soil temperatures at 0 °C for extended periods ('zero curtain effect'). The thermal regime of the saturated active layer during the summer may be understood from assuming density driven convection as the mechanism of heat transfer. Convective transfer also appears to be dominating during fall, when large amounts of latent heat are released by freeze-back.

Seasonal fluxes of heat and water are calculated using a simple zero-dimensional model of water and energy balance. Although this model neglects processes such as sensible heat fluxes and lateral water flow, it reveals that the dominant heat sink during spring and summer is evaporation. During fall freeze-back, the dominant heat-producing process is phase change.

The soil heterogeneity strongly impacts hydrological and thermal processes in the active layer. Two direct consequences are the development of preferential flowpaths and preferential freezing of the profile during freeze-back.

The geochemical composition of precipitation and active layer water was investigated using $\delta^{18}O$ and δD. Based on precipitation samples from 1994 and 1995, a local meteoric water line (LMWL) was established that deviates from the global meteoric water line (GMWL) for the summer precipitation. The reason is that the summer air masses carry moisture which has been exposed to a high degree of evaporative stable isotope enrichment. The $\delta^{18}O$ and δD values of the saturated and unsaturated zone of the active layer demonstrate that the active layer is mostly fed by rainwater or melting of active layer ground ice. Small differences in $\delta^{18}O$ and δD within the catchment are interpreted as a result of variabilities in microclimate, morphology and hydrology of each slope and site. Therefore, it is suggested that the interpretation of $\delta^{18}O$ and δD in these waters should be backed of with physical measurements.

Kurzfassung

Ungefähr 65 % der Landfläche Rußlands liegt im Permafrostgebiet. In diesen Gebieten kommt es zum saisonalen Auftauen und Gefrieren in der oberflächennahen Schicht. Ziel dieser Arbeit ist es, die gekoppelte Dynamik des thermischen, hydrologischen und geochemischen Regims dieser Schicht in einem kontinuierlichen Permafrostgebiet durch Feldexperimente zu verstehen. Dafür wurden Experimente im Einzugsgebiet des Levinson-Lessing-Sees auf der Taymyr Halbinsel in Nordsibirien (74° 32'N; 98° 35'E) von Juli bis September 1994 und Mai bis Oktober 1995 durchgeführt. Insbesondere sollten die saisonalen Wärme- und Massenflüsse in der Auftauschicht vom Beginn des Tauens im Frühjahr bis zum Zurückfrieren im Herbst quantifiziert sowie die Quellwässer der Auftauschicht anhand der stabilen Isotope $\delta^{18}O$ und δD identifiziert werden.

TDR ('Time Domain Reflectometry') wurde als Feldmethode für die Bestimmung des volumetrischen Wassergehaltes θ und der Gesamtleitfähighkeit σ_b des Bodens eingesetzt. Um diese Methode zu testen, wurden auf drei für dieses Einzugsgebiet charakteristischen Hängen Kalibrierungen durchgeführt. Der Vergleich der mit zwei unterschiedlichen TDR-Ansätzen berechneten Wassergehalte mit den gravimetrisch bestimmten zeigte eine gute Übereinstimmung. Für die Berechnung der elektrischen Leitfähigkeit des Bodenwassers σ_w aus der Gesamtleitfähigkeit des Bodens wurden zwei Modelle angewandt, die auf der theoretischen Beschreibung der Geometrie des Porenraumes beruhen. Der Vergleich der durch die TDR-Messungen berechneten σ_w mit den σ_w-Werten aus Wasserlösungen der Saugkerzen zeigte starke Abweichungen, was zu der Entwicklung eines neuen Modells führte. Im Vergleich zu den theoretischen Modellen wurden die besten Ergebnisse mit diesem Regressionsmodell erzielt, wobei die höchste Präzision durch sondenspezifische Eichung erreicht wurde. In diesem Permafrostgebiet bietet die TDR-Methode für eine Reihe von arktischen Böden quantitativ gute Meßwerte für θ und σ_w. Um die TDR-Methode zur Bestimmung von σ_w des Bodenwassers anderer Böden anzuwenden, muß jedoch vorher eine Eichung zur Erfassung der Beziehung zwischen σ_b und σ_w durchgeführt werden. Insgesamt ist die TDR-Methode zur *in situ*-Bestimmung von zeitlich hochauflösenden Messungen des Wasser- und Stofftransportes in der Auftauschicht zu empfehlen.

Mit Hilfe der TDR-Methode wurde Wasser in der gefrorenen Auftauschicht im Frühjahr bei Bodentemperaturen bis zu minus 12°C nachgewiesen. Dieser flüssige Anteil erhöhte sich mit steigender Bodentemperatur vor dem Auftauen des Bodens. Während des Auftauens und Gefrierens des Bodens dominieren die latenten Wärmeflüsse. Sie stabilisieren die Bodentemperaturen für längere Zeit um 0°C ('Nullschleier-Effekt'). Das thermische Regime der gesättigten Auftauschicht des Sommers kann mit der Annahme erklärt werden, daß Konvektion ein wichtiger Wärmetransportmechanismus ist. Diese wird durch die Dichteanomalie des Wassers

gesteuert. Konvektive Wärmeflüsse dominieren auch im Herbst, wenn große Mengen von latenter Wärme durch das Gefrieren des Bodens freigesetzt werden.

Die saisonalen Wärme- und Wasserflüsse wurden durch ein einfaches Wasser- und Energiebilanzmodell berechnet. Obwohl dieses Modell einige Prozesse vernachlässigt, wie z. B. den sensiblen Wärmestrom und den lateralen Abfluß in der Auftauschicht, zeigt es, daß die Verdunstung im Frühjahr und Sommer den höchsten Energieverbrauch hat. Während des Zurückfrierens der Auftauschicht erweist sich der Phasenübergang als dominanter wärmeproduzierender Prozeß.

Die Heterogenität des Bodens beeinflußt stark die hydrologischen und thermischen Prozesse in der Auftauschicht. Direkte Auswirkungen sind die Entwicklung von bevorzugten Fließwegen und ungleichmäßges Gefrieren der Auftauschicht im Herbst.

Die geochemische Zusammensetzung der Niederschläge und des Wassers in der Auftauschicht wurde mit Hilfe der stabilen Isotopenverhältnisse $\delta^{18}O$ und $\delta^{2}H$ untersucht. Die $\delta^{18}O$ und $\delta^{2}H$ Werte der Niederschläge in den Jahren 1994 und 1995 definieren eine lineare Beziehung, die von der globalen Beziehung meteorischer Wässer abweicht. Die Werte von $\delta^{18}O$ und $\delta^{2}H$ in der gesättigten und ungesättigten Zone der Auftauschicht zeigen, daß diese Wässer hauptsächlich aus sommerlichen Niederschlägen bzw. dem Tauen des in der Auftauschicht vorhandenen Eises gespeist werden. Geringe Variationen von $\delta^{18}O$ und $\delta^{2}H$ in der Auftauschicht innerhalb des Einzugsgebietes sind das Ergebnis kleinräumiger Variabilitäten des Mikroklimas, der Bodenmorphologie und Hydrologie des jeweiligen Meßpunktes. Es ist daher notwendig, die isotopengeochemischen Methoden mit Hilfe der bodenphysikalischen Parameter (Bodenfeuchte, Temperatur) wie in der vorliegenden Arbeit zu interpretieren.

List of Figures

List of Tables

Symbol notations

a	air	[-]
α	phase	[-]
b	bulk	[-]
c	composite	[-]
i	ice	[-]
nr	net radiation	[-]
r	rainfall	[-]
s	soil	[-]
sf	solid to fluid	[-]
sv	solid to vapor	[-]
sat	saturated	[-]
t	total energy	[-]
v	vapor	[-]
w	water	[-]
ℓ	depth	[m]
A, B	soil geometric constants	[-]
a, b	soil specific constants in Rhoades model	[-]
β	geometry factor in Roth model	[-]
C	volumetric heat capacity	[J m^{-3} K^{-1}]
c_α	specific heat capacity of phase α	[J kg^{-1} K^{-1}]
C_t	mass of solute per unit volume	[kg m^{-3}]
D	Deuterium	[-]
d	Deuterium excess	[‰]
δ	isotope ratio	[‰]
E_t	areal density of thermal energy relative to reference state down to depth ℓ	[J m^{-2}]
ε	dielectric number	[-]
j_{nr}	energy flux from net radiation	[J m^{-2} s^{-1}]
j_r	water flux due to rainfall	[m s^{-1}]
j_t	total energy flux into soil	[J m^{-2} s^{-1}]
j_v	vapor flux across soil surface	[m s^{-1}]
$\hat{j}_v^E$, $\hat{j}_v^W$	estimate of j_v from energy and water balance	[m s^{-1}]
K	saturated hydraulic conductivity	[m s^{-1}]
k	thermal conductivity	[J m^{-1} K^{-1} s^{-1}]
L	specific latent heat of phase change for water	[J kg^{-1}]
λ	constant for soil texture in Mualem and Friedmann model	[-]
N	number of data points	[-]
n	parameter in Mualem and Friedmann model	[-]

η	porosity	[-]
R^E, R^W	energy and evaporation residual	[J m^{-2} s^{-1}]
ρ_α	specific mass density of phase α	[kg m^{-3}]
r^2	correlation coefficient	[-]
SD	standard deviation	[-]
σ_α	electrical conductivity of phase α	[mS m^{-1}]
T	temperature	[°C]
t	time	[s]
τ	transmission factor in Rhoades model	[-]
Θ_ℓ	areal density of total water content to depth ℓ	[m]
θ_α	volumetric density of phase α	[m^3 m^{-3}]
θ	volumetric water content	[m^3 m^{-3}]
ν	kinematic viscosity	[m^2 s^{-1}]
ψ_m	matric potential	[Pa]
ψ_0	air entry value in Brooks and Corey model	[Pa]
z	vertical space coordinate	[m]
σ_w^{mod}	σ_w determined from model estimates	[mS m^{-1}]
σ_w^{meas}	σ_w determined from suction lysimeter solution	[mS m^{-1}]

Chapter 1

Introduction

Approximately 25 % of the earth's continental area and 65 % of Russia is underlain by permafrost (Ershov, 1995), which is defined as ground or substrate that is continuously below 0°C for two or more years (NRCC, 1988). The increasing demands on natural resources, growing tourism, the high potential for environmental disturbances and possible climate change call for integrated studies of arctic ecosystems. To date, we have a limited understanding of the physical and biological interactions within a permafrost system, which makes small and large scale modeling of these systems rather complex and hence leads to uncertain predictions.

A multidisciplinary framework was established in 1993 for the project, 'Late Quaternary environmental history of northern Central Taymyr', involving the Alfred Wegener Institute of Polar and Marine Research, Potsdam, the Institute of Soil Science, University of Hamburg, and the Institute for Polar Ecology, University of Kiel. Research was carried out along an approximately 1400 km north to south transect extending along the Taymyr Peninsula from the high arctic desert on Severnaya Semlya to the northern taiga zone close to Norilsk (Figure 1.1). Details of the expeditions and preliminary results of the multidisciplinary projects have been summarized in a series of expedition reports (Melles, 1994; Siegert and Bolshiyanov, 1995; Bolshiyanov and Hubberten, 1996). By covering this wide range of climatic, landscape and vegetation conditions, the project yields information on present and past processes in the permafrost landscape, specifically on the interaction between permafrost and atmosphere and the formation of sediments. These sediments are sensitive indicators of past and recent climate and give information on the long-term climatic (in)stability of the permafrost system. Although similar integrated studies have been undertaken in the Alaskan Arctic (Shaver, 1996), the Siberian Arctic is distinct due to a more continental climate (Gavrilova, 1981). Consequently, this study will not only add to the regional history and recent processes of the Taymyr Peninsula, but also to our circumpolar knowledge in permafrost regions.

The overall objectives of this thesis are an integrated understanding of hydrological and thermal dynamics of the active layer, the upper seasonally thawing and freezing ground, and the ranking of processes controlling seasonal changes of the geochemical and stable isotope ratios ($\delta^{18}O$, δD) of active layer water and ice. It contains the results of two expeditions, the first from August to September 1994 and the second from May to October 1995, carried out in the Levinson-Lessing Lake catchment on the Taymyr Peninsula (Figure 1.1). Hydrological processes in the active layer are the synthesis of a complex interplay between hydrological inputs (snow and ground ice melt, rain) and microclimatological factors (*e.g.*, net radiation, evaporation, vegetation

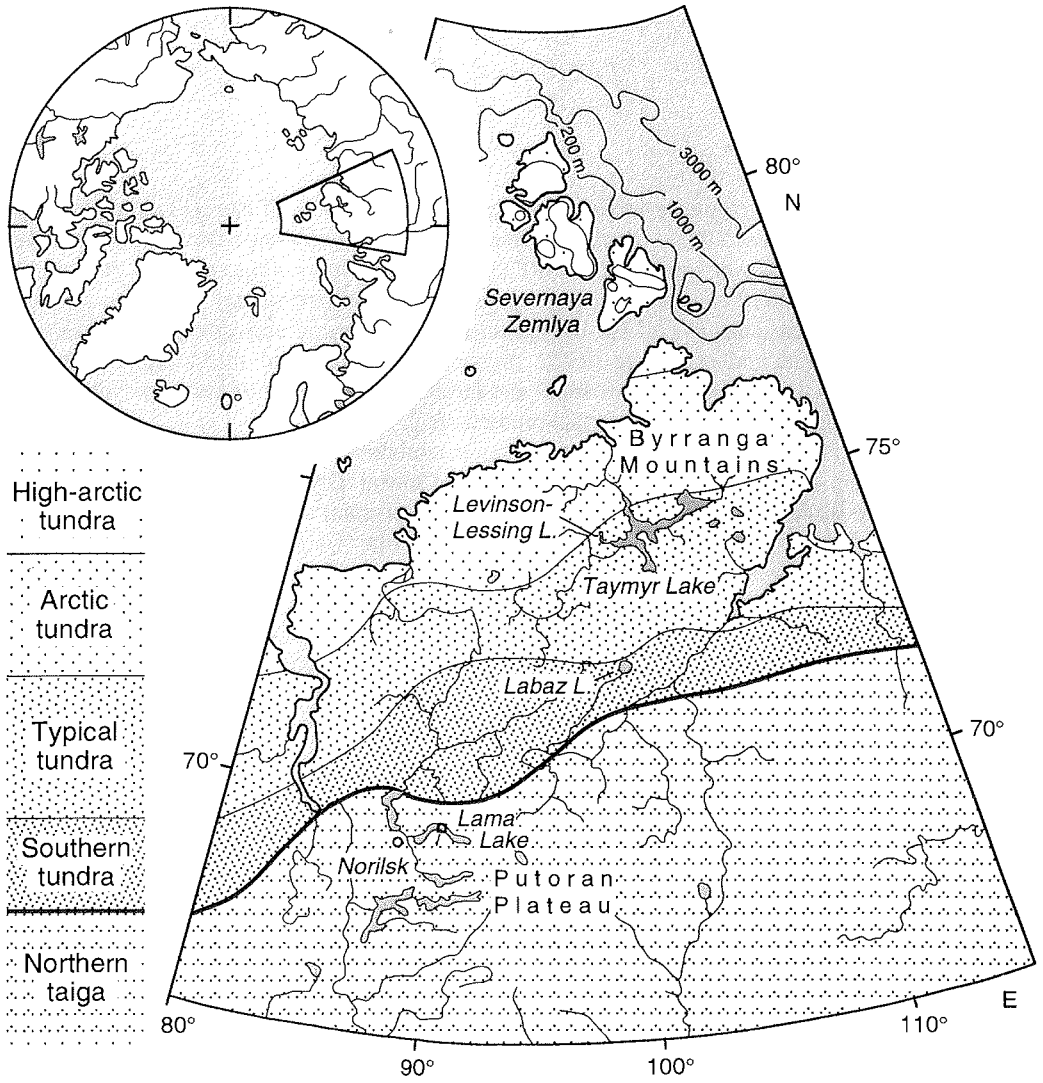

Figure 1.1. Location of Taymyr Peninsula with the research areas around Levinson-Lessing lake and Labaz lake.

and snow cover; Figure 1.2). Since the thermal and moisture regime of the active layer are strongly coupled through phase transitions, measurements of these quantities become especially important during the times of phase change. However, to date no study has been undertaken that investigates the seasonal active layer dynamic through simultaneous *in situ* measurements of the hydrological, thermal and geochemical regimes. This is largely because of lack of acceptable techniques as well as logistical constraints that limit field work in these remote areas.

The thesis is written in the form of four main papers that represent self-contained units which are filed on a common thread. Chapters 2, 3 and 4 have been submitted for publication to various journals (Boike *et al.*, 1997a; Boike *et al.*, 1997b; Boike and Roth, 1997), whereas Chapter 5 reports the current state of ongoing research. The order of their appearance in this thesis also describes the temporal path this research evolved.

A major component of this thesis deals with the development of an *in situ* technique for the determination of physical parameters required for measuring mass transport in permafrost soils. Chapter 2 describes the test of a model for the calculation of solute concentrations in the active layer and is applied for the observation of solute movement in the active layer. The results called for a detailed evaluation of currently applied models and resulted in the development of a new model for determining solute concentrations in the active layer (Chapter 3). The fourth chapter examines the seasonal hydrological and thermal dynamics of the active layer for one complete thaw-freeze cycle with the aim of understanding the dominant heat transfer processes. Chapter 5 describes the spatial and temporal variability of stable isotopes (^{18}O, D) in recent permafrost waters in the Levinson-Lessing Lake catchment with respect to their application as hydrological tracers and paleoenvironmental data archives. The last chapter synthesizes the results and discusses the future direction of permafrost-active layer related research.

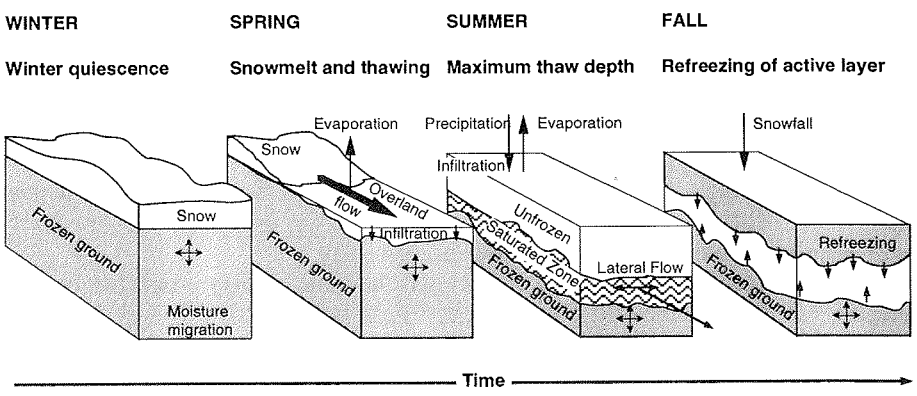

Figure 1.2. Conventional scheme of hydrological processes in the active layer from spring to fall.

Chapter 2

Solute movement in the active layer, Taymyr, Siberia

Paper by:
J. Boike, W. K. P. van Loon, P. P. Overduin and H. W. Hubberten. Accepted for publication in *Int. Symp. on Physics, Chemistry, and Ecology of Seasonally Frozen Soils*

2.1 ABSTRACT

Time domain reflectometry (TDR) has been used extensively for determining the dielectric number and water content of soils, and relationships for measuring soil water conductivity are being developed. The technique is particularly well-suited to use in the Arctic, where *in situ* and potentially remote methods are important. The objective of this study is to evaluate TDR as a field technique for bulk electrical conductivity σ_b and soil water electrical conductivity σ_w in arctic soils. Calibration measurements of σ_b were carried out at a field site in Siberia (74° 32'N; 98° 35'E). TDR-determined σ_w using the model of van Loon *et al.* (1991) is compared to electrical conductivity σ_w of solution obtained with suction cups. Best results are obtained when using a probe specific calculated soil electrical conductivity σ_s, rather than one value for this soil type. This is thought to be a reflection of soil coarseness and heterogeneity. Data of σ_w were obtained for for one field site in Siberia from spring to fall 1995. Infiltration into the frozen soil in spring and exclusion of solutes during fall freeze-back were observed using TDR.

2.2 INTRODUCTION

Understanding the processes of solute and water migration in frozen ground and during phase changes (thawing and freezing) has become a major challenge and resulted in the development of new techniques. Adequate *in situ* methods for determining soil water electrical conductivity (σ_w) for arctic field applications are still being developed. One method for measuring the temporal evolution of solute concentrations at specific depths is the use of suction cups. Its major disadvantages are the unknown, but potentially large measuring volume and failure in frozen ground.

Time domain reflectometry (TDR) has become widely used for *in situ* determination of soil volumetric water content (θ) and bulk electrical conductivity (σ_b). Whereas the determination of θ has been widely applied (Patterson and Smith, 1980; Stein and Kane, 1983; Roth *et al.*, 1990), the use of TDR determined σ_b for the calculation of σ_w in frozen and unfrozen ground is still under discussion. Although a number of theoretical and empirical methods have been proposed (Mualem and Friedman, 1991; Rhoades *et al.*, 1989), no simple relationship between σ_w and σ_b is applicable to all soils. In addition, arctic field soils are often very coarsely structured

(regolithic) and can exhibit a heterogeneous texture. They have a high mineral or high organic matter content and are subjected to a seasonal thawing and freezing cycle possibly damaging or deforming instruments. Moreover, controlled laboratory experiments and field data often appear to be inconsistent. For example, Heimovaara *et al.* (1995) report that the same soil studied in the field under natural conditions and in laboratory experiments through the addition of salt gave different relationships between σ_w and σ_b. To parameterize this relationship in a way useful for field use, it thus seems necessary to collect data for calibration via *in situ* instruments in the field.

Dynamics of solutes during freezing and thawing from a field site in northern Sweden (north of Uppsala) were reported by Lundin and Johnsson (1994). They applied the quasi theoretical model for frozen soils by van Loon *et al.* (1991) to calculate solute concentrations in frozen soils from TDR determined σ_b. Our objective is to evaluate the use of TDR as a method for *in situ* field measurements of σ_b using the model of van Loon *et al.* (1991) within the context of results from an arctic soil type in Siberia.

2.2.1 Bulk soil electrical conductivity

The amplitude of the TDR signal at very long times can be used to determine σ_b (Heimovaara *et al.*, 1995), which is a compound of σ_w and soil surface electrical conductivity σ_s. For calculation of σ_b, calibration of triple-wire probes and the TDR system were carried out with a range of solutions with known electrical conductivities following the method of Heimovaara *et al.* (1995). The value of σ_b was corrected for the temperature dependence of the water viscosity ν (van Loon *et al.*, 1991):

$$\sigma_b[T] = \sigma_b[25]\nu[T] \approx \sigma_b[25]\left[0.588 + 0.0193\,T + 0.00014T^2\right] \qquad [2.1]$$

where T is temperature in [°C].

Van Loon *et al.* (1991) developed the following theoretical model for σ_b in frozen soils between water content θ, saturated water content θ_{sat}, electrical conductivity of the liquid phase σ_w and soil surface conductivity σ_s:

$$\sigma_b = \sigma_s(1+3\theta) + \frac{(2-\theta)\,\theta^2}{(2-\theta_{sat})\,\theta_{sat}}\,\sigma_w \qquad [2.2]$$

The coefficients σ_w and σ_s are determined through multiregression analysis and were shown to be highly significant for the frozen soil-water system studied in the laboratory columns.

2.3 STUDY SITE AND METHODS

This paper reports results from field work carried out in 1994 and 1995 in the Levinson-Lessing catchment, Taymyr Peninsula, Siberia, the northernmost continental area of the circumpolar Arctic (74° 32'N; 98° 35'E). This study uses data collected from a single site (2x) which is located midway up on a calcareous, south west-facing slope with low inclination (7°). It is classified as loamy skeletal carbonatic calcareous Pergelic Cryorthent. Soil grain size characteristics of one bulk sample are given in Table 2.1.

Solifluction lobes and soil stripes indicate active cryogenic processes. Vegetation covers less than 5 % and is dominated by patches of *Dryas octopetala* and *Salix spec.*

Table 2.1. Soil characteristics of site 2x.

Bulk density [kg m^{-3}]	Porosity	Saturated hydraulic conductivity [cm s^{-1}]	Grain size [% weight] >2 mm	Sand	Silt	Clay
$1.69 \cdot 10^{3}$	0.34-0.42	$7.9 \cdot 10^{-6}$ (at 73 cm depth) $3.0 \cdot 10^{-4}$ (at 37 cm depth)	44	36.2	17.8	2

During the summer of 1994, soil pits were excavated to the depth where frozen ground was encountered. At each site, triple wire TDR probes, PT 100 temperature probes, wells, piezometers and suction cups (5 cm long, pore size 2 µm; Gravquick) were installed. The TDR probes used in this study consist of three parallel steel rods (0.5 cm diam., 25 cm long, 3 cm spaced apart), connected to a 50 Ω coaxial cable and held in place by an epoxy resin (Heimovaara, 1993). TDR waveforms were recorded in the field using a Tektronix 1502 B cable tester, a portable laptop and the program of Heimovaara and de Water (1993). Volumetric water content θ in unfrozen soils was calculated from the dielectric number ε using the composite approach of Roth *et al.* (1990) and in frozen soils using the formula of Smith and Tice (1988). Although Spans and Baker (1995) found that their independent calibration of TDR in frozen soils deviated from the formula of Smith and Tice (1988) we used the latter formula since no calibration for this soil was undertaken.

2.4 RESULTS AND DISCUSSION

2.4.1 Relationship between σ_b and σ_w at site 2x

The σ_b is a function of σ_s and σ_w, therefore reflecting the heterogeneity of the soil matrix (differences in θ, σ_s and soil geometry). This relationship is not easily defined, as demonstrated in Figure 2.1 where TDR measured values of σ_b are compared to values of σ_w from suction cup solutions. The nonlinearity of these two parameters was also demonstrated by Dasberg and Dalton (1985).

As a next step, we investigated the importance of σ_s for defining σ_b. Values of σ_s were determined in two different ways: 1) through multiregression analysis following the model of van Loon *et al.* (1991) and 2) using the soil suction lysimeter data as σ_w in [2.2] and calculating σ_s as the unknown variable. These calculations were undertaken for each probe and for the entire site to account for heterogeneity of the soil.

As can be seen in Table 2.2, the σ_s determined by multiregression analysis is generally small, but positive, with two exceptions. This suggests that the model is consistent within itself. However, the σ_s determined using the suction lysimeter data as σ_w yields negative σ_s values. Negative σ_s values were also calculated by van Loon *et al.*

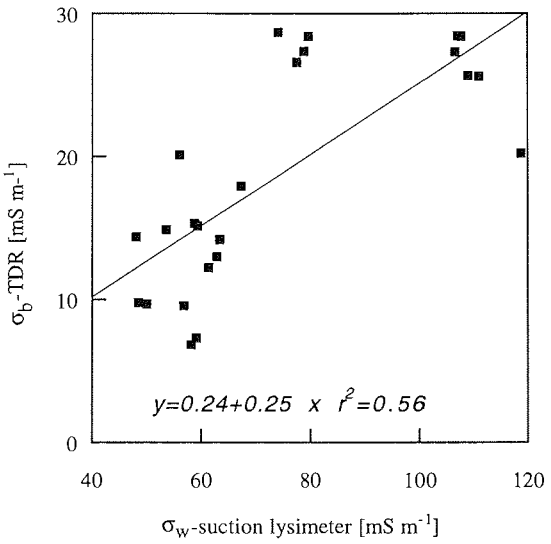

Figure 2.1. Comparison of σ_b calculated from TDR measurements with σ_w from suction lysimeters.

Table 2.2. Values of σ_s estimated for model [2.2] for site 2x. Parameter obtained by simultaneously fitting all data obtained from this site are marked "all sites" in the first column. The number of data points in each set is *N*.

	1 σ_s determined by multiregression analysis			2 σ_s calculated using equation [2.2] and suction lysimeter data as σ_w	
probe depth [cm]	σ_s [µS cm^{-1}]	r^2	*N*	average σ_s [µS cm^{-1}]	*N*
11	51 (51)	0.4 (0.65)	40 (34)*	n.a.	n.a.
23	26	0.72	39	-24	7
34	34	0.74	42	-28	6
47	-1	0.92	39	-21	4
52	-14	0.84	38	-55	2
65	22	0.96	43	-58	4
78	13	0.99	43	n.a.	n.a.
all sites	23 (22)	0.61 (0.61)	284 (278)*	-33	23

* Six outliers taken out

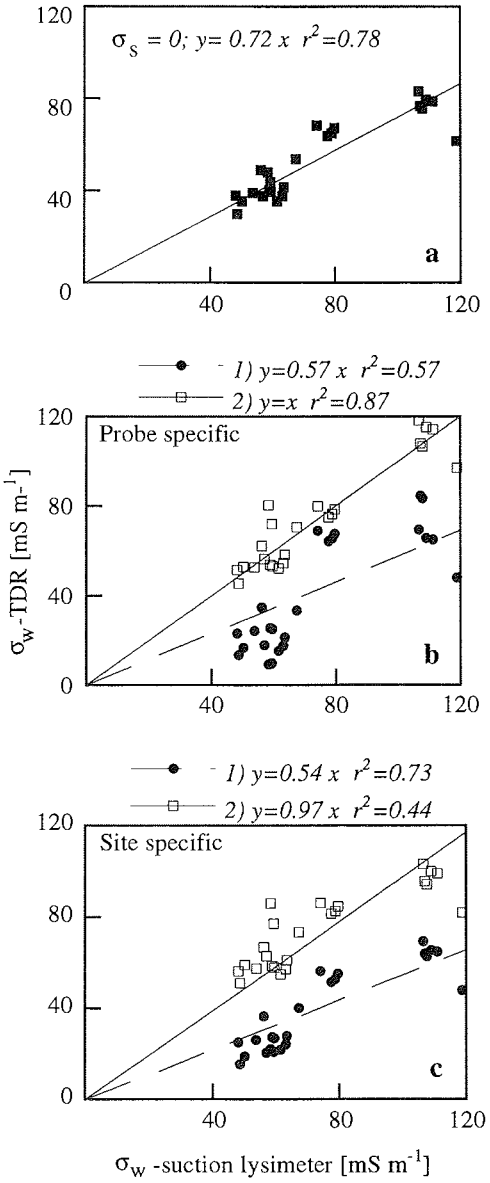

Figure 2.2. TDR determined σ_w using equation [2.2] compared with σ_w from suction lysimeters. a) σ_s = 0; b) σ_s determined probe specifically through 1) multiregression analysis and 2) calculated using suction lysimeter σ_w and c) σ_s determined site specifically through 1) multi regression analysis and 2) calculated using suction lysimeter σ_w.

1990) when data of Hayhoe and Balchin (1988) were analyzed the same way. They interpreted these negative σ_s as a result of limited water contents. A generally low σ_s for site 2x is to be expected based on the observed soil coarseness (Table 2.1).

The relationship between σ_w from suction lysimeters and TDR-calculated σ_w is shown in Figure 2.2. Figure 2.2a shows this comparison for TDR-calculated σ_w omitting σ_s in [2.2]. When this term is omitted, the TDR-determined σ_w are generally too low compared to the suction lysimeter σ_w, although there is a relatively good linear correlation (r^2= 0.78; Fig. 2.2a). This suggests that a basis for refining the relationship is including the contribution of σ_s. Figures 2.2b and 2.2c show the relationship when σ_s is considered. In Figure 2.2b, probe specific σ_s values determined through 1) multiregression analysis and 2) calculated on the basis of suction lysimeter data σ_w (Table 2.2) are used in [2.2] and graphed against the suction lysimeter σ_w data. The same comparison is undertaken using one site specific σ_s value from the multiregression analysis (σ_s =23 μS cm^{-1}) and one average calculated value (σ_s = - 33 μS cm^{-1}) in Figure 2.2c. Using probe and site specific σ_s determined through multiregression analysis, the model consistently underestimates σ_w by about 50 %. The best fit between TDR determined σ_w and suction lysimeter σ_w is obtained when using the probe specific calculated σ_s values (Fig. 2.2b). However, these negative values may rather represent a fitting parameter for model [2.2] than a physical quantity since σ_s values should be ≥ 0. These results demonstrate that the multiregression approach of van Loon *et al.* (1991) is only a good method for calculating relative σ_w for this site. For the absolute determination of σ_w for this field soil, probe specific calibration in addition to suction lysimeter data are required.

2.4.2 Seasonal dynamics of σ_w

Figure 2.3 shows the seasonal dynamics of σ_w in frozen and unfrozen ground in the profile 2x from 14 June to 15 October, 1995. The σ_w values are calculated using [2.2] and probe specific, calculated σ_s values for depths 23 to 65 cm. For depths 11 and 78 cm, the site calculated average value of σ_s = - 33 μS cm^{-1} is used since no probe specific value is available. Although this approximation might not give an accurate absolute value of σ_w at these depths, relative statements are justified.

Overall, the σ_w values during the summer in the unfrozen ground are relatively stable, ranging around 100 mS m^{-1}, whereas in the frozen ground they are about 4 to 15 times higher. In the lower, unfrozen ground (65 and 78 cm), σ_w values are higher compared to the upper depths. A possible explanation for this could be the dissolution of a concentrated solute layer at the previous years' thawed-frozen interface observed in permafrost-affected soils.

Infiltration into frozen ground

Data for σ_w are not available for the snowmelt that started on 5 June, which could give indication of snowmelt water infiltration into the frozen ground. However, in soil depths below 52 cm, an increase in σ_w is observed in the frozen ground before thawing. This could indicate the infiltration of suprapermafrost groundwater into the frozen ground. An increase of σ_w in frozen ground during snowmelt was observed using TDR by Lundin and Johnsson (1994), which they interpreted as infiltration of snowmelt water.

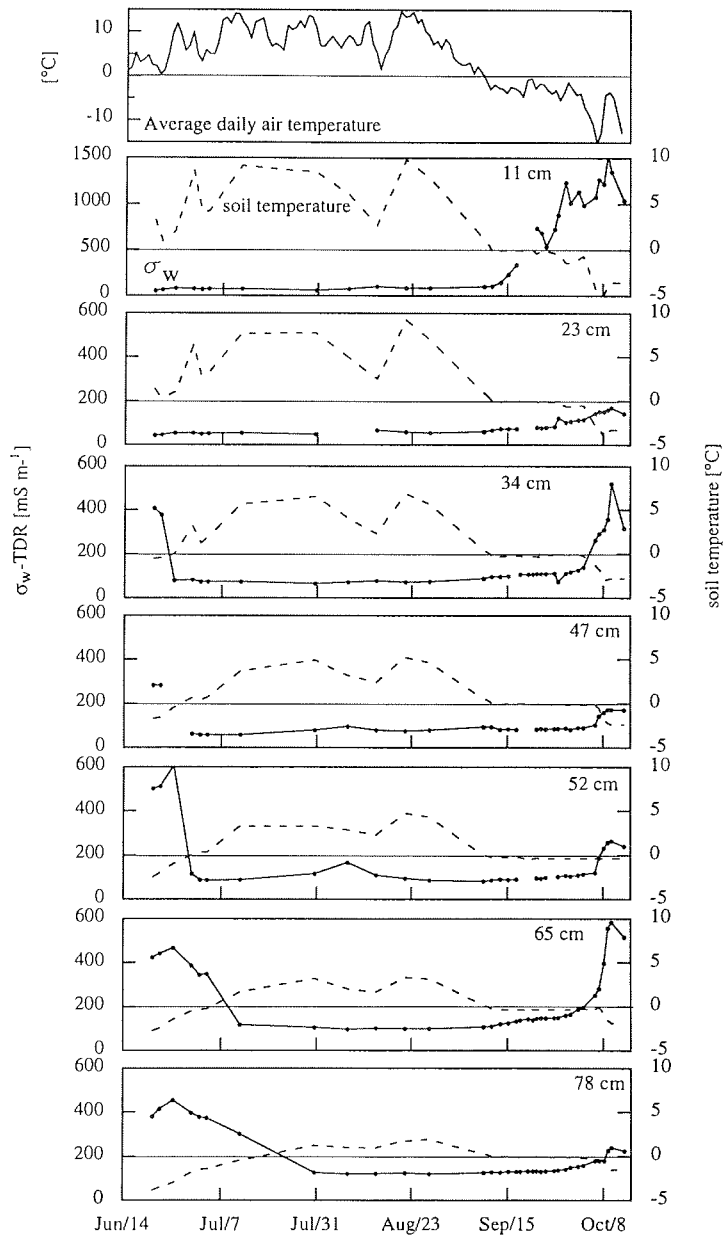

Figure 2.3. Seasonal dynamics of σ_W at site 2x from 14 June to 15 October 1995. Probe specific calculated σ_S are used to calculate σ_W for depths 23, 34, 47, 52 and 65 cm. For depths 11 and 78 cm, the average site specific calculated σ_S value is used.

Freeze-back

The active layer is saturated up to about 8 cm below the surface before freeze-back starts (Boike *et al.*, 1997b). In the frozen ground, σ_w range between 200 to 600 mS m^{-1} with the exception of highest values of up to 1500 mS m^{-1} at 11 cm depth. With the exception of 1500 mS m^{-1}, these values lie in the range reported by Lundin and Johnsson (1994).

In September, when air temperatures decrease and fall below 0 °C, soil temperatures decrease quite uniformly at all depths and the phase change, characterized by the zero curtain effect, is initiated. During the first part of the phase change in September, soil temperatures are just below 0°C and σ_w increases slowly (Fig. 2.3). Starting in October, air temperatures fall sharply down to -15 °C, soil temperatures decrease and σ_w increases rapidly. This increase of σ_w during the period of phase change can be explained by exclusion of solutes from the ice during freezing which has been reported by Hallet (1978). Differences in σ_w within the profile are related to the initial water content of the soil. At depths of 11, 34 and 65 cm, freezing proceeds somewhat faster and σ_w are higher relative to other depths due to faster decreasing water contents (Boike *et al.*, 1997b) (Fig. 2.3). The preferential freezing within the profile apparently depends on the heterogeneity of the soil and the resulting differences in water content. These results support the observation by Panday and Corapcioglu (1991) that the exclusion of solutes within a freezing soil system is determined by a complex interplay between hydraulic and thermal properties.

2.5 CONCLUSIONS

Generally, TDR is a promising *in situ* technique to calculate σ_w from σ_b for arctic field soils. Optimal results are achieved when the model of van Loon *et al.* (1991) is used with a probe specific calibrated σ_s through the use of suction lysimeter data. Further improvements could be made by incorporating a soil characteristics term that is related to the coarseness and tortuosity of the soil.

TDR measurements have been used to study the seasonal dynamics of σ_w in frozen and unfrozen ground. Strong temperature dependence of σ_w in the frozen ground was observed in the range of 50-100 mS m^{-1}, but variations in σ_w as a result of phase change were much greater, in the range of 200-500 mS m^{-1}. The magnitude of conductivity changes associated with phase changes, *i.e.*, of solute exclusion, depends on the freezing rate and therefore the initial water content of the soil.

Chapter 3

Using time domain reflectometry to measure water content and soil water electrical conductivity in the active layer of a continous permafrost site

Paper by:
J. Boike and K. Roth. Permafrost and Periglacial Processes (accepted).

3.1 ABSTRACT

Time domain reflectometry (TDR) is evaluated as a field technique for measuring volumetric water content θ and bulk electrical conductivity σ_b in arctic soils. Calibration measurements of θ and σ_b were carried out on three different slopes at a field site in Siberia (74° 32'N; 98° 35'E). Comparison of θ calculated from TDR using two different approaches and gravimetrically determined water contents show a close correlation. TDR determined σ_b applying theoretical relationships and a simple regression model are compared to the electrical conductivity σ_w of soil solutions obtained with suction cups. Best results for σ_w are obtained using the regression model, with highest precision when probe specific calibration is carried out. In this permafrost setting, TDR can be applied to obtain quantitative estimates of θ and σ_w in the active layer. The application of the regression model in different permafrost soils to infer σ_w requires additional calibration.

3.2 INTRODUCTION

In situ measurements of volumetric water content θ and soil water electrical conductivity σ_w give estimates of the spatial and temporal distribution of water and solutes in the unfrozen and frozen ground. These data are essential for identifying transport properties and the calibration and verification of mass and energy transport models for the frozen and unfrozen ground. Adequate *in situ* methods for determining θ and σ_w for arctic field applications are still being developed. Methods widely used in temperate climates are not necessarily transferable to arctic regions. One example is the use of suction lysimeters for measuring the temporal evolution of solute concentrations at specific depths. Their major disadvantages in arctic regions are the freezing of tubes above ground at subzero air temperatures and complete failure in frozen ground.

Conventional methods for the *in situ* determination of θ include thermalization of neutrons and gamma ray attenuation. These methods are not always suitable for Arctic regions due to the limitations of transporting radioactive equipment to these

remote areas. Furthermore, they require vertical access holes which are difficult to drill in regolithic soils. Another disadvantage is that these methods measure the total water content (water and ice) rather than estimates of liquid water content in frozen soils. Techniques for field measurements of θ and σ_w in arctic regions should fulfill the following conditions: (i) the equipment (probes and instruments) should be largely unaffected by subzero temperatures and a seasonal freeze-thaw cycle and (ii) the method should be suitable for use in remote areas and automation. In addition to these technical requirements, the method should yield parameters for θ and σ_w for the frozen and unfrozen active layer under a wide range of soil conditions. Arctic soils are generally coarsely textured (regolithic), often very heterogeneous and vary from soils with high organic content to soils with a high mineral content over different water content and temperature ranges.

In this paper we evaluate the use of time domain reflectometry (TDR) as a method for *in situ* field measurements of θ and σ_w for a variety of arctic soil types in Siberia. Within the framework of a larger project on 'transport processes of water and solutes in the active layer', our objective was to obtain quantitative estimates of θ and σ_w in active layer from TDR field measurements. Existing models for the calculation of θ from the dielectric number ε and σ_w from σ_b will be tested using data taken from the field site in Siberia. Introduced by Topp *et al.* (1980), TDR has been discussed and applied to measure θ in temperate (*e.g.* Herkelrath *et al.*, 1991; Roth *et al.*, 1990) and arctic field soils (Stein and Kane, 1983). In temperate soils, TDR has become an established method to determine σ_b (Dasberg and Dalton, 1984; Nadler *et al.*, 1991). In contrast, TDR has not been used to derive σ_w from σ_b in arctic regions. Results from laboratory and field studies have yielded various theoretical and empirical models (Rhoades *et al.*, 1976; Mualem and Friedman, 1991; van Loon *et al.*, 1991).

A further advantage of the TDR method in the permafrost environment is that other parameters in addition to θ and σ_w can be measured. This includes the location of the frozen-unfrozen boundary (Baker *et al.*, 1982) and estimates of the porosity η of the soil. The latter can be obtained under saturated soil conditions (assuming that $\theta_{sat}=\eta$) which can be determined using wells.

3.3 THEORY

3.3.1 Soil volumetric water content θ

In the TDR method for θ determination, an electromagnetic pulse is propagated through the soil along a transmission line, here a triple wire probe, and its reflections are recorded. From the travel time of the signal along the soil probe the soil dielectric number ε can be calculated. This value can be related to θ using empirical or theoretical relationships. Two different approaches for the calculation of θ from ε were applied for this study. The third-order polynomial relationship proposed by Topp *et al.* (1980)

$$\theta = -0.053 + 0.29\varepsilon - 5.5\times10^{-4}\varepsilon^2 + 4.3\times10^{-6}\varepsilon^3 \qquad [3.1]$$

is independent of soil texture, density and temperature. The composite dielectric number ε_c used by Roth *et al.* (1990) describes the soil as a three-phase medium consisting of the solid, liquid and gaseous phases and leads to

$$\theta = \frac{\varepsilon_c^{\beta} - (1-\eta)\varepsilon_s^{\beta} - \eta\varepsilon_a^{\beta}}{\varepsilon_w^{\beta} - \varepsilon_a^{\beta}} \qquad [3.2]$$

where $\varepsilon_{s,a,w}$ are the dielectric numbers of the soil particles, air and water, η is the porosity and β is a geometry factor with β =0.5 for a random arrangement of the soil constituents. This approach therefore requires additional soil parameters such as porosity and soil temperature for the calculation of θ.

3.3.2 Electrical conductivity of soil

The amplitude of the TDR signal at very long times can be used to determine σ_b, which is treated as the sum

$$\sigma_b = \sigma_w + \sigma_s \qquad [3.3]$$

of the electrical conductivities of the water phase and the matrix surface, respectively. Using data from the 4-electrode probe, Rhoades *et al.* (1976) found for σ_b the empirical parametrization

$$\sigma_b = \tau\theta\sigma_w + \sigma_s; \quad \tau = a\,\theta + b \qquad [3.4]$$

where τ is called the transmission factor and a and b are soil specific constants. The factor τ accounts for the geometry of the network of electrically conductive paths. In a porous medium, individual paths are highly tortuous and exhibit a highly variable cross section.

Mualem and Friedmann (1991) assume that the network of electrically conductive paths in an electrical gradient is identical to the network of hydraulically conductive paths in the corresponding hydraulic gradient. They further postulate that τ is the ratio between the hydraulic conductivity obtained from the statistical model of Mualem (1976) and a bundle of parallel capillaries with the same pore size distribution. Assuming that this distribution may be calculated from the measurable soil water characteristic function $\theta(\psi_m)$, they find a description for $\tau(\theta)$ that depends only on a single parameter n and on $\theta(\psi_m)$. Using the parametrization $\theta(\psi_m) = \theta_{sat}[\psi_m/\psi_0]^{-\lambda}$ (Brooks and Corey,1966) where ψ_0 is the air-entry value and λ is a constant expressing soil texture, Mualem and Friedmann (1991) finally arrive at

$$\tau(\theta) = \frac{\theta^{n+1}}{\theta_{sat}} \frac{1+2/\lambda}{[1+1/\lambda]^2} \qquad [3.5]$$

For coarse-textured soils, which are associated with large values of λ, this may be simplified to

$$\tau(\theta) \approx \frac{\theta^{n+1}}{\theta_{sat}}; \quad \lambda >> 1. \qquad [3.6]$$

Inserting this approximation into [3.4] finally yields

$$\sigma_b = \frac{\theta^{n+2}}{\theta_{sat}}\sigma_w + \sigma_s . \qquad [3.7]$$

Van Loon *et al.* (1991) obtain an empirical model for the electrical conductivity of wet soil by using a third order polynomial for interpolating approximate descriptions of two limiting cases, dry soils and soil suspensions, to the intermediate range of water saturation. For the limiting case in the dry range, they presume that the electrical properties of soil can be calculated from a model where soil matrix and soil solutions are thin layers orthogonal to the electrical field. The electrical properties of the soil suspensions are obtained from assuming a homogeneous mixture. Using this approach, they arrive at

$$\sigma_b = \sigma_w[2-\theta]\theta^2 + \sigma_s[1+3\theta] \qquad [3.8]$$

for the case $\sigma_w >> \sigma_s$.

3.4 STUDY SITE AND METHODS

This paper reports results from field work carried out in 1994 and 1995 in the Levinson-Lessing Lake catchment, Taymyr Peninsula, Siberia. The peninsula is the northernmost continental area of the circumpolar Arctic (Figure 1.1). Three slopes differing with respect to slope aspect and inclination and soil characteristics were instrumented (Figure 3.1, Table 3.1). At each site, triple wire TDR probes, PT 100 temperature probes, wells, piezometers and suction cups (5 cm long, pore size 2 microns; Gravquick, Denmark) were installed. The TDR probes used in this study consist of three parallel steel rods (diameter 5 mm) with a length of 25 cm, separated by 3 cm, connected to a 50 Ω cable and held in place by an epoxy resin (Heimovaara, 1993). TDR waveforms were recorded in the field using a Tektronix 1502 B (Tektronix, 1988) cable tester, a portable laptop and the program of Heimovaara and de Water (1993).

Calibration measurements for θ were undertaken at sites representative of the soil material in this area. For calibration, a small profile was dug and TDR probes inserted horizontally at different depths. After recording TDR signals, volumetric soil samples were taken at these depths using steel cylinders (100 cm^3). These samples were oven dried in the field following standard gravimetric methods (Klute, 1986). For calculation of σ_b, the cell constant of the triple-wire probes and the resistance of the TDR system (cable tester, cables and connectors) were carried out with a range of solutions with known electrical conductivities, following the method of Heimovaara *et al.* (1995). The value of σ_b was corrected for the temperature dependence of the water viscosity ν (van Loon *et al.*, 1991):

$$\sigma_b[T] = \sigma_b[25]\nu[T] \approx \sigma_b[25]\left[0.588 + 0.0193\,T + 0.00014T^2\right] \qquad [3.9]$$

where T is temperature in [°C].

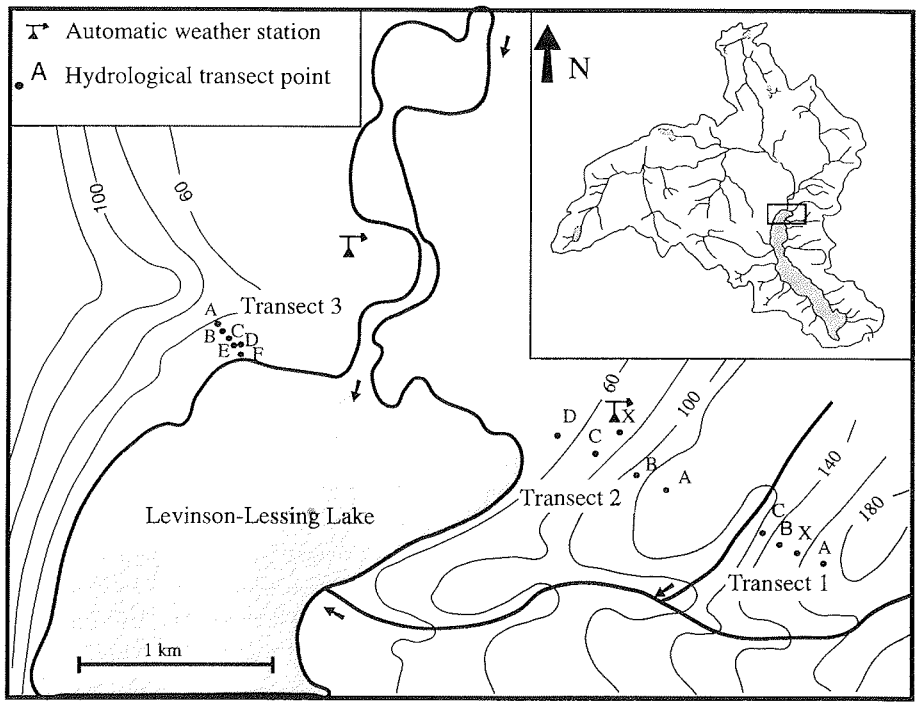

Figure 3.1. Location and field installation of 3 slopes in the Levinson-Lessing watershed, Taymyr, Siberia.

Table 3.1. Soil characteristics of slopes 1, 2 and 3. Data are averaged from all transect points on each slope.

Slope	porosity+	C_{org} [%]	bulk density [kg m^{-3}]	saturated K* [m s^{-1}]	>2 mm [%weight]	sand	silt	clay
1 average	0.36	3.9	1470	$2*10^{-4}$	59	18	17	6
range	0.3-0.53	3-4.7	1340-1560	$1*10^{-3}$-$6*10^{-8}$				
N	16	6	12	6				
	soil tax#:	lower slope: sandy-skeletal pergelic cryaquept						
		upper slope: sandy-skeletal pergelic cryorthent						
2 average	0.34	1.6	1700	$5*10^{-6}$	36	41	20	13
range	0.3-0.44	0.8-2.5	1430-1820	$2*10^{-5}$-$8*10^{-8}$				
N	22	6	18	8				
	soil tax#:	loamy skeletal carbonatic calcareous pergelic cryorthent						
3 average	0.5	4.2	1160	$2*10^{-5}$	14	48	29	9
range	0.4-0.58	1.9-8.7	930-1380	$3*10^{-5}$-$3*10^{-7}$				
N	14	5	19	4				
	soil tax#:	sandy nonacid pergelic cryaquept						

+ determined using TDR probes at saturation, * determined using bail tests in mini-piezometers (Lee and Cherry, 1978), # after Pfeiffer *et al.* (1996)

3.5 RESULTS

3.5.1 Field evaluation

Figure 3.2 shows the grain size distribution of instrumented sites on slopes 1, 2, and 3. Generally, the sites are characterized by a high percentage of coarse material larger than 2 mm with slope 1 having the greatest fraction. Furthermore, the poor sorting of the soils is reflected in the large variation of grain size percentages. For TDR measurements we chose triple instead of double wire probes since the measuring accuracy is higher and a balancing transformer is not required (Zegelin *et al.,* 1992). However, triple-wire probes are more difficult to install in these stony and concrete soils and limit the length of the rods. In addition, the probe should be constructed following the optimal ratio between rod diameter and outer and inner spacing between the probes (Heimovaara, 1993). Zegelin *et al.* (1992) further suggest that as a 'rule of thumb' the probe diameter should be larger than 10 times the average grain size diameter to obtain maximum accuracy. For coarse-textured soils, as encountered at our sites, this leads to unrealistically large rod diameters. Apart from the technical difficulty of installing the resultingly huge probe, a fundamental problem arises with its cut-off frequency. Depending on the geometry, a wave guide is generally able to support higher modes of the electromagnetic field which travel at different velocities (Jackson, 1975). Since the TDR technique essentially measures the travel time of an electromagnetic impulse, this impulse is required to form a single mode. The easiest way to accomplish this is to choose the dimensions of the probe such that the cut-off frequency, beyond which higher order modes can emerge, is so high that only a negligible fraction of the TDR's frequency spectrum is above it. For the instrument used, this limits transverse dimensions of the probe to some 0.1 m. As will be demonstrated in the following section, our TDR probes can be used and yield sufficiently accurate results at these coarse-textured site even though the probes are significantly smaller than suggested by the 'rule of thumb'.

During installation it is important to avoid air gaps and deformation of the probes since this reduces the measuring accuracy of θ and σ_w. Problems with the installation of triple wire probes in the stony soil were overcome by using robust probes in addition to a guide that was inserted and removed into the soil prior to the TDR probes. The 60 probes that stayed in the ground for two winters were excavated in 1996; only two were deformed and no frost heave effects were observed.

The measurement equipment, a cable tester and computer, were used in the field at temperatures as low as -20°C. In addition, an automatic TDR station (using the cable tester, Campbell Scientific datalogger and multiplexer powered by a 12V solar station) were set up to continuously record data under these temperature conditions. Another benefit of the TDR method is that fast measurements can be made, once one is familiar with the technique. The raw data are stored in the form of waveforms in the field. The time consuming analysis of the waveforms can be carried out later.

3.5.2 Testing the TDR method for volumetric water content

Figure 3.3 compares the results of thermogravimetrically determined water content to TDR measurements at 8 different sites on all 3 slopes. Water contents calculated using

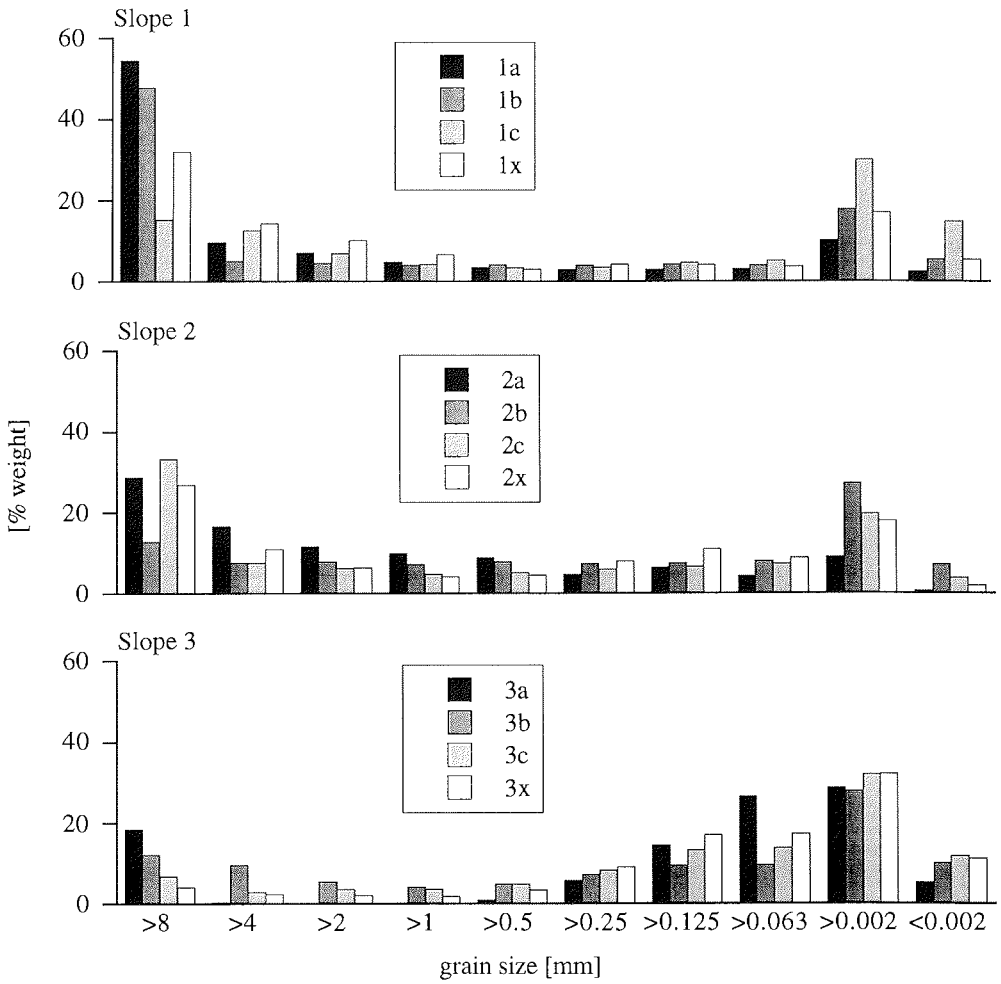

Figure 3.2. Grain size distribution of instrumented sites on slopes 1, 2 and 3 expressed as % of total weight. Soil grain size analysis was carried out using standard methods (Klute, 1986).

[3.1] and [3.2] are relatively close to the thermogravimetrically determined values (Figure 3.3).

However, the approach based on a mixing model [3.2], yields a slightly higher correlation coefficient between the gravimetrically determined and the calculated water content. Values of r^2 calculated from 18 data points were = 0.87 for [3.2] and 0.82 for [3.1]. The standard error of estimate in θ is 0.031 $m^3\ m^{-3}$ for [3.2] and 0.033 $m^3\ m^{-3}$ for [3.1]. Despite limits for probe design and installation, we have a good accuracy of the θ-measurements in these coarse and variable soils with both equations using TDR.

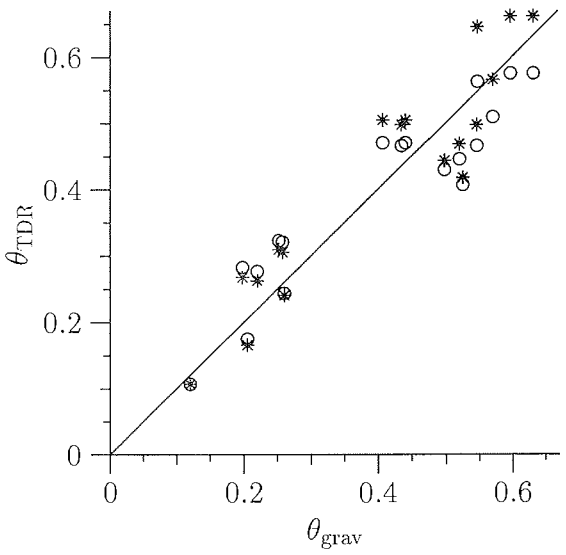

Figure 3.3. Comparison between volumetric water content measured gravimetrically and calculated using equation [3.1] (circles; r^2= 0.82) and [3.2] (stars; r^2= 0.87; N=18).

3.5.3 Relationship between σ_b and σ_w

To study the relationship $\sigma_b(\sigma_w)$, we compare estimates of σ_w calculated from the TDR measurements of σ_b to values measured in soil solutions extracted with suction cups. The tacit assumption underlying such an approach is that both instruments, TDR and suction cups, sample the same volume of the water phase. Such an assumption is probably not true in general because (i) suction cups extract solution from the largest pores only while TDR measures the entire water phase, (ii) the region from which solution is extracted is determined by the hydraulic properties of the soils whereas the measuring volume of the TDR is determined mainly by the geometry of the probe, and (iii) the two instruments are generally located at different positions. We believe that the first point is of minor importance for the coarse-textured soils considered here. The other two points will lead to an additional scatter of the data, however.

The relationship between TDR determined σ_b and σ_w from suction lysimeters at all sites from transects 1, 2 and 3 is shown in Figure 3.4. The three transects fall into three different groups; sites on transect 2 have the highest and widest range in σ_w and sites on transect 3 have the lowest σ_w. There is no common relationship between σ_b and σ_w for the set of all sites which illustrates the importance of different soil properties of the slopes.

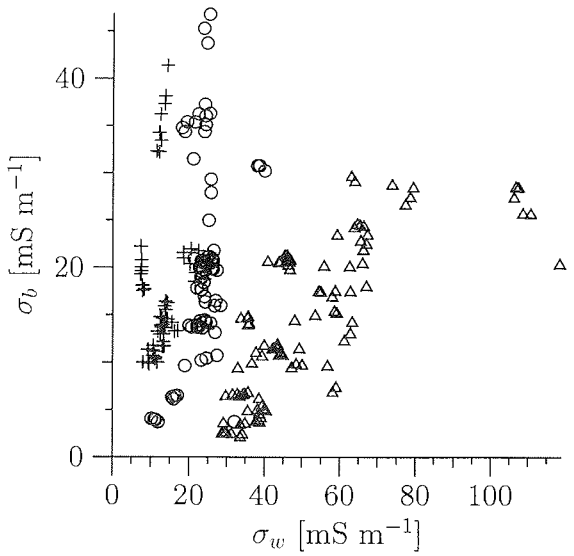

Figure 3.4. Comparison between σ_b calculated from TDR measurements and σ_w from suction lysimeters for each slope (circles: slope 1; triangles: slope 2; crosses: slope 3).

Parameterization

Three different parametrizations are used to describe $\sigma_b(\sigma_w)$: the model of van Loon *et al.* (1991) as given by [3.8], the model of Mualem and Friedmann (1991) in the approximation [3.7], and the regression model

$$\sigma_b = A\theta^B\sigma_w + \sigma_s \qquad [3.10]$$

where A and B are constants. This last model is formulated in analogy to Rhoades *et al.* (1976). The first two models are chosen because they have been applied for frozen (Lundin and Johnsson, 1994) and unfrozen soils (Heimovaara *et al.*, 1995).

Estimation of Parameters

Optimal values for the parameters of the three models are estimated by minimizing the sum of squares

$$\Delta^2(p) := \frac{1}{N}\sum_{i=1}^{N}\left[\sigma_{w_i}^{\mathrm{mod}}(p) - \sigma_{w_i}^{meas}\right]^2, \qquad [3.11]$$

where N is the number of data points. Minimization was done using a modified version of the Levenberg-Marquardt algorithm as given by Press *et al.* (1992). For each model optimal parameters are estimated (i) for the entire slope, (ii) for each soil profile, and (iii) for each TDR probe. This succession leads to decreasing deviation between model and measurement at the cost of reduced generality and higher requirements for the calibration.

The three models considered require between 1 and 3 parameters. Their descriptive power is thus not directly comparable. During the estimation process we found, however, that some parameters were either insignificant or highly correlated with each other. As a consequence, we formulated one-parameter models and estimated optimal values for their parameters. The models used are (i) the original model [3.8] of van Loon *et al.* (1991), (ii) the model [3.7] of Mualem and Friedman (1991) with $\sigma_s = 0$ and (iii) the regression model

$$\sigma_b = A\,\theta\,\sigma_w \qquad [3.12]$$

derived from [3.10]. The descriptive power of these models, expressed as the mean deviation Δ, was found to be somewhat lower than that of their multi-parameter formulation. However, the consistency of the estimated parameters increased dramatically, *i. e.*, they varied much less among different sites or probes.

Comparison between models with one parameter estimates

Figure 3.5 shows the measured results compared to the TDR determined results applying the three relations described above for slope and site specific calibration. Parameter values estimated for each relation at each site are given in Table 3.2. While models in the theory section have been ordered with decreasing theoretical justification, here they are ordered with increasing descriptive power, *i. e.*, with decreasing mean deviations Δ as indicated in Figure 3.5.

Values for σ_s of relation [3.8] were estimated between 1.2 and 8.3 mS m^{-1} for the site calibration. Contrary to the laboratory results of van Loon *et al.* (1991), this parameter is always positive as would be expected intuitively. For the Mualem-Friedmann model [3.7] we notice that values of n are between -2.81 and +0.26 which deviates considerably from the value of 0.5 which is suggested to be used when data for calibration are unavailable.

The simple regression model [3.12] turned out to yield the best description of the data both for the slope and for the site specific calibration. Comparing [3.12] with the empirical parametrization [3.4] of Rhoades *et al.* (1976) shows that A and τ have identical functions, namely to account for the geometry of the network of electrically

Table 3.2. Values of model parameters estimated for each of the models [3.8], [3.7] and [3.12] for all the sites. The first column indicates the site with the number giving the slope. Parameters obtained by simultaneously fitting all data obtained from a slope are marked "all" in the first column. The number of data points in each set is *N*; SD is the standard deviation of the parameter estimate.

		model [3.8]		model [3.7]		model [3.12]	
site	N	σ_s	$SD_{\sigma s}$	n	SD_n	A	SD_A
1x	12	6.43	0.52	-1.13	0.12	2.48	0.22
1a	9	2.83	0.13	-0.83	0.07	2.35	0.32
1b	21	7.27	0.98	-1.25	0.11	3.32	0.29
1c	31	6.88	0.32	-0.87	0.03	2.12	0.06
all	73	3.74	0.27	-1.04	0.04	2.59	0.11
2x	24	1.42	0.26	0.26	0.03	0.72	0.03
2a	14	1.24	0.05	-0.21	0.06	0.70	0.02
2b	9	4.63	0.45	-0.35	0.07	1.35	0.11
2c	29	2.02	0.11	-0.24	0.04	0.83	0.03
2d	29	1.76	0.24	0.16	0.03	0.86	0.02
all	105	1.74	0.09	-0.10	0.03	0.83	0.02
3a	16	8.34	0.61	-2.81	0.07	4.80	0.09
3b	16	4.66	0.13	-0.89	0.04	2.09	0.08
3c	14	3.63	0.23	-1.01	0.05	2.13	0.09
3e	6	2.51	0.07	-1.09	0.05	1.96	0.06
3f	6	2.59	0.07	-1.02	0.07	2.02	0.10
all	58	4.84	0.31	-1.71	0.13	2.95	0.17

conductive paths. While Rhoades *et al.* (1976) found this parameter to be a linear function of θ, it is independent of θ for our data set, although a range of θ is covered (*i. e.*, slope 2: 0.11 to 0.46; slope 1: 0.1 to 0.5). Table 3.2 further indicates that the value of A for model [3.12] varies much less within a slope than between slopes. Slopes 1 and 3 have generally a higher value of A than slope 2. Laboratory measurements (Table 3.1) and soil profile descriptions during instrumentation indicate a higher content of organic matter and a more pronounced skewness of the grain size distribution on slopes 1 and 3 as compared to slope 2 (Figure 3.2). While these broad observations would hint at a different geometric structure for slopes 1 and 3 relative to slope 2, our data set is too limited to show a general relationship between soil physical parameters and A.

Scale of calibration

Calibration of σ_w^{mod} to σ_w^{meas} is affected by the spatial variability of the soil at different scales, and by the differences of the TDR and the suction cup measurement. We consider variability at the scale of the slope, of the site, and at a probe. Estimating parameters for a particular scale corresponds to assuming homogeneity at that scale. Consequently, the actual heterogeneity is lumped into the value of Δ. The extent of heterogeneity at the different scales is reflected by the steep decrease of Δ with decreasing scale. For example, Δ^{slope} to Δ^{site} values for slopes 1 and 3 using model [3.12] decrease from 7.8 to 6.4 for slope 1 and 5.4 to 1.8 for slope 3 (Figure 3.6).

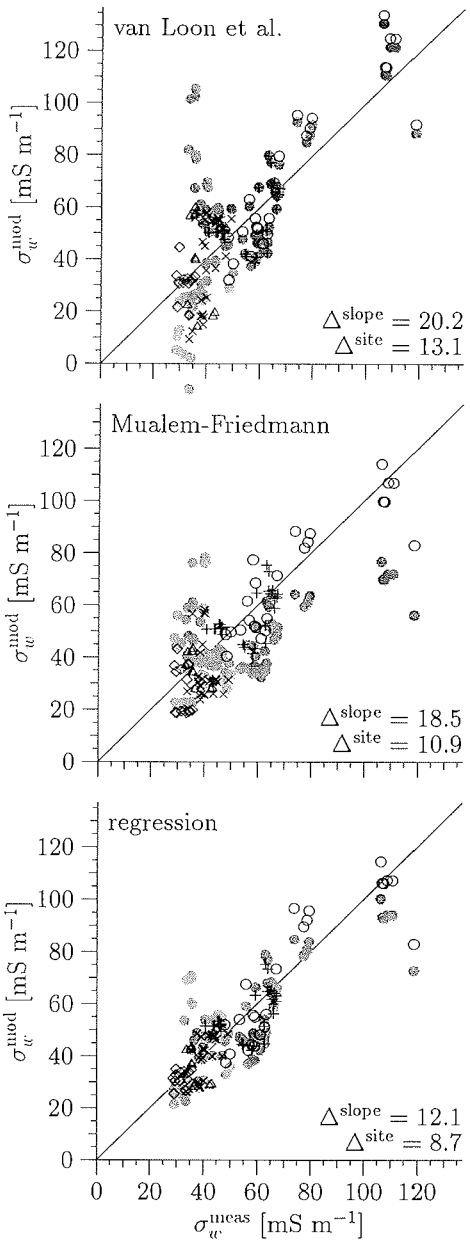

Figure 3.5. Comparison between σ_w^{meas} and σ_w^{mod} using the models [3.7], [3.8] and [3.12] for slope (grey circles) and site specific analysis for slope 2. For site specific analyis one symbol is used for each site.

Results are expressed as $\Delta^2(p) := \frac{1}{N}\sum_{i=1}^{N}\left[\sigma_{w_i}^{mod}(p) - \sigma_{w_i}^{meas}\right]^2$.

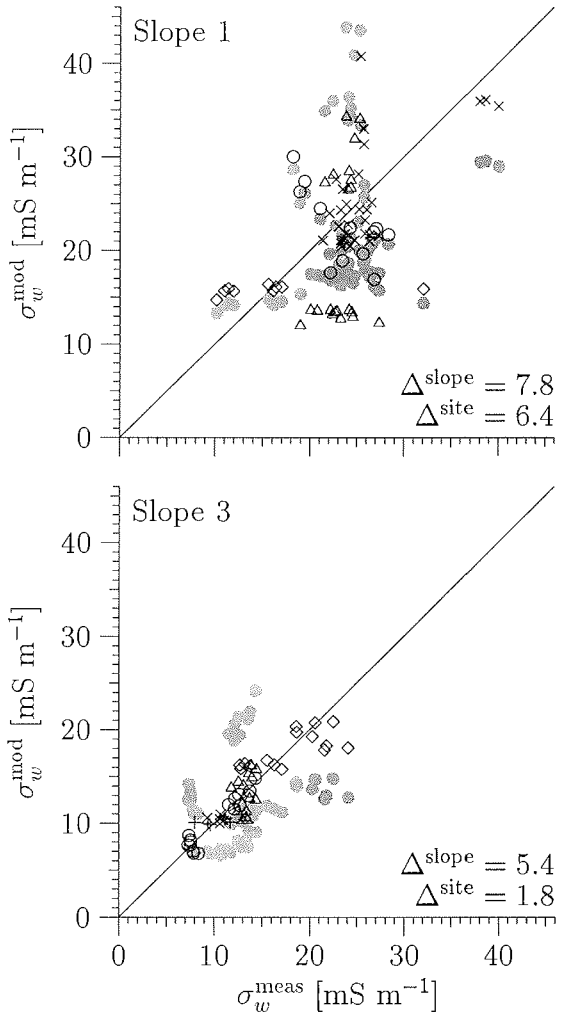

Figure 3.6. Comparison between σ_w^{meas} and σ_w^{mod} using the model [3.12] for slope (grey circles) and site specific analysis for slopes 1 and 3. For site specific analyis one symbol is used for each site.

Smallest Δ values are obtained for probe specific calibration, *i. e.* for slope 2 Δ^{slope}=12.1, Δ^{site}=8 and Δ^{probe}=6.5 (Figure 3.7). Moving from the largest to the smallest scale the value of Δ does not drop to 0 because of three facts: (i) the linear regression model is only an approximation of the real, unknown, relation $\sigma_w(\sigma_b)$, (ii) measurements with the TDR and the suction cups are taken at nearby, but still different positions and the measuring volumes of the two instruments are different and (iii) omission of σ_s in the regression model as a result of insignificantly low values. Notice that the TDR measurement may be biased if the probe has been deformed during installation and if, consequently, the cell constant is different from what has been determined in the

laboratory. This is compensated, however, in the probe specific calibration, but it would contribute to the larger values of Δ at the larger scales. It should be noted, however, that the number of lysimeters and concomitant field or laboratory work required for probe specific calibration does not necessarily justify the relatively small improvement in predicting σ_w (i .e. slope 2 Δ^{site}=8.7 versus Δ^{probe}=6.5).

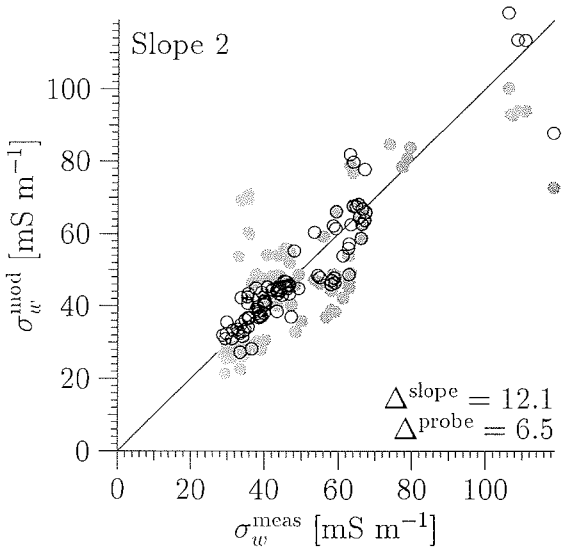

Figure 3.7. Comparison between σ_w^{meas} and σ_w^{mod} using the model [3.12] for slope (grey circles) and probe specific analysis for slope 2. For probe specific analyis one symbol is used for each probe.

Discussion

For our data, the simple regression model [3.12] is more accurate in quantitative prediction of σ_w than currently used theoretical models. A possible explanation is, that the pore geometry models (Mualem and Friedman,1991; van Loon *et al.* 1991) do not describe the ion flow lines sufficiently well. Contrary to their results, *A* is independent of θ for our data set. A possible interpretation for this finding is that in the coarse-textured soils considered in this study, the pore geometry is such that a decrease of θ leads, in a first approximation, to a proportional decrease in the cross-sectional areas of the water phase, but not to a change in the lengths of the ion flow paths. This discrepancy between results from coarse- and fine-textured soils warrants further experimental investigations.

The major improvement of Δ values from slope to site calibration with respect to probe calibration implies that soil physical variations within the slope are much greater compared to variations within sites. Each site can be considered more or less

homogeneous. This is also supported by the lack of distinct layering or the formation of horizons which was observed during the excavation of these soil profiles.

The major improvement of Δ values from slope to site calibration with respect to probe calibration implies that soil physical variations within the slope are much greater compared to variations within sites. Each site can be considered more or less homogeneous. This is also supported by the lack of distinct layering or the formation of horizons which was oberverd during the excavation of these soil profiles.

With the exception of two sites, 2b and 3a, the variability of A between slopes is much larger than within them (Table 3.2). This indicates that A depends only weakly on soil properties. While the deviating values found at sites 2b and 3a could be the result of analytical errors, they may also indicate morphological/topological differences on these slopes. Site 2b, for example, is located in a small trough, has a higher percentage of surface vegetation and the highest silt and clay fraction compared to other sites on slope 2 (Figure 3.2). As stated earlier, our data set is too limited to expand this discussion. Nevertheless, A only varies by a factor of about 5 for all slopes (with the exclusion of 3a; Table 3.2). Without further calibration, we may thus use an average value A=2 to obtain acceptable estimates for σ_w in this permafrost setting.

However, caution should be applied to transfer this factor to other permafrost settings without calibration. The ultimate goal could be to develop an universally applicable model which relates A to some easily measurable soil physical parameters. This requires further detailed experimental research.

3.6 SUMMARY

In situ measurements of θ and σ_b were undertaken at a Siberian field site using TDR. Independent methods, such as gravimetrically determined θ and σ_w from suction cups were compared to values calculated from TDR measurements. Generally, the use of TDR to determine θ and σ_w yields good results for a range of arctic field soils. For the determination of θ, no special calibration is needed. This is an advantage compared to alternative methods such as neutron thermalization or gamma ray attenuation.

The linear regression model was found to yield significantly better results than the theoretical models for calculation of σ_w. Estimating σ_w from TDR measured values of σ_b using the linear regression [3.12] with A=2 produces values that are within a factor of about 2 of the true values for our sites. As expected, the precision in predicting σ_w increases for all models when the scale of calibration decreases (slope<site<probe). The site specific calibration offered the best track-off between precision and experimental effort for calibration. However, our current understanding does not permit calculation of σ_w from measured σ_b without calibration at other permafrost sites.

Based on these results, TDR is recommended as an *in situ* technique for studying the temporal dynamics of soil water and solutes in the unfrozen active layer. As a next step, the application of TDR for the calculation of σ_w in frozen soils and the relationship between the geometry factor A and soil properties should be explored. In the Appendix of this paper we suggest a simple model for the calculation of σ_w in the frozen active layer.

3.7 APPENDIX

We suggest a simple model for extending [3.12], which was obtained for non-frozen soil, into the realm of partially frozen soil. The premises of this model are:

(i) dissolved solutes are expelled from the ice
(ii) migration of water and solutes is negligible
(iii) electrical conductivity is proportional to solute concentration in liquid water phase and the geometric factor is constant, independent of the degree of freezing.

Consider a small volume of unfrozen soil with total concentration C_t (mass of solute per unit volume of soil) and volumetric water content θ. The concentration in the liquid water phase is then

$$C_w = \frac{C_t}{\theta} \qquad [3.13]$$

and $C_w \propto \sigma_w$. Assume that a fraction of this volume freezes, bringing the liquid water content to θ'.
Then the electrical conductivity in frozen ground becomes

$$\sigma_w' = \sigma_w \frac{\theta}{\theta'} \qquad [3.14]$$

Inserting into [3.12] finally leads to

$$\sigma_b' = A\, \sigma_w\, \theta \qquad [3.15]$$

where θ is the water content before the onset of freezing. We recognize that premise (i) can be considered as generally satisfied (Anderson and Morgenstern, 1973), (ii) may only be true for short times and (iii) need not necessarily be true. The third assumption is rather speculative since the geometric factor is likely to change from an unfrozen soil-water system to a frozen soil-ice-unfrozen water system. However, we determined parameter A for θ down to 0.1 on slopes 1 and 2 in the unfrozen soil. During the spring 1995 field campaign, θ' was measured up to 0.1 in these frozen soils (Boike *et al.*, 1997b). The hypothesis is that at low water contents, as in frozen or dry unfrozen soils, the geometric factor would not change. This is corroborated by our previous results that A is independent of θ. We suggest that equation [3.15] can be applied to obtain estimates of solute concentrations in frozen soils, but needs to be tested through experimental work.

Chapter 4

Thermal and hydrological dynamics of the active layer at a continuous permafrost site (Taymyr Peninsula, Siberia)

Paper by:
J. Boike, K. Roth and P. P. Overduin. Water Resources Research (accepted). Awarded the *First Annual Arctic Research Consortium of the U.S. (ARCUS) Student Award for Arctic Research Excellence 1997*

4.1 ABSTRACT

The ground thermal and hydrological regime of a site located in the continuous permafrost landscape of Taymyr Peninsula, northern Siberia was studied in 1994 and 1995. The aim was to quantify the seasonal fluxes of water and heat in the active layer from spring thaw to fall freeze-back. Liquid water content was measured in frozen and unfrozen soils using time domain reflectometry (TDR). Liquid water was present in frozen soil at temperatures down to -12 °C and its volumetric fraction increased with temperature before melting occurred. The ground thermal regime during spring thaw and fall freeze-back is dominated by latent heat fluxes that stabilize soil temperatures at 0 °C for extended periods. During the summer, the thermal regime of the saturated active layer may be understood from assuming density driven convection as the mechanism of heat transfer. Convective transfer also appears to be dominating during fall, when large amounts of latent heat are released by freeze-back.

Seasonal fluxes of heat and water are calculated using a simple zero-dimensional model of water and energy balance. Although this model neglects processes such as sensible heat fluxes and lateral water flow, it reveals that the dominant heat sink during spring and summer is evaporation. During fall freeze-back, the dominant heat-producing process is phase change.

The soil heterogeneity strongly impacts hydrological and thermal processes in the active layer. Two direct consequences are the development of preferential flowpaths and preferential freezing of the profile during freeze-back.

4.2 INTRODUCTION

The active layer, the annually freezing and thawing upper ground in permafrost areas, is of pivotal importance. Conditions for plant growth, gas fluxes, groundwater flow regimes and soil formation are all limited and to some extent determined by this zone. The moisture and heat transfer characteristics of this layer also determine the boundary layer interactions of the underlying permafrost and the atmosphere and are therefore

important input parameters for geothermal or climate modeling. Finally, changes in the characteristics of the permafrost and permafrost related processes may be used as indicators of global ecological change (Lachenbruch and Marshall, 1986) provided the system permafrost-active layer-atmosphere is understood sufficiently well.

The thermal and moisture states of the active layer are coupled (Guymon and Luthin, 1974). This coupling becomes especially important during the spring and fall when thawing and freezing processes comprise substantial portions of the heat energy balance. Nonetheless, the mechanisms of heat and mass transfer during these periods are poorly understood, owing to the complexity of the systems and to the inaccessibility of the permafrost regions.

Active layer heat transfer is a complex process. Three phases of water coexist and redistribute over time with changing temperature and pressure conditions and the active layer itself is underlain by permafrost, a source of unfrozen water. In a frozen soil, a film of unfrozen water, whose thickness depends on the temperature and soil texture, surrounds the soil matrix. Unfrozen water may also be preserved in pockets of highly concentrated, depressed freezing point waters. The unfrozen water in frozen soil has major implications: 1. thermal and hydrological properties, such as volumetric heat capacity (C) and thermal conductivity (k), depend on the liquid water content (θ) and therefore change over time in seasonally freezing and thawing soil (Farouki, 1981; Williams and Smith, 1989), 2. a liquid water phase system that is connected with the surface may provide a fast conduit for convective heat flow. The mobility of the water and vapor phase in frozen soil has been shown through laboratory and field experiments (*e.g.*, Cheng and Chamberlain 1988; Mackay, 1983; Parmuzina, 1978).

A basic understanding of thermodynamic and hydrological transfer mechanisms in the active layer is needed to understand seasonal fluxes of heat energy. Several studies have been carried out to understand the hydrological and energy balance of the active layer during springmelt and summer (*e.g.* Hinzmann *et al.*, 1996; Ohmura, 1982) and the heat transfer during freeze-back (Outcalt, 1990). During spring and summer, high positive net radiation provides an energy source for thawing and warming and the ground heat flux is directed downward (Rouse, 1984). Evaporation becomes the dominant heat sink in summer (Ohmura, 1982). As a result of falling air temperatures in the fall, the heat flux is directed outward, cooling the active layer from above. A downward-moving freezing front evolves, whose progress can be slowed by increases in soil water content, or by the migration of water to the freezing front. In general, a wet active layer provides a large reservoir of latent heat and slows freeze-back. Various roles for sublimation, vapor driven moisture redistribution and water convection within the soil column have been proposed (Hinkel *et al.*, 1994). It is clear that the energy requirements of thawing ground ice in the spring and energy released by freezing in the fall slow the progress of both processes. The large energy density that is associated with the phase change at 0 °C stabilizes soil temperature at this value for extended periods of time. Together with the density anomaly of water it may also lead to a constant zero temperature over quite a large depth interval. This happens at the onset of freeze-back, when the disturbance of the system by the energy flux through the surface is minimal, and is referred to as the zero-curtain effect (Harris *et al.*, 1988).

There already exist several numerical simulation models to describe coupled heat and moisture transfer processes including phase transitions (e.g. Guymon and Luthin, 1974; Hromadka *et al.*, 1981; Taylor and Luthin, 1978). Modeling the complex

processes in permafrost soils is hindered by a paucity of data in two areas: 1. material properties like effective heat capacities and effective conductivities for water and heat and 2. state variables like temperatures and phase densities of solid matrix, ice and water with a sufficient spatial and temporal resolution and extent. The first area is notorious for its difficulty, particularly noting that permafrost soils are often very coarse textured, their hydraulics consequently highly nonlinear and that they are affected by considerable deformation and transport of soil material during thaw-freeze cycles (Ray *et al.*, 1983). In contrast, state-of-the-art instrumentation makes it feasible to obtain data in the second area and allows a quantitative glimpse at the dominating processes of the thermal and hydrologic dynamics of permafrost soils.

The data presented in this work originate from two expeditions to the Siberian field site and focus on the heat and moisture transfer from spring to fall 1995. Our objective is twofold: 1. to describe hydrological and thermal processes for a complete thaw-freeze-back cycle of the active layer and 2. to calculate moisture and heat fluxes vertically in the active layer in order to check the consistency of the data with a very simple energy model.

4.3 METHODS

4.3.1 Field site

Field work was carried out during the summer of 1994 and from May to October 1995 within the framework of a cooperative Russian-German research project in the Levinson-Lessing lake catchment, Taymyr peninsula, Siberia (74° 32'N; 98° 35'E). The Levinson-Lessing lake catchment is situated approximately 80 km west of Taymyr lake in the Byrranga mountain range. The peninsula is the northernmost continental area of the circumpolar arctic and is underlain by continuous permafrost extending down to 1100 meters depth (Ershov, 1989).

The site of intensive soil and weather data collection is located midway up on a calcareous, south-west facing slope with low inclination (7°) classified as loamy skeletal carbonatic calcareous Pergelic Cryorthent (Pfeiffer *et al.*, 1996). Soil grain size characteristics of one bulk sample are given in Table 4.1. Solifluction lobes and soil stripes indicate active cryogenic processes. Vegetation covers less than 5 % and is dominated by patches of *Dryas octopetala* and *Salix spec.*

During the summer of 1994, soil pits were excavated until frozen ground was encountered. In the pit, soil moisture and temperature probes were installed horizontally in the upslope wall at 11, 23, 34, 47, 52, 65, 78 cm depths.

Unfrozen water contents in frozen and unfrozen soils were determined using time domain reflectometry (TDR). Automatic and manual TDR measurements were undertaken from at least once a week during the summer to up to 12 times a day during spring. For unfrozen soils, the dielectric approach of Roth *et al.* (1990) was used to calculate volumetric water content. This method leads to a good agreement with gravimetrically determined values (Boike and Roth, 1997). Unfrozen moisture contents in frozen soils were calculated using the empirical relationship of Smith and Tice (1988). The relative error of the measured volumetric water content is estimated as 3 %. Soil temperatures were recorded 4 to 12 times a day using PT100 temperature probes calibrated in ice water with an accuracy of 0.1°C.

Climatic data were collected within 5 meters distance of the soil microclimate station. They include air temperature and humidity, rainfall, wind speed and direction and net radiation using a Q7 net radiometer probe (Campbell Scientific). Climatic data were measured every 20 seconds and averaged over 15 and 60 minute and 24 hour intervals.

At least every 5 days, groundwater levels and ground thaw depths were determined. Groundwater levels were measured with a water level tape with 0.5 cm accuracy. Depth of unfrozen ground was measured by pounding a steel rod into the ground until frost was encountered. Saturated hydraulic conductivities (K) were determined in the field using bail tests in the mini-piezometers (Lee and Cherry, 1978). Soil grain size analysis was carried out using standard methods (Klute, 1986).

Table 4.1. Soil characteristics of site 2x.

>2 mm [% weight]	44
sand	36.2
silt	17.8
clay	2
bulk density [kg m^{-3}]	$1.69 \cdot 10^{3}$
porosity	0.34-0.42
saturated hydraulic conductivity [cm s^{-1}]	$7.9 \cdot 10^{-6}$ (at 73 cm depth) $3.0 \cdot 10^{-4}$ (at 37 cm depth)

4.3.2 Water and Energy Balance Model

To relate the measured data to each other, we describe permafrost soil, which in reality is a complex system, by a simple, zero-dimensional model. Consider a compartment of the soil which extends from the surface to depth l, where l is larger than the penetration depth of the water and energy fluxes through the soil surface. Assume that all the fluxes are perpendicular to the surface and that the system is forced at the surface by the net radiation flux j_{nr}, the vapor flux j_v, and the water flux j_r due to rainfall. Within the compartment, three phases are considered, soil matrix (s), ice (i), and unfrozen water (w). Transfer processes within the unfrozen part of the soil are assumed to be instantaneous, *e.g.*, that energy which enters through the surface is immediately available at the melting front.

A number of processes are neglected in this model. They include lateral water fluxes within the soil and on its surface and transfer of sensible heat through wind, rain and vapor. Such a simple model is useful because the energies associated with phase transitions are often much larger than those associated with convective processes and because energy transfer within the soil is fast due to the very high hydraulic conductivity that results from the coarse texture of the material and due to internal distillation that occurs when the soil is not water-saturated.

To formulate the water balance for this model, first define the areal density Θ of the water content to depth l, *i.e.*, the volume of liquid and solid water per unit area in the compartment to depth l, as

$$\Theta_l(t) := \sum_{\alpha\in\{i,w\}} \int_0^l \theta_\alpha(z,t)dz, \qquad [4.1]$$

where the sum indicates summation over the ice (i) and fluid water (w) phase. The water balance may then be formulated as

$$\Theta_l(t_1) - \Theta_l(t_0) - \int_{t_0}^{t_1} j_r(t)dt - \int_{t_0}^{t_1} j_v(t)dt = 0, \qquad [4.2]$$

where the first term is the change of total water content within the compartment during the time interval $[t_0, t_1]$, the second term is the water input due to rainfall, and the third term is the water input due to vapor flux. This last term is generally negative since it reflects evaporative loss of water.

To formulate the energy balance, define the areal density E_l of the soil's thermal energy to depth l with respect to the reference state where the soil is at temperature T_0 = 0°C and contains neither water nor ice. Hence

$$E_l(t) = \sum_{\alpha\in\{s,w,i\}} c_\alpha \rho_\alpha \int_0^l \theta_\alpha(z,t)T(z,t)dz \quad - L_{sf}\rho_i \int_0^l \theta_i(z,t)dz, \qquad [4.3]$$

where the first term accounts for the thermal energy stored as sensible heat, with the sum indicating summation over all phases, and the second term represents the latent heat of the ice. Energies associated with capillarity are not considered since their change is negligible compared to the other energy components. Notice that for the choice T_0 = 0°C the temperature difference $T(z,t)$ - T_0 equals $T(z,t)$. Since we assume that the time required for thermal equilibration over depth l is small on the temporal scale of interest, the energy balance may be written as

$$E_l(t_1) - E_l(t_0) - \int_{t_0}^{t_1} j_{nr}(t)dt - L_{fv}\rho_w \int_{t_0}^{t_1} j_v(t)dt = 0, \qquad [4.4]$$

With the exception of the vapor flux j_v, all the components of [4.2] and [4.4] can be estimated from the measured data. Hence j_v may be calculated from either the water balance [4.2] or from the energy balance [4.4] yielding the estimates $\hat{j}_v^W$ and $\hat{j}_v^E$, respectively. These two estimates for j_v generally differ from each other, most importantly because a number of processes have been neglected in formulating the model. Further sources of discrepancy are the limited spatial and temporal resolution of the data and the measurement error. To quantify the deviation of the actual dynamics from that described by the model, we define the energy residual

$$R^E(t_1,t_0) := \frac{L_{fv}\rho_w}{t_1-t_0}\int_{t_0}^{t_1}\left[\hat{j}_v^E(t)-\hat{j}_v^W(t)\right]dt$$
$$= \frac{1}{t_1-t_0}\left[E_l(t_1)-E_l(t_0)-\int_{t_0}^{t_1}j_{nr}(t)dt\right]-\frac{L_{fv}\rho_w}{t_1-t_0}\left[\Theta_l(t_1)-\Theta_l(t_0)-\int_{t_0}^{t_1}j_r(t)dt\right] \quad [4.5]$$

It is sometimes convenient to express the residual R^E as an equivalent water loss rate. We thus define the evaporation residual

$$R^W(t_1,t_0) := R^E(t_1,t_0)/\left[L_{fv}\rho_w\right]. \quad [4.6]$$

All the terms in [4.5] can be estimated from the measured data by approximating the integrals using the trapezoid rule. This leads for [4.1] to

$$\Theta_l(t_k) \approx \tfrac{1}{2}\sum_{\alpha\in\{i,w\}}\sum_{j=1}^{N}\left[\theta_\alpha^{j+1,k}+\theta_\alpha^{j,k}\right]\left[z_{j+1}-z_j\right] \quad [4.7]$$

and in analogy for the other integrals. Notice that $R^E(t_1, t_0) = 0$ if the model correctly represents all the processes and if the measurements are sufficiently resolved and exact. Recalling that j_v is generally negative, periods with $R^E(t_1, t_0) > 0$ indicate that evaporating the amount of water calculated from the water balance requires more energy than appears available based on the energy balance. This may result from surface runoff which causes actual infiltration to be smaller than measured rainfall with the difference being interpreted by the model as additional evaporation. The reverse is signaled by $R^E(t_1, t_0) < 0$, *i.e.*, more energy available than required for evaporation. This is typically caused by convective cooling (sensible heat transfer) of the surface.

Data on phase densities below 78 cm were estimated. Porosities were taken as averages from lower layers. This can be a critical point for the determination of ice content, since the lower active layer zone is often ice enriched. Values used for material properties and temperature-dependent properties are given in Table 4.2.

Table 4.2. Material properties (values for T = 0°C).

Specific Heat [kJ kg^{-1} K^{-1}]	
c_s	0.733
c_w	4.22
c_i	2.11
Latent Heat [MJ kg^{-1}]	
L_{sf}	0.333
L_{fv}	2.45

4.4 RESULTS AND DISCUSSION

4.4.1 Weather, thaw depths and groundwater

The weather record for the 1995 season is displayed in Figure 4.1. The average daily temperature rose above 0 °C on June 4 and initiated snowmelt on June 5. After September 10, average temperatures stayed continuously below 0 ° C. In between, daily temperatures increased and reached a maximum value of 19.6 °C on August 20. The daily average net radiation reaches its maximum in June and becomes negative after mid-September. The ground thaws rapidly until mid-July after which thaw rates are somewhat slower (Figure 4.1). Maximum thaw depths greater than one meter are reached at the beginning of September when freeze-back had already started from the surface and the upper 7 cm of the ground were frozen. The ground freezes back from both above and below, which is typical for a cold soil. A similar, but schematic freeze-back mechanism was shown by Mackay (1982) for the western arctic coast, Canada.

Figure 4.1 also demonstrates the (methodical) limitations for determining the boundary between thawed and frozen ground. Ground thaw depths determined using the probe method deviate considerably from the thaw depths determined by soil temperatures during the period when the active layer is dry (Figure 4.1). This may be explained by the greater ease of penetration of the frost probe when the active layer is saturated. During the unsaturated period we therefore used ground temperatures at 0°C as the limit of frozen ground. During fall freeze-back, permafrost probe measurements were limited to 20 cm depth. Therefore the freezing front was extended with TDR measurements choosing an unfrozen volumetric water content of 0.22 as the limit between frozen and unfrozen ground.

With the onset of snowmelt, the shallow unfrozen ground is quickly saturated to the surface; overland flow occurred due to the limited storage capacity of the ground. After snowmelt stopped, the groundwater level dropped rapidly to the frost table. Rainfall began to saturate the active layer in mid-July and kept the groundwater level stable at 15 cm below surface. Over the entire summer a total of 169 mm rain fell with a maximum intensity of 32 mm/day on July 17. The active layer is saturated up to about 8 cm below the surface before freeze-back starts (Figure 4.1).

4.4.2 Seasonal soil moisture and temperature from spring to fall

Figure 4.2 shows the seasonal trend of moisture and soil temperatures at depths from 11 to 65 cm. The minimum soil temperature recorded was -12.2 °C at 78 cm in May, the maximum of 12 °C degrees at 11 cm on June 11. Soil temperatures show strong variations near the surface (following changes in air temperature) and less variation with depth. The fall freeze-back progresses slowly and the zero curtain effect is much more pronounced compared to spring thaw.

Volumetric water content rises sharply at all depths once the spring phase change has been completed. After a drop in water content following snowmelt, the active layer water content stays at a stable level for the entire summer, supplied by rather small but frequent precipitation events. Similar seasonal changes in water content and temperature were presented by Hinzman *et al.* (1991) for the active layer of the Alaskan Arctic. Volumetric water contents were generally 0.15 higher in the mineral soils due to the higher porosities.

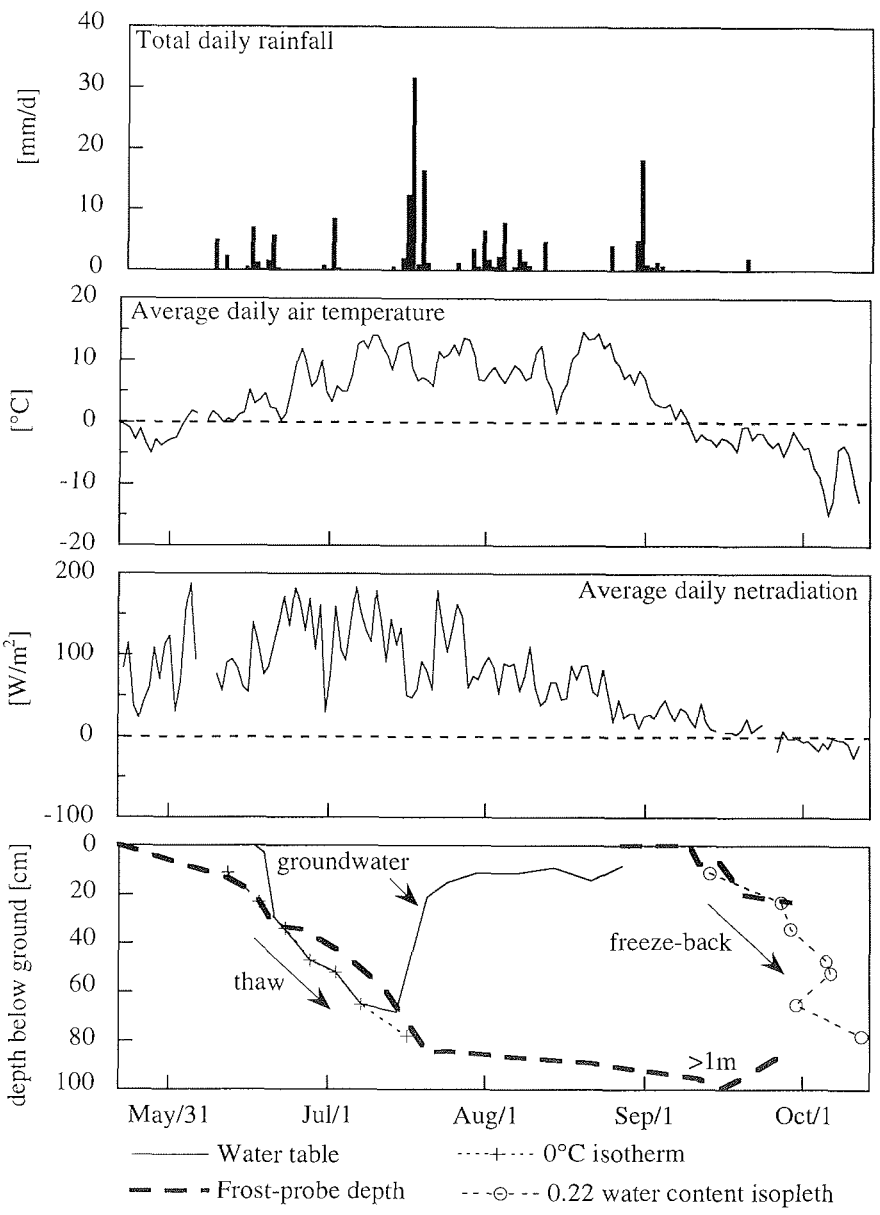

Figure 4.1. Weather data and frost depths for the study site. Thaw depths are measured with a frost probe and with the thermistor-determined 0 °C isotherm. Freeze-back depths are determined with the frost probe and with the TDR-determined 0.22 water content isopleth.

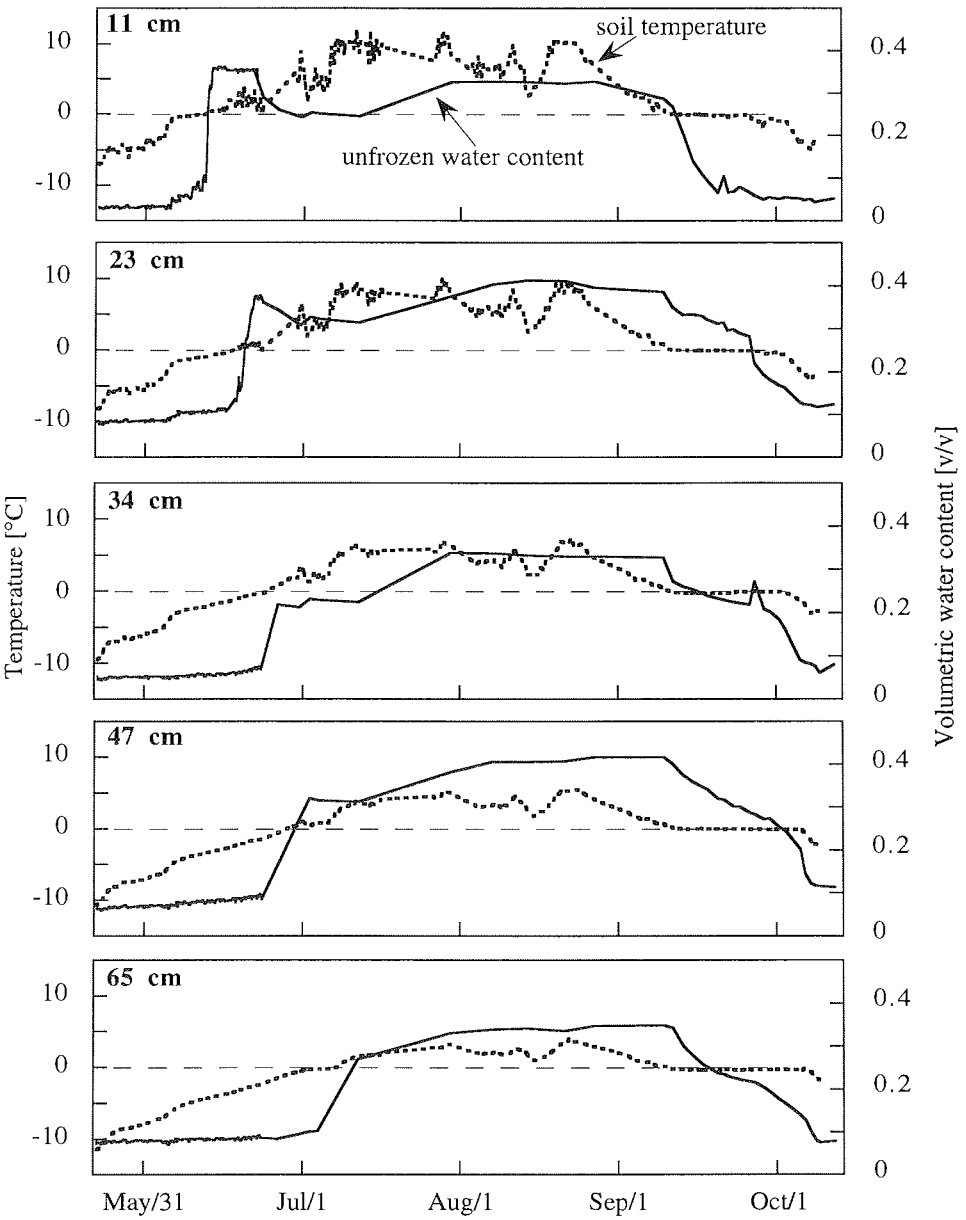

Figure 4.2. Seasonal variations in soil temperature and volumetric water content at 5 depths. The dashed line indicates 0 °C.

4.4.3 Spring

Figure 4.3 shows unfrozen water in frozen ground and soil temperatures at depths from May 22 to June 24. Volumetric unfrozen water content in the frozen soils ranges from 0.03 at 11 cm to 0.09 in the lower layers even at temperatures down to -12 °C. This is the same range as given by Nersesova and Tsytovich (1963) for a loam to a sandy loam.

Unfrozen moisture content increases in the frozen soil with increasing soil temperatures at all depths, more pronounced after the onset of the snowmelt when soil temperatures increase rapidly (Figure 4.3). For the upper soil at 11 cm depth, the additional increase in unfrozen water content from 0.03 to 0.05 on June 5 is due to infiltration of snowmelt water (Figure 4.3). On June 8, infiltrating rain increases the unfrozen water content from 0.05 up to 0.07 in the frozen ground. The rapid increase of soil temperatures with the onset of snowmelt was also observed by Marsh and Woo (1993). They did not observe an increase in unfrozen water content, however.

The thawing front, as given by the 0 °C isotherm, gradually penetrates to greater depths (Figures 4.2 and 4.4) and the temperature gradient indicates that heat conduction is an important process.

4.4.4 Fall

The fall dynamic is in stark contrast to the spring dynamic. During spring, temperatures increased gradually as the thawing front progressed. In fall, when air temperatures decrease in September, soil temperature decreases quite uniformly throughout the unfrozen soil profile and freezing sets in abruptly after the 0 °C isotherm has been passed. While the onset of freezing, as given by the 0 °C isotherm, is rather uniform, its progress is not as indicated by the contorted form of the isotherms for temperatures between 0 and -1 °C (Figure 4.4). It apparently depends on the heterogeneity of the soil. This may be understood as a result of the complex interplay between the thermal and hydraulic conductivities which both decrease with decreasing unfrozen water content and the larger amount of latent heat that is released in regions with higher water content. Regions with an initially lower water content may thus be expected to initially freeze somewhat faster because the release of latent heat is smaller. Figure 4.4 indicates that in the temperature range between 0 and -1 °C, transfer of heat to the soil surface proceeds mainly through convective processes since temperature gradients are small and in opposite directions.

Notice that the dynamics in fall, and to a lesser degree also in spring, is consistent with the assumption that the unfrozen soil is well-mixed, *i.e.*, transfer processes are instantaneous at the scale of interest.

Air temperatures fall sharply down to -15 °C on October 8; soil temperatures begin to decrease (Figure 4.2) and unfrozen moisture content remains stable indicating that phase change is practically complete. This is further corroborated by the isotherms shown in Figure 4.4, which show conduction of heat has again become an important process of energy transfer.

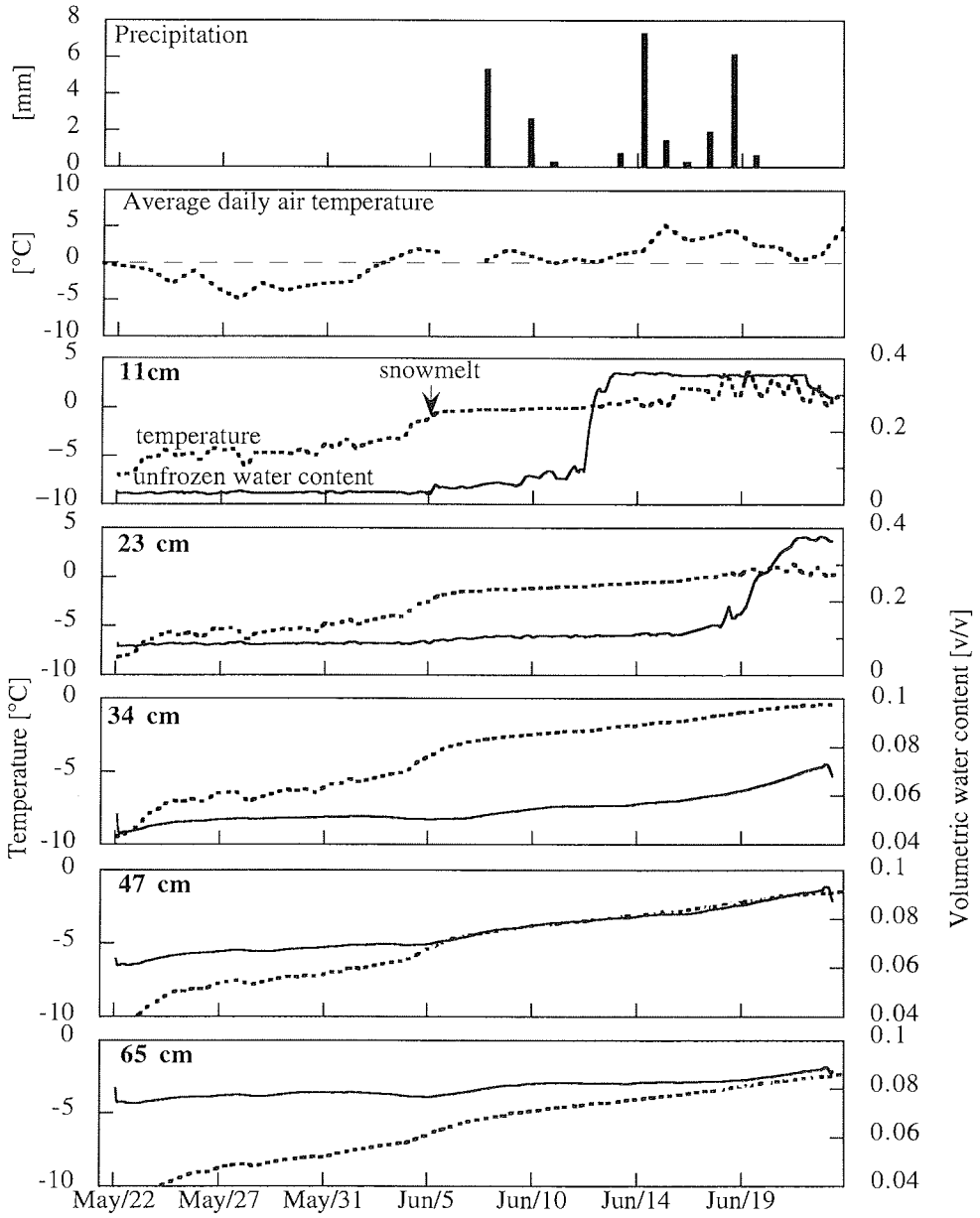

Figure 4.3. Weather data, soil temperature and volumetric water content at 5 depths from May 22 until June 24. Water content data for the lower 3 depths have a higher resolution and have been smoothed to remove noise, resulting in the aberrant values at the ends of the datum series. The start of snowmelt is indicated (June 5). Notice different vertical scales for last three frames.

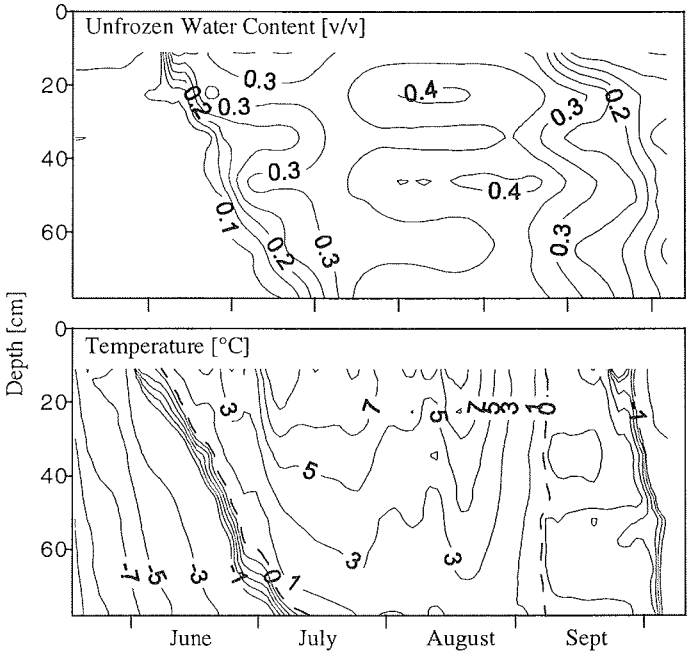

Figure 4.4. Soil temperature and volumetric water content variation within the soil profile over time. The contour interval for the unfrozen water content is 0.05 [v/v] and 2 °C for temperature. Additional contour lines at intervals of 0.2 °C have been added from 0 to -1 °C.

4.4.5 Dynamics associated with soil heterogeneity

Figure 4.4 displays the results of the seasonal unfrozen water content and soil temperatures over time and depth. Zones of higher volumetric water content within the thawed active layer during the summer suggest a heterogeneous soil system with varying porosities. The heterogeneous structure of the soil was also observed directly and its influence on water flow was visualized by a dye tracer and is possibly caused by cryorturbation and solifluction. This complex soil system would therefore imply a spatially variable infiltration, *e.g.*, during snowmelt or rain events. A large spatial variability in soil infiltration was observed by Marsh and Woo (1993) at three sites near Resolute, N.W.T., Canada, which they attributed to the occurrence of flow fingers in the snowpack.

The seasonal soil temperatures plotted against depth in Figure 4.4 demonstrate that the phase change in spring is different from the fall's. While in spring the soil warming and phase change gradually penetrate the soil, the fall soil profile undergoes a drastic temperature drop to 0°C over the entire profile. The freezing of the active layer between 0 and -0.8 °C is dependent on the soil's spatially variable phase density. It is difficult, therefore, to determine the progression of the freezing front without measuring soil texture and initial water content. Our case also implies that we have a freezing zone, rather than a freezing front.

During late summer when the ground is saturated, soil temperatures down to 78 cm depth respond to cycles of average daily air temperatures, *e.g.* between August 12 and 20 (Figure 4.2). Within a short time period, the temperature first drops and then increases as shown by 'temperature curtains' moving up and down the soil profile. This phenomenon may be explained by convection cells which facilitate a rapid transfer of heat within the soil profile. The driving force of such cells is the density anomaly of water which below 4 °C makes cooler water less dense than warmer water. Dense warm water would thus sink and be replaced by rising less dense cool water. In the process, the falling water would cool while the raising water would warm thereby perpetuating the cell as long as the corresponding temperature reservoirs are available. This convection theory has been postulated for water saturated soils by Ray *et al.* (1983) and is, in their opinion, a mechanism for the formation of frost structures such as sorted circles and polygons. We recognize, however, that while convection cells would explain our data, the data constitute no direct evidence for the existence of such cells.

4.4.6 Thermal and hydrological dynamics using the energy balance model

The residuals R^E and R^W of the energy balance for the entire season are shown in Figure 4.5. Notice that R^E and R^W, as defined by [4.5] and [4.6] respectively, represent the same quantity but express it in different units. The residual is positive when the net energy flux into the soil compartment during a time interval is smaller than the associated change of total energy. Correspondingly, a negative residual indicates an energy flux that is too large. Such deviations are mainly caused by components of the water balance that have not been accounted for in the model.

An example is runoff during heavy rainfall which leads to a positive residual because measured rainfall is assumed to infiltrate and to increase the total water content of the soil compartment. If the measurements do not reflect the corresponding increase of water content, the evaporation flux calculated from [4.2] is too large, hence the total

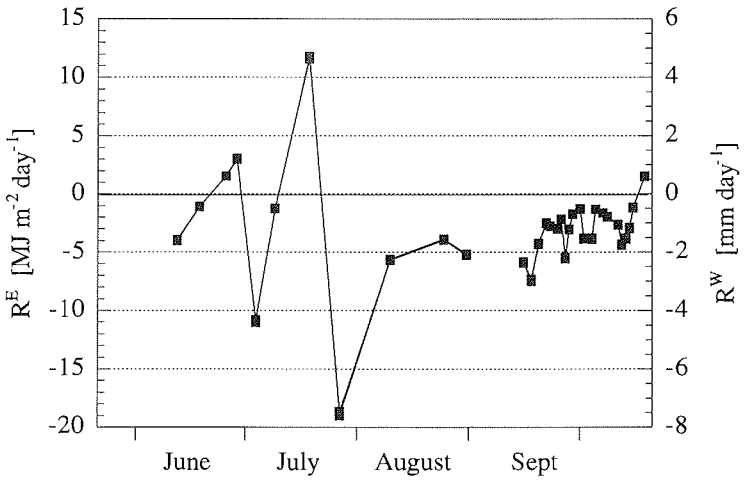

Figure 4.5. The seasonal variation in the residual, R^E, and the evaporative residual, R^W.

energy flux obtained from [4.4] too small and consequently the residual [4.5] positive. On average, the residual is negative which may be explained as resulting from net flux into the compartment with lateral flow, and transfer of sensible heat due to convection. Studies by Ohmura (1982) on Axel Heiberg Island, Canadian High Arctic and by Weller and Holmgren (1974) at Barrow, Alaska have shown that sensible heat transfer can consume up to 3.6 MJ m^{-2} day^{-1} and 5 MJ m^{-2} day^{-1}, respectively. However, the high minimum and maximum residuals on July 17 and 25 cannot be explained through the omission of sensible heat transfer. On July 17, 32 mm of warm rain (air temperature was at 13 °C) added between 0.47 and 1.3 MJ m^{-2} day^{-1} to the soil when taking soil temperatures at 11 and 78 cm as maximum and minimum values of temperature difference. Although it has been postulated that intense summer rains can deepen the dry active layer by transport of sensible heat (Hinkel *et al.*, 1993), our data suggest that this would have only a minor effect relative to the other energy components. This energy source is thus too small to explain the large maximum residual. As a response to the rain event, widespread overland flow was observed on the slope which is not included in our water balance. The following minimum residual could be interpreted as a large amount of energy used to evaporate water from oversaturated/overland flow surfaces.

During the fall, large amounts of energy must be removed from the refreezing soil due to the release of latent heat of fusion. Since the temperature is colder at the surface, the temperature gradient would promote moisture transfer upwards, either as vapor or liquid thereby leading to rapid transfer of energy from the region of release, the freezing front, to the soil surface. The non-conductive transfer of heat during fall may also be deduced from Figure 4.4. It shows that the temperature gradient, the driving force of conductive heat transfer, is considerably smaller in September and October than from May to July although comparable amounts of heat are transferred. Hinkel and Outcalt (1994) also suggest that non-conductive processes such as vapor transport, volatilization, or sublimation are important during and after the freeze back in Alaska.

The latent heat released in the soil compartment is eventually lost to the atmosphere, either directly by evaporation and sublimation from the soil surface or, at a slower rate, through a snowcover. Our site had only a very thin and incomplete snowcover until October 8, allowing the direct transfer of heat to the atmosphere. Based on the simple energy balance model which neglects transfer of sensible heat, we find a total loss of energy between September 9 and October 13 which corresponds to 33 mm of sublimated water. While this amount appears quite large, it is in agreement with the findings of Santeford (1978) who measured a loss of 30 mm at the end of the winter from a profile near Fairbanks, Alaska, using 'vapor traps'. In contrast, Smith and Burn's (1987) and Woo's (1982) results from vapor trap experiments in the Yukon Territories and at Resolute, N.W.T., are an order of magnitude lower. Notice, however, that in these studies the water loss was measured over different time intervals: Smith and Burns's in time periods of September, November, March, April and Woo's continuously from August to May. These results are not directly comparable to ours, however. Our data also indicate that after freeze-back, water loss is much smaller than during the freeze-back, when large amounts of latent heat have to be dissipated from the soil surface. Due to a lack of data for late fall, we cannot quantify this flux, however.

The last residual on October 13 is positive, coinciding with rapid cooling of the active layer. The snowcover was still thin but complete during this time. At this time, air temperatures dropped and the phase change was more or less complete.

The average of all residuals from June to October is -4.5 MJ m^{-2} day^{-1} (-1.7 mm evaporation), *i.e.*, there was more energy available in the soil compartment than was dissipated from the soil surface. This value lies in range of sensible heat transferred by convection as given by Weller and Holmgren (1974) and Ohmura (1982). This implies that the energy fluxes in the active layer are approximately balanced for this period. Since we did not estimate the energy flux due to sensible heat and do not have data to complement the energy balance for the winter, we cannot estimate the annual energy balance. This would be very useful for estimating the long-term net heat flux into the underlying permafrost which would help in interpreting geothermal climate records in the permafrost (Lachenbruch *et al.*, 1988).

4.4.7 Percentage of total energy

Figure 4.6 gives an overview on the distribution of net radiation on evaporation, soil warming and soil thawing as calculated from the energy balance [4.4] with evaporation obtained as the residual term. This calculation does not include sensible heat flux and consequently the evaporation is greatly overestimated. Considering that approximately 38 % of the total energy is used by sensible heat flux on the Arctic tundra during the snow free period (Ohmura, 1982), the average evaporation lies in the range of approximately 25 to 50 % of the total energy. These values are consistent with results from Ohmura (1982) and Rouse *et al.* (1977) who determined evaporation fluxes from Arctic tundra surfaces by independent methods (aerodynamic profile or Bowen ratio).

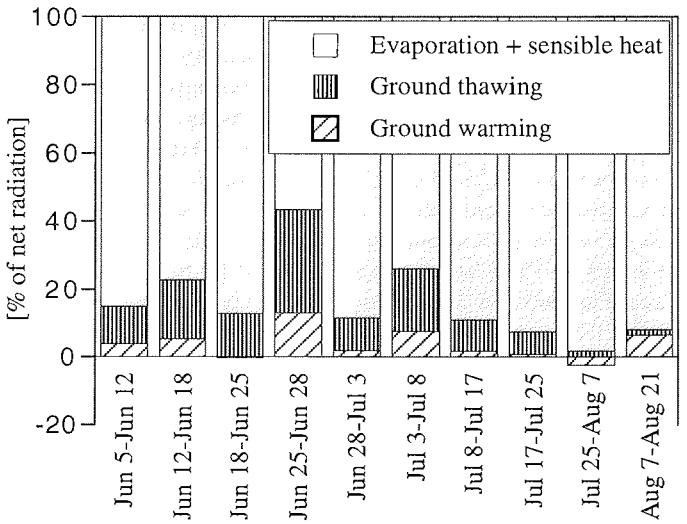

Figure 4.6. Relative importance of the energy balance components, expressed as percentage of the net radiation from June 5 until August 21. Note that the bars do not represent equal spans of time.

The second largest energy sink is the thawing of the active layer which can consume more than 20 % of the total available energy (Figure 4.6). Ohmura (1982) calculates that a maximum of 17 % of the total net radiation is conducted in the ground in June and July using heat flux plates. His estimate is that half of this energy is used for the increase in soil temperature and the other half for thawing of the active layer. Our data indicate that between 70 to 100 % of the heat transferred into the ground during this period is consumed for thawing. This apparent discrepancy resolves by noting that heat flux plates do measure fluxes of sensible, but not of latent heat. This supports the expectation that convective processes are also important during the spring thaw and not only during fall freeze-back. This was already pointed out by Rouse (1984) who found that the latent heat term represents a large flux component which is often underestimated with soil heat flow plates. This term is largest when the active layer is driest (Figure 4.1). Energy loss by evaporation is then reduced by the soil's strongly decreased hydraulic conductivity.

4.4.8 Conclusions

Temporally and spatially resolved measurements of liquid soil water content and soil temperature together with time series of freezing depth, rainfall, and net radiation allowed determination of the hydrological and thermal dynamics of a thaw-freeze cycle at a permafrost site. It was found that the dominating components in this system are the energy input by net radiation and the latent heat associated with melting and evaporation. Particularly during summer and during autumn freeze-back, convective processes appeared to be responsible for quite rapid energy transfers within the thawed part of the soil. This characteristic of the system facilitated the application of a simple water and energy balance model which allows a check of the consistency of the data and, within the accuracy of the model, quantification of the individual heat and water flux components as well as assessment of the impact of neglected processes.

From the TDR measurements we deduce that liquid water was present well below the freezing point, at least down to -12 °C, and that the fraction of liquid water in frozen soil increases with temperature. A continuous liquid water phase with a significant volume fraction may dramatically increase the transfer of heat through frozen soil by allowing convection. It was furthermore found that freezing depth measurements by pounding a steel rod into the ground agrees with values calculated from temperature and TDR measurements only for saturated conditions. For unsaturated soils, the steel rod underestimates the freezing depth. Future research should consider the following: (i) a more accurate description of the local dynamics would demand the direct non-destructive measurement of the ice content, *e.g.*, through the combination of TDR and twin-gamma probe, and the measurement of the vapor flux through the soil surface. (ii) a very simple model already leads to a good agreement between the major components of the energy and water budget of this permafrost site. It may thus be feasible to invert the approach used in this work and to use independently estimated vapor fluxes, *e.g.* by the method of Priestley and Taylor (1972), together with measurements of net radiation to predict values for the depth of the thawing front. While the first point aims at an improved understanding of the physics of permafrost soils, the second facilitates flux estimation at a larger scale and could be based on data from remote sensing.

Chapter 5

Climatological and hydrological influences on stable hydrogen and oxygen isotopes of active layer waters, Levinson-Lessing Lake area, Taymyr Peninsula

5.1 ABSTRACT

Stable isotope data ($\delta^{18}O$, δD) of precipitation and active layer waters were collected in the Levinson-Lessing Lake catchment, Taymyr, Siberia during 1994 and 1995. They are used here in conjunction with hydrological and microclimate data to provide information on water forming processes in the active layer. Summer precipitation defines a local meteoric water line different from the global meteoric water line, suggesting that the source of summer precipitation has been exposed to evaporative isotopic enrichment. Annual precipitation levels and the stable isotope composition of active layer waters from the saturated and unsaturated zone indicate that these waters are mostly fed by summer precipitation. Isotopic variabilities between sites in the catchment indicate differences in microclimatic and hydrologic characteristics between sites. Furthermore, the isotope ratios have been successfully applied to discern different sources of active layer waters (snow and ground ice melt, rain water) within slopes underlining the usefulness of isotopes for small scale interpretation of source waters.

5.2 INTRODUCTION

The previous chapters have examined the physical dynamics of the active layer (heat and water transfer) from spring to fall. In order to accurately assess the hydrological character of the active layer, information on water pathways and formation is required. The abundance of the heavy stable isotopes ^{18}O and D in water makes them suitable natural hydrological tracers (under the assumption that they behave conservatively) and have been used in a variety of studies on arctic hydrological processes. Bursey *et al.* (1991) and Gibson *et al.* (1993) calculated water balance components in two northern lake catchments in Canada using stable isotopes. Cooper *et al.* (1993) applied them in the Imnavait watershed in Alaska to trace the contribution of snowmelt and rain to streamflow runoff.

Furthermore, any significant climatic variation results in changes of the ^{18}O and D content of meteoric waters. Paleowaters therefore reflect paleoenvironmental conditions. Within the multidisciplinary project on 'Late Quaternary environmental history of Central Siberia' it was important to establish the ^{18}O and D content of recent waters as reference for the interpretation of paleowaters. This is of special interest in this region where paleo data archives such as ice cores are absent. First data on the stable isotope and geochemical composition of ground ice in the Labaz lake area

(Figure 5.1) suggest a more continental climate during the Middle-Weichselian (Wisconsin) compared to the Holocene (Melles *et al.*, 1996). In East-Siberia, $\delta^{18}O$ analysis of ground ice and ice wedges has been used to identify the transition zone between the Pleistocene and Holocene epoch (Vaikmäe, 1991).

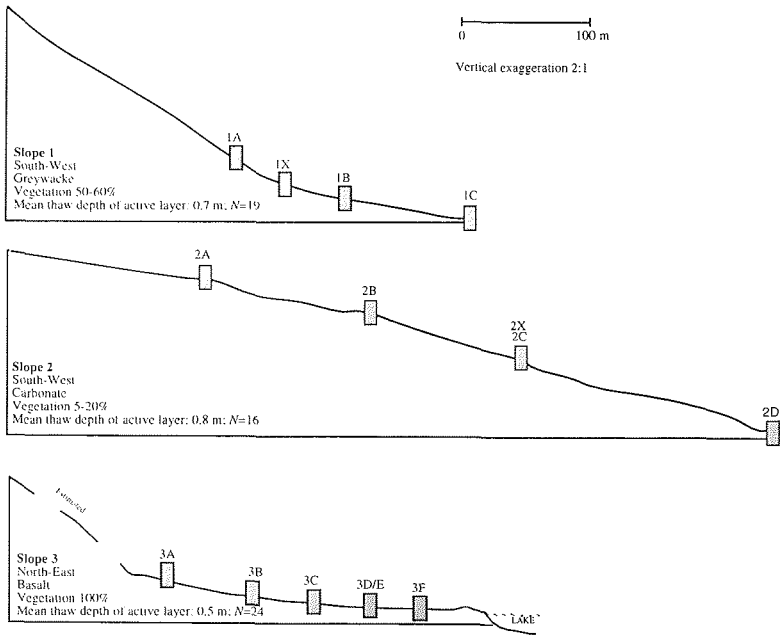

Figure 5.1 Cross section of the three installed transects in the Levinson-Lessing lake catchment.

For the correct understanding of permafrost waters, information on how permafrost waters are formed is necessary. This includes a survey of permafrost waters under current climate conditions and a study of processes that affect the isotopic composition of permafrost waters which will be discussed in 5.4.2. In the permafrost landscape, hydrological inputs (snow and ground ice melt, rain) and site characteristics influence the isotopic composition of groundwater in the active layer. Site characteristics that influence the isotopic composition are position and aspect, ice content, vegetation, snow coverage and lithology. A detailed study on $\delta^{18}O$ in active layer groundwaters in differing geomorphological and lithological locations was undertaken by Mikhalev (1989) in the Kolyma Lowland. He concluded that the main source of active layer groundwater is the late summer and fall precipitation which

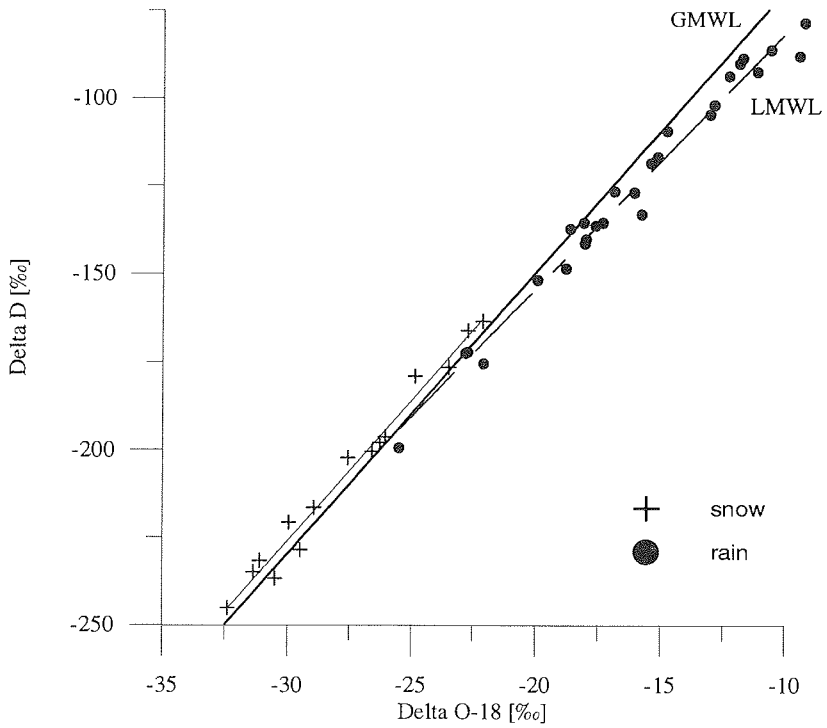

Figure 5.2. Plot of $\delta^{18}O$ versus δD of precipitation samples collected in 1994 and 1995. The LMWL (determined from summer rain samples) is presented relative to the GMWL.

would be reflected in the isotopic composition of active layer ground ice.

This study examines the spatial and temporal variation of stable isotopes in permafrost affected waters in the Levinson-Lake catchment collected during 1994 and 1995. The following questions were raised: 1. What are the recent, seasonal isotopic variations in the local precipitation? 2. What are the sources of active layer waters and is there a seasonal change in their isotopic composition? 3. Based on our current knowledge, is it useful to apply stable isotopes for arctic hydrological processes and paleoenvironmental interpretation in this permafrost setting?

5.3 METHODS

Levinson-Lessing lake is situated in the Byrranga mountain range approximately 50 km west of Taymyr lake (Figure 1.1). A varying topography (slopes and flat areas) and arctic tundra vegetation enable a study of transport processes in the active layer under different geological and geomorphological conditions. Three transects with a sum of 16 sites were instrumented during the summer 1994 in the Levinson-Lessing lake catchment (Figure 3.1). These slopes differ in: slope aspect and inclination, soil parent material, vegetation and thaw depth of the active layer (Figure 5.1). At each site, triple wire time domain reflectometry (TDR) probes, PT 100 temperature probes, wells, piezometers and suction lysimeters were installed. Figure A.1 gives a schematic

overview of the technique and installation depths. After installation, the following parameters were measured daily from July to the end of August 1994: volumetric moisture content and bulk electrical conductivity using TDR, water level in wells and piezometers, electrical conductivity and pH of ground and soil waters. Depth of thaw of the active layer was recorded at least once a week. Ground water samples were collected from wells and piezometers using PVC tubing and plastic syringes and from the vadose zone using suction lysimeters. Precipitation was sampled from each event. At least two samples (each 30 ml) were taken from each type of water: one was analyzed for pH and electrical conductivity in the field; the second one was kept cool for stable isotope and radionuclide analysis. Laboratory analysis of water samples was undertaken using the Epstein-Mayeda technique for oxygen isotopes (Epstein and Mayeda, 1953) with an analytical error of 0.2 ‰ and a new water-H_2 gas equilibration technique for hydrogen isotopes with an error of 2 ‰. The stable isotope ratios $r_H = D/^1H$ (δD) and $r_O = {}^{18}O/{}^{16}O$ ($\delta^{18}O$) are calculated relative to Vienna Standard Mean Ocean Water (V-SMOW) in permil:

$$\delta = \frac{r_{sample} - r_{V-SMOW}}{r_{V-SMOW}} \times 10^3 \qquad [5.1]$$

Positive $\delta^{18}O$ and δD values therefore indicate an enrichment of the heavy isotopes ^{18}O and D compared to the SMOW, negative values a depletion.

5.4 RESULTS AND DISCUSSION

5.4.1 Sources of precipitation

The ocean is the major source for atmospheric water vapour. By evaporative processes this vapour is depleted in heavy isotopes relative to the water which remains in the ocean. With increasing latitudinal cooling, progressive condensation of water forming precipitation removes the heavy isotopes from the vapour in the air mass. As a result, precipitation is most depleted in high latitudes and depending on the temperature it can reach values as low as -50 ‰ $\delta^{18}O$ (Dansgaard, 1964).

Craig (1961) defined on a large number of precipitation samples from all latitudes the following linear relationship between $\delta^{18}O$ and δD, which is called the Global Meteoric Water Line (GMWL):

$$\delta D = (8.0 \pm 0.1)\, \delta^{18}O + (10 \pm 10) \qquad [5.2]$$

However, any region will define a local water line, depending on the origin of vapour which depends on local climatological factors such as latitude, altitude, distance from coast and season (Gat,1980). The Deuterium excess *d* defined by Dansgaard (1964)

$$d = \delta D - 8\, \delta^{18}O \qquad [5.3]$$

is useful to identify sources of precipitation on a global scale. In particular, *d* is mainly a function of the mean relative humidity of the air mass, where water is evaporating (Merlivat and Jouzel, 1979). A high *d*-value is associated with conditions of low

humidity and a low *d* value with a high humidity (assuming subsequent evaporation is negligible).

Figure 5.2 depicts the relationship between $\delta^{18}O$ and δD of meteoric water samples collected in the Levinson-Lessing lake catchment in 1994 and 1995. Values for $\delta^{18}O$ range between -32.4 and -9.1 ‰, δD values between -245.3 and -78.6 ‰ with an average of $\delta^{18}O$ = -20.1 ‰ and δD=-154.5 ‰ (N= 42). The average values agree well with the theoretical predicted values using the equations by Dansgaard (1964). Given a mean annual air temperature of -10 to -15 °C for the Taymyr peninsula (Ershov,1989), this theoretical equation produces $\delta^{18}O$ values between -20.6 to -24.1 ‰ and δD values between -156 to -184 ‰.

The seasonal variations of precipitation correspond to variations of air temperature, *i.e.* the winter and fall snow is depleted in heavy isotopes compared to summer precipitation (Figure 5.2). Using the least squares fit, winter snow samples define a linear relationship of

$$\delta D = (8.02 \pm 0.31)\,\delta^{18}O + (14.2 \pm 8.7) \qquad [5.4]$$

$$N=15,\ r^2=0.98$$

where N is the number of data points and r^2 is the correlation coefficient. The slope and intercept are within the uncertainties of the GMWL therefore suggesting the oceans as the source of precipitation. Since the Arctic ocean is ice covered until at least early summer, the vapour must originate from the Atlantic ocean which is consistent with observed cyclone trajectories during the winter months (Murray and Simmonds, 1995). Summer rain, however, deviates from the GMWL and scatters around a local meteoric water line (LMWL) defined as:

$$\delta D = (7.23 \pm 0.21)\,\delta^{18}O - (9.9 \pm 3.5) \qquad [5.5]$$

$$N=27,\ r^2=0.98.$$

The scattering of precipitation data along the LMWL (Figure 5.2) reflects seasonal differences in air mass history that depend on temperature during condensation of vapour. The smaller slope compared to the GMWL and the intercept of -9.9 suggest a different origin of summer air masses compared to the winter snow. The slope suggests that the summer air masses carry some moisture from terrestrial surface waters which are already enriched in heavy isotopes by evaporation. Although the average monthly air temperatures are low and relative humidities are high (Table 5.1), evaporation is enhanced due to the water surplus in the typical tundra setting (bogs and open water bodies) and the continuous 24 hour input of netradiation during the summer months (Ohmura, 1982). Evaporation is a major loss in the water and energy budget at these (Boike *et al.*, 1997) and other tundra sites in the Canadian High Arctic (Woo and Marsh, 1990) and Alaska (Kane *et al.*, 1990). However, the isotopic fractionation of water is limited by the high relative humidity during vapourization; the slope of fractionation decreases with increasing relative humidity of the air and reaches a constant level after about 25 % of the water is lost by evaporation (IAEA, 1983). This

would explain why, despite large evaporative loss, the slope of the LMWL is not smaller than 7.2.

The importance of the relative air humidity during vapour formation is further given by seasonal changes of *d*-values (Figure 5.3). For winter snow samples, *d*-values are between 12 to 18 ‰ and they fall into the range of the GMWL. From June to September, *d*-values decrease as a result of increasing relative air humidities from 79 to 85 % (Table 5.1).

Table 5.1. Summary of weather conditions during 1995 in the Levinson-Lessing lake area (data from climate station at site 2x; for location see Figure 3.1).

Date 1995	Air temp. [°C]	Max. air temp. [°C]	Min. air temp. [°C]	Relative humidity [%]	Total rainfall [mm]
May (23-31)	-2.6	-2.8	-10.2	84	0
June (1-6, 15-30)	3.0	15.9	-5.0	79	25
July (1-31)	9.9	18.3	0.6	79	86
August (1-31)	8.9	19.6	0	82	52
September (1-14; 27-30)	0	10.1	-7.6	85	6

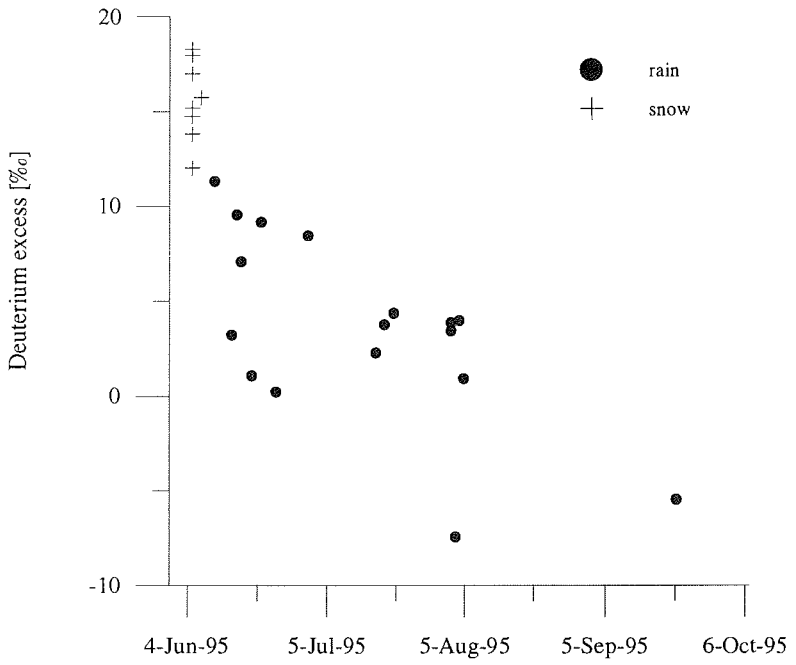

Figure 5.3. Seasonal development *d*-values of precipitation samples collected in 1995.

Without knowledge of regional air mass movements it is difficult to assess the source of evaporative summer precipitation. For example, isotopically heavier vapour masses from continental areas could mix with isotopically lighter vapour masses originating from the oceans. The local climatic conditions at Levinson-Lessing lake can vary greatly and do not necessary reflect the regional climatic pattern. With establishment of the LMWL, however, permafrost waters in this catchment can be interpreted with respect to recent meteoric water input.

5.4.2 Survey of waters in the Levinson-Lessing lake catchment

Processes affecting the stable isotope composition in the active layer

The isotopic composition of ice in the active layer (texture ground ice) can preserve paleoclimatic information (Vaikmäe, 1991). This information can be interpreted properly provided the origin of the active layer water and processes of ice formation are understood. $\delta^{18}O$ and δD in the active layer are influenced by:

1. fractionation during phase change (freezing, thawing, condensation and evaporation)
2. mixing of (ground) waters from different sources
3. migration of water (vapour)in the freezing or frozen ground

Possible sources of water for the active layer are meltwaters from snow, ground ice or rain water. Ground ice is stored in the active layer and formed from previous' years active layer waters. It should reflect the isotopic composition of the active layer water assuming that the isotopic fractionation during freezing is negligible. The magnitude of fractionation in the active layer depends on the freezing rate, but generally does not exceed 2 to 3 ‰ for $\delta^{18}O$ relative to the water (Michel, 1982) and is therefore of minor importance. Small scale changes in isotope composition can also be the result of migration of moisture in frozen or freezing ground. In a freezing soil, heavy isotopes migrate towards the freezing front while the unfrozen soil becomes isotopically depleted (Michel, 1982).

The two different types of water in the active layer above the frozen ground are groundwater (also called suprapermafrost groundwater or phreatic water) and water in the unsaturated zone (soil waters or vadose water). Groundwater samples are extracted from the entire saturated zone using wells and over a defined interval using piezometers. Soil waters are extracted from the unsaturated zone of the active layer with the help of suction lysimeters at specific depths.

Differences in stable isotope composition between slopes

The three slopes where data were collected are different with respect to their microclimatologic conditions (Figure 5.1). Slope 1 is south-west exposed, but located in the trough of a valley and therefore receives some shadow. Slope 2 has a south-west exposure, little vegetation cover and is steeply inclined. Thaw depths are greatest on this slope and it is well drained. Slope 3, which faces north-east, has the lowest inclination, thickest vegetation cover, receives a considerable amount of shadow and is poorly drained. As a consequence, the water table reaches the surface during most of the summer. Upslope of site 3a is a shattered block field with steep inclination.

Figure 5.4 shows the isotopic composition of active layer water samples (ground and soilwater) collected from July to August 1994. These values are displayed in relation to the GMWL and LMWL. For all slopes, ground and soilwaters fall between the GMWL and LMWL. Values for slope 1 and 2 fall in the same range: $-19 \leq \delta^{18}O \leq -15$ ‰ and $-140 \leq \delta D \leq -110$ ‰. In comparison, some water samples of slope 3 are isotopically lighter, ranging from -21 to -15 ‰ and -160 to -120 ‰. A closer examination shows that all depleted samples are from site 3a, the uppermost site on slope 3.

This suggests that site 3a receives water from an additional source, possibly from melting snow or basal ice. Basal ice, first defined by Woo *et al.* (1982), refers to ice that is formed by refreezing snow meltwater. For example, when snowmelt water infiltrates large rock fields, it refreezes at the base of the rockfield due to negative temperatures (Boike, 1993). In addition, basal ice can supply meltwater over the entire summer since it is protected from direct sunlight or strong air temperature variation. Supporting evidence was found in the field, where meltwater leaving the rock field was observed. Furthermore, snow was absent suggesting basal ice was an important source of active layer waters at site 3a.

The range of active layer stable isotope composition for the entire set of slope water samples ($-20.8 \leq \delta^{18}O \leq -14.7$ ‰ and $-156 \leq \delta D \leq -109$ ‰) relative to summer precipitation (Figure 5.2) indicates that active layer waters are mostly fed by rainwater or melting of active layer ground ice. In 1995, a few samples were collected from the upper centimetres of the frozen active layer. The extracted waters have the isotopic ratios of $\delta^{18}O$=-17.5 ‰, δD=-129 ‰ (N=1) on slope 2 and $\delta^{18}O$=-17.9 ‰, δD=-132 ‰ (N=2) on slope 3 which is essentially unchanged relative to the 1994 active layer waters.

Therefore it can be assumed that processes during the fall and winter, such as outward vapour flux detected on slope 2 (Boike *et al.*, 1997b), essentially leave the isotope composition of the active layer unchanged. This similarity in isotopic values between the frozen active layer and summer precipitation makes the isotopic quantification of these active layer water budget components more difficult.

Some waters show an offset to the left of the LMWL (1b, 2d) which are difficult to interpret and requires further investigations using additional geochemical data (*e. g.* pH, anions, cations).

Local variability in stable isotope composition within one slope-example slope 2

An examination of slope 2 waters reveals site specific differences in active layer waters (Figure 5.5). Site 2a is located furthest upslope and 2d at the base of the slope (Figure 5.1). Site 2x and 2c are located at the same height on the slope, approximately 50-80 metres apart from each other (Figure 3.1).

With the exception of waters from 2x, all samples fall in the range of -110 to -135 ‰ and -15 to -18 ‰ (Figure 5.5). The waters of site 2x are isotopically depleted compared to other sites on slope 2 and range between -125 to -145 ‰ δD and -17 to -20 ‰ $\delta^{18}O$ suggesting snowmelt water as an additional source of active layer water. Field observation supports this trend in the isotopic data. Site 2x received meltwater from a small snowpatch until the latter half of July while the rest of the slope was already snow free.

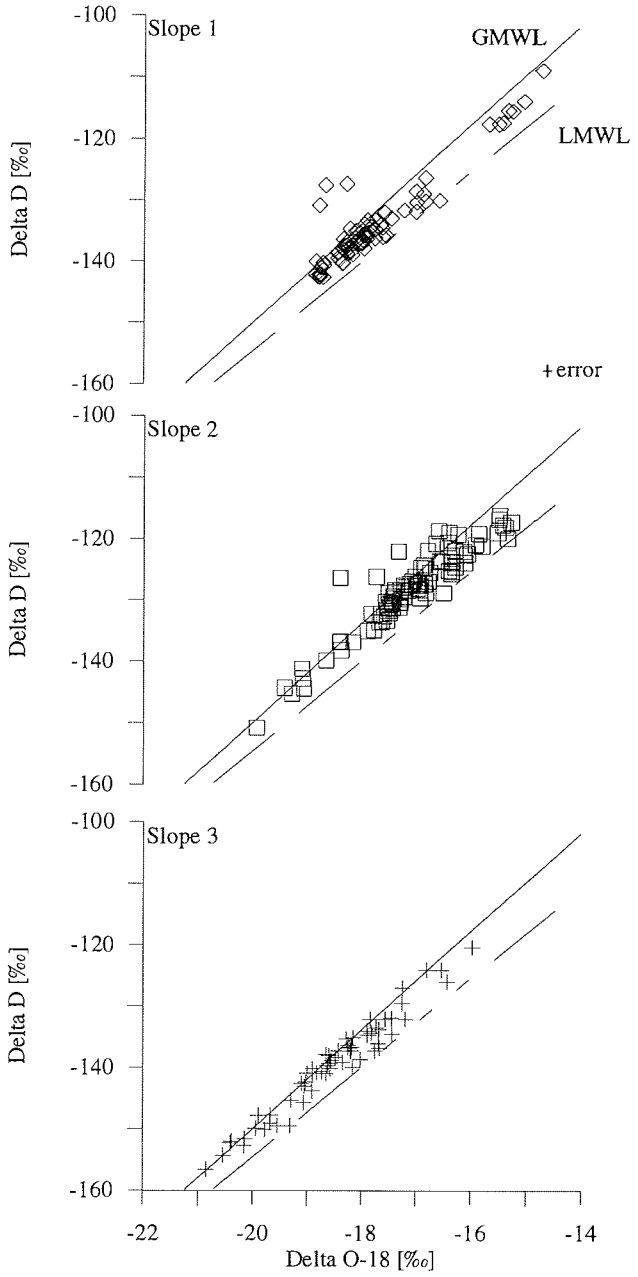

Figure 5.4. Plot of $\delta^{18}O$ versus δD for each slope for samples collected from July to August 1994.

The active layer groundwater is isotopically different than waters from the unsaturated zone (Figure 5.5). An explanation for the difference is that the two sampling methods generally extract different water types. Groundwater samples are sampled from wells and represent 'free bulk water samples', while water samples from suction lysimeters are extracted under negative pressure and thus sample a greater portion of bound water ('immobile water'). Another possibility would be that after a precipitation event, wells fill up faster while sampling of soil suction lysimeters generally takes longer (up to 2 days). The difference in soil water-groundwater isotopic composition could therefore reflect a time lag effect caused by different sampling techniques.

Soil temperature and $\delta^{18}O$

Figure 5.6 depicts the relationship between soil temperatures in the active layer and the $\delta^{18}O$ of the soilwater at that depth. For most sites, $\delta^{18}O$ values become heavier with increasing soil temperatures which is most pronounced for sites on slope 2. Sites that do not show this trend are located in the upper soil profiles (1a-9 cm, 3a-9 cm, 2x). These samples reflect the infiltration of rainwater (1a) or mixing of active layer waters with snow (2x) or basal ice contribution (3a). At site 1a, samples from the unsaturated zone could only be extracted after precipitation events, since the soil was usually very dry (the maximum water content at this site was 15 %).

The positive relationship between $\delta^{18}O$ and soil temperatures supports the observation that at higher soil temperatures, evaporation is enhanced and fractionation increases. Another explanation is that, concomitant with progress of the summer and warming of the active layer, precipitation $\delta^{18}O$ values become more enriched. The latter hypothesis cannot be supported by precipitation $\delta^{18}O$ values since they do not follow a seasonally increasing trend.

Using the $\delta^{18}O$ values as a 'microthermometer' for these slopes, slope 3 has the coldest active layer which corresponds to lowest isotope values. Slope 2 is warmest, with highest $\delta^{18}O$ values. Furthermore, the slope of the $\delta^{18}O$-soil temperature relationship indicates the magnitude and type of evaporation. Although soil temperatures of slopes 1 and 2 extend over a similar range, the inclination of the $\delta^{18}O$ - soil temperature relationship on slope 2 is greatest. This can be explained by distinguishing between evaporation and evapotranspiration dominated fractionation. As stated earlier, slope 2 has almost no vegetation cover compared to slope 1. Therefore, evaporation on slope 2 will cause an isotopic fractionation. On slopes 1 and 3, however, a considerable part of evaporation may proceed as evapotranspiration which has no fractionation effect on the isotopic composition (Gat, 1995).

5.4.3 Conclusions: Application of stable isotopes for paleoclimatic and hydrological studies

The deviation of the LMWL relative to the GMWL in this permafrost setting underlines the importance of long-term, seasonally resolved isotope measurements of precipitation in catchments where hydrological studies are undertaken. The active layer waters of this site are of meteoric origin, fed mostly by summer precipitation. This is in agreement with results presented by Mikahalev (1989) who found that the main source of active layer waters in the Kolyma region is summer and fall precipitation. In contrast, Mackay (1983) found that the isotopic composition of active layer waters of the Tuktoyaktuk

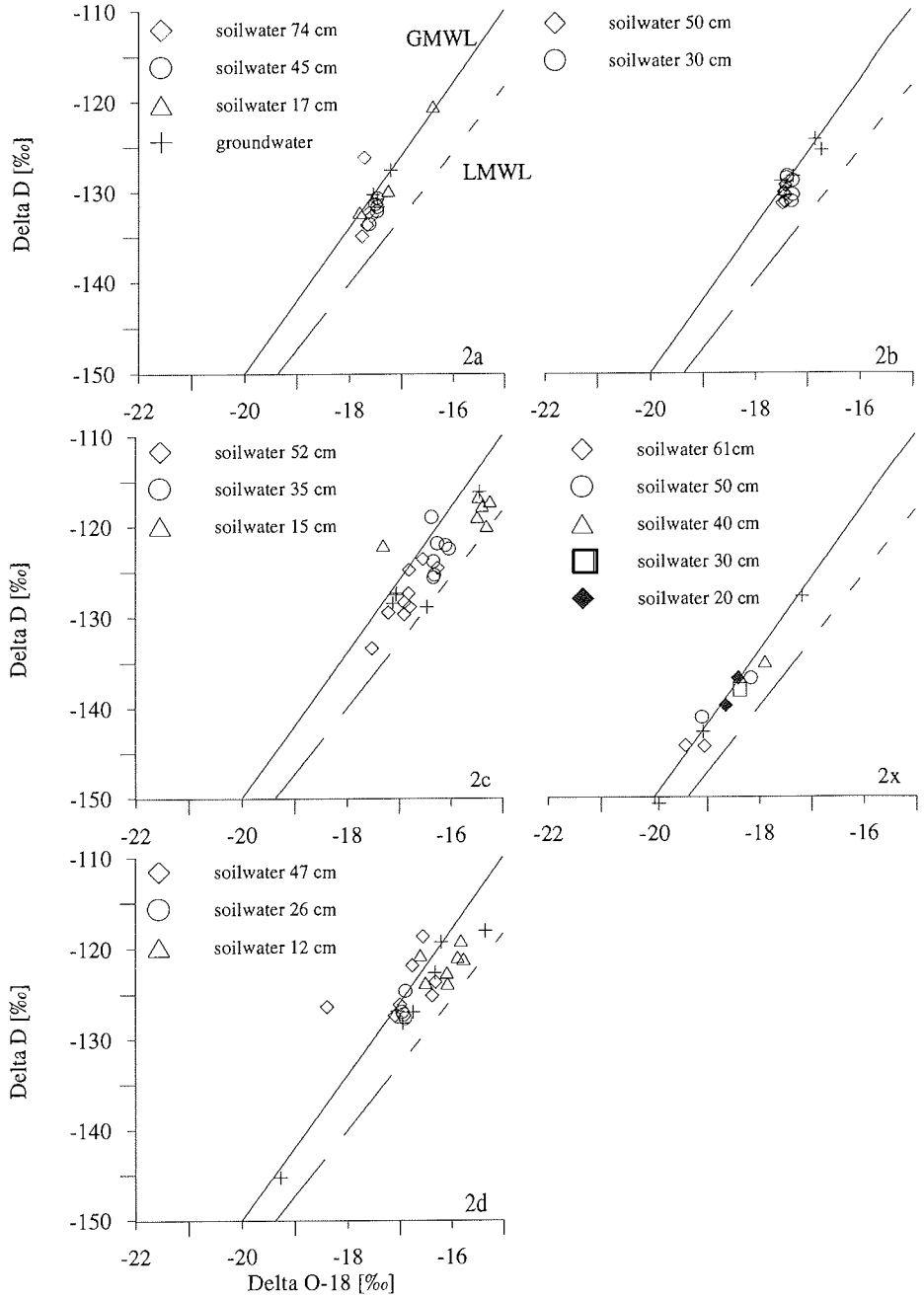

Figure 5.5. Plot of $\delta^{18}O$ versus δD for each site on slope 2. Symbols denote the type of water and sampling depth.

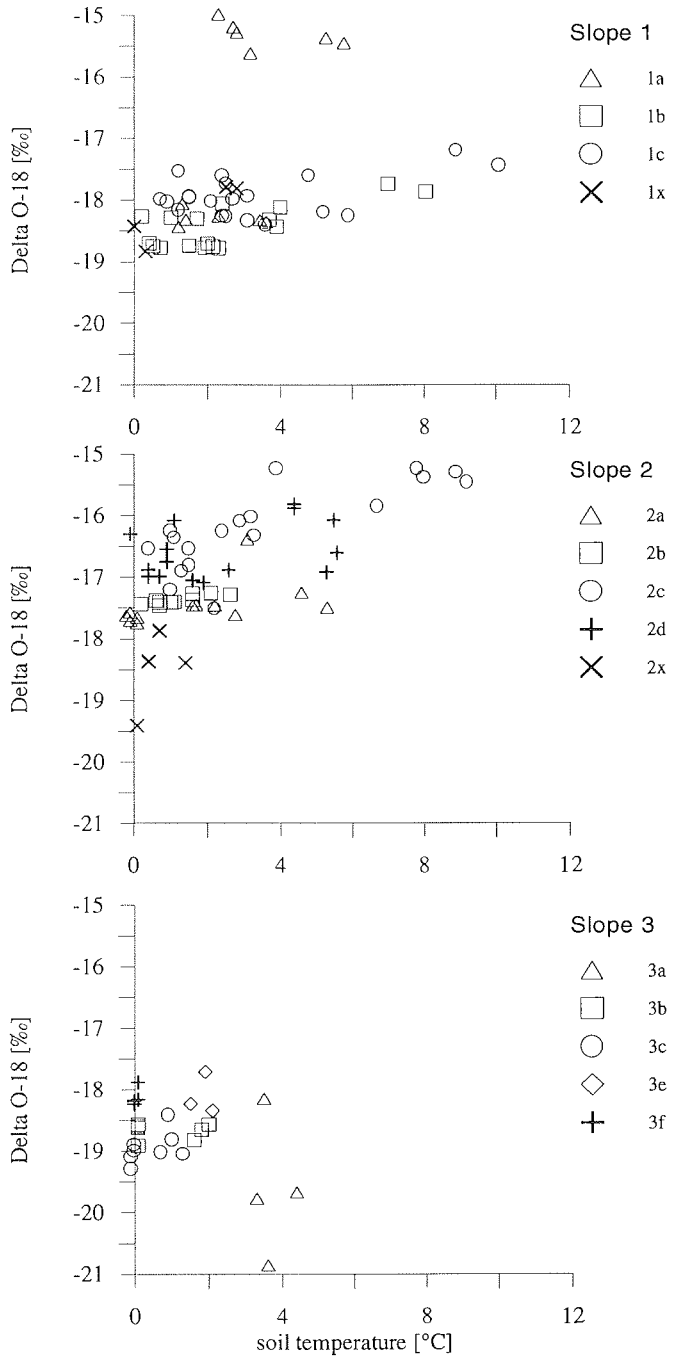

Figure 5.6. Plot of soil temperature versus $\delta^{18}O$ from soilwaters at the same depths. Within each slope one symbol represents one site.

Peninsula, Canada, is composed of snowmelt water and rainfall. These differences are probably related to the different field sites. Mackay's study was carried out in the western Arctic of North-America where the climate is less continental compared to the Taymyr peninsula or Kolyma region. As a result, the snow cover on the Tuktoyaktuk Peninsula is probably thicker and extends over a longer period. This furthermore underlines the importance a good understanding of the site, so that local effects (such as runoff from a late lying snowpack) can be excluded when isotope ratios are discussed.

At our sites, the active layer is fed mainly by summer rain, therefore the isotopic signatures reflect the late summer air temperatures. This is useful for the paleoclimatic interpretation of isotopic composition of texture ice preserved in the active layer in this setting. However, these results are contrary to Nikolayev and Mikhalev (1995) who found the best correlation between $\delta^{18}O$ of active layer texture ice and average air temperature of the winter season, although the active layer was also fed by late summer precipitation. The role of active layer isotopes as paleothermometers is not yet fully understood. Future process studies should therefore investigate the relationship between stable isotopes in active layer waters, formation of texture ice and air temperatures on a long-term basis.

The interpretation of stable isotope ratios on the basis of physical parameters of the active layer (soil water content and temperature) allows the identification of microclimatic differences between slopes. Moreover, the isotopes have been applied to discern different sources of waters within one slope (such as basal ice at site 3a). This stresses the fact that on a small scale, i.e. within one catchment, isotopes are sensitive indicators for microclimatic and hydrological processes affecting the active layer. However, independent hydrological measurement should be carried out in support of stable isotope measurements.

The results of this study are prerequisites for hydrological budget studies based on isotopic mass balance equations. For example, a lake water isotopic budget requires knowledge of the isotopic components of snow, rain, groundwaters and inflows.

Chapter 6

Summary and conclusions

6.1 SUMMARY

The goal of this research was to gain an overall understanding of the seasonal heat and water transfer processes in the active layer at a field site in Siberia. To accomplish this, the following strategy was used: (i) evaluation of the time domain reflectometry (TDR) as a technique for obtaining accurate and temporally highly resolved measurements of volumetric water content θ and bulk electrical conductivity σ_b for the active layer (ii) characterizing the dominant heat and mass transfer processes using a simple water and energy model for a complete thaw-freeze cycle (iii) classification of active layer waters with respect to global meteoric waters, and on a smaller scale, to hydrological and microclimatological variances within the catchment using the stable isotopes D and H.

As a first step, currently applied models were tested for calculation of θ and σ_b in the active layer, based on *in situ* application of TDR. The result was that the determination of θ is well-established with current models and does not require calibration. However, the application of theoretical models for determination of the soil water electrical conductivity σ_w resulted in unacceptably high deviations of predicted from measured values. A model was developed for this permafrost setting to calculate σ_w with sufficient accuracy from TDR data, *i. e.*, to within a factor of about 2 of the true values. Based on these results, TDR is recommended as an *in situ* technique for studying the temporal dynamics of soil water and solutes in the active layer.

Field experiments carried out for one continuous thaw-freeze cycle gave insight into the thermal and hydrologic dynamics and the dominant heat and mass transfer mechanisms in the active layer. A simple water and energy balance model allowed quantification of the individual energy and water balance components across the surface of the ground. It was found that the dominant components in this system are the energy input by net radiation and the latent heat associated with melting and evaporation. The average amount of energy taken for evaporation lies in the range of approximately 25 to 50 % of the total available energy during the spring and summer period. The second largest energy sink is the thawing of the active layer which can consume more than 20 %. In contrast to other studies, a much higher percentage of the energy transferred into the ground is consumed for thawing. Of 100% energy transferred into the ground, between 70 to 100 % is consumed for thawing and the rest for the warming of the ground. Overall, the calculations indicate that the energy fluxes in the active layer are approximately balanced for the studied period May to October 1995 which indicates that there is no large net inflow or outflow of energy.

Liquid water up to 9 % was present in frozen soil even at -12 °C and increased in volumetric content with temperature. During spring thaw, temperature gradients led to heat conduction as an important process of heat transport. During summer and during autumn freeze-back in particular, convective processes appeared to be responsible for efficient energy transfer within the thawed part of the soil. The heterogeneity of the soil profile has the effects of (i) routing water along preferential flowpaths and (ii) allowing freezing to occur in 'cells' within the active layer rather than through the descent of a distinct freezing front (Figure 6.1). Areas with an initially lower water content freeze earlier compared to regions with a higher water content.

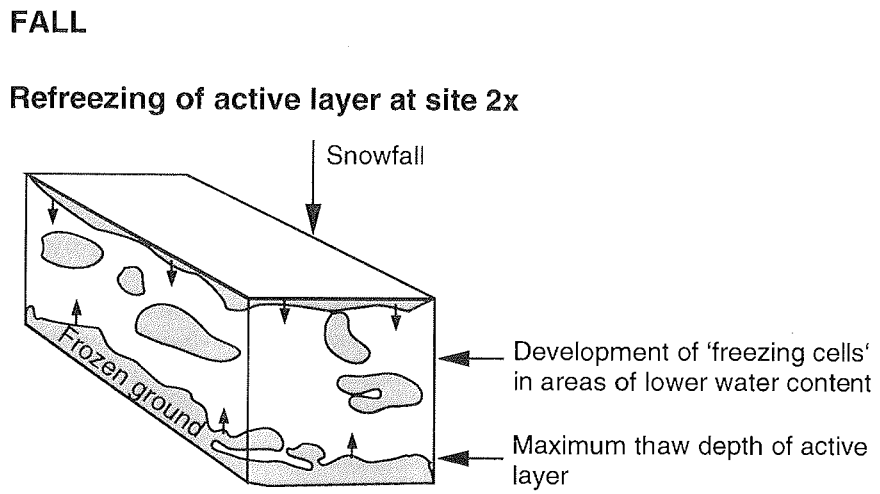

Figure 6.1. Revised scheme of freeze-back in the active layer at site 2x.

During the freeze-back of the active layer, solutes are excluded from the ice matrix which results in an increase of σ_W in the freezing ground. Compared to σ_W changes during the summer, variations in σ_W as a result of phase change in the fall are one order of magnitude greater.

Based on precipitation samples from 1994 and 1995, a local meteoric water line (LMWL) was established that deviates from the global meteoric water line (GMWL) for the summer precipitation. The stable isotope ratios $\delta^{18}O$ and δD in water of the active layer indicate that they are of meteoric origin, fed mostly by summer precipitation. Moreover, the isotope ratios have been used to discern different sources of active layer waters within the catchment. Isotopic variabilities between sites in the catchment indicate differences in microclimatic and hydrologic characteristics between sites.

6.2 CONCLUSIONS

- Calibration of TDR enables the determination of σ_w in the active layer of this investigated Siberian permafrost setting. However, calibration of the TDR determined σ_b is required *in situ* with an independent means of conductivity measurement at other permafrost sites.
- The dominant energy sinks in this system are the latent heat associated with melting and evaporation. Several models exist for the quantification of evaporative fluxes at the active layer-atmosphere boundary (*e. g.*, Priestley Taylor), but the quantification of latent heat fluxes (thawing) in the active layer is often neglected. Heat flux plates, commonly used in the active layer, largely underestimate latent heat fluxes, since they only measure the sensible heat flux, as was already pointed out by Halliwell and Rouse (1987). Furthermore, the latent heat flux in the active layer should be incorporated into models where the distribution of permafrost is predicted under climate change scenarios (Anisimov and Nelson, 1996). Especially in permafrost regions with high content of ground ice, a lag time is expected due to the importance of latent heat consumption (Riseborough, 1990).
- Convective heat flow is an important heat transfer mechanism in the active layer, but is often neglected in models for water and heat transport (Kennedy and Lielmezs, 1973; Nixon, 1975), large scale predictive models for simulation of climate change scenarios in arctic watersheds (Hinzman and Kane, 1992) and models for the prediction of permafrost ages (Lunardini, 1993). Hence, this creates differences of simulated model data relative to experimental results as the observed temperature difference between simulated and measured data for the active layer at Toolik Lake, Alaska illustrates (Kane *et al.*, 1991).
- The determination of the local meteoric water line in this setting is necessary for the interpretation of hydrological processes affecting $\delta^{18}O$ and δD, since it deviates from the global meteoric water line.

Which direction should future research take?

Future studies should extend the performed measurements across a larger spatial and temporal scale.

- The application of TDR for the calculation of σ_w in frozen and unfrozen soils and the relationship between the geometry factor A and soil properties should be experimentally explored. The ultimate goal must be to develop an generally applicable model for frozen and unfrozen soils relating A to some easily measurable soil physical parameters.
- In addition to estimates of θ in frozen soils, a more accurate description of the local dynamics demands the direct non-destructive measurement of the ice content, *e. g.*, through the combination of TDR and twin-gamma probe, and the measurement of the vapor flux through the soil surface concomitant with microclimatic data.
- Further investigations of $\delta^{18}O$ and δD in the active layer with respect to temporal and seasonal changes, soil morphological, hydrological and climatological characteristics should be carried out. Only with a complete understanding of these processes, the paleoclimatic interpretation of $\delta^{18}O$ and δD in active layer texture ice should be undertaken.

- The start of long term circumpolar programs to monitor climate, active layer θ and temperatures should be initiated. This should be undertaken in active layer sites varying in ice content, fraction of mineral and organic, snow cover and vegetation. Only if this complex problem is understood on a small scale, we can detect changes in the atmosphere-permafrost disequilibrium as a result of climatic change.
- With a comprehensive understanding of the physics of permafrost soils, the energy and water fluxes can be estimated on a larger scale, potentially based on data from remote sensing.

References

Anderson, D. M. and N. R. Morgenstern (1973). Physics, chemistry and mechanics of frozen ground: A review, 257-288. In *North American Contribution, Permafrost, 2nd Int. Conf.*, July 1973, Yakutsk. National Academy of Sciences, Washington, D. C.

Anisimov, O. A. and F. E. Nelson (1996). Permafrost distribution in the Northern Hemisphere under scenarios of climatic change. *Global and Planetary Change* 14, 59-72.

Baker, T. H. W., J. L. Davis, H. N. Hayhoe and G. C. Topp (1982). Locating the frozen-unfrozen interface in soils using time domain reflectometry. *Can. Geotech. J.* 19, 511-517.

Boike, J. (1993). Seasonal hydrology and geochemistry of two small high arctic catchments, Axel Heiberg Island, N. W. T. *Unpubl. M.A. thesis*, Wilfrid Laurier University, Waterloo, Ontario, Canada, 190 pp.

Boike, J., W. K. P. van Loon, P. P. Overduin and H. W. Hubberten (1997a). Solute movement in the active layer, Taymyr, Siberia. *In*: Int. Symp. on Physics, Chemistry, and Ecology of Seasonally Frozen Soils, Fairbanks, Alaska, June 10-12, 1997 (in press).

Boike, J., K. Roth and P. P. Overduin (1997b). Thermal and hydrological dynamics of the active layer at a continuous permafrost site (Taymyr Peninsula, Siberia). *Water Res. Res.* (accepted).

Boike, J. and K. Roth (1997). Using time domain reflectometry to measure water content and soil water electrical conductivity in the active layer of a continous permafrost site. *Permafrost and Periglacial Processes* (accepted).

Bolshiyanov, D. Y. and H. W. Hubberten (1996). Russian-German Cooperation: The Expedition Taymyr 1995. *Reports on Polar Research* 211, 208 pp.

Brooks, R. H. and A. T. Corey (1966). Properties of porous media affecting fluid flow. *J. Irrigation and Drainage Div., Proc. Am. Soc. Civil Eng.* (IR2) 92, 61-88.

Bursey, G. G., T. W. D. Edwards and S. K. Frape (1991). Water balance and geochemistry studies in a tundra watershed, district of Keewatin, Northwest Territories, 17-31. In *Northern Hydrology, selected perspectives, Proc. of the NHRI Symp.* 6 (eds. T. D. Prowse and C. S. L. Ommanney).

Cheng, G. and E. J. Chamberlain (1988). Observations of moisture migration in frozen soils during thawing. *Proc. Fifth Int. Conf. on Permafrost* 1, August 1988, Trondheim, Norway, 308-312.

Cooper, L. W., C. Solis, D. L. Kane and L. D. Hinzmann (1993). Application of $\delta^{18}O$ tracer technique to arctic hydrological processes. *Arctic and Alpine Res.* 25 (3), 247-255.

Craig, H. (1961). Isotopic variations in meteoric waters. *Science* 133, 1702-1703.

Dansgaard, W. (1964). Stable isotopes in precipitation. *Tellus* 16, 436-468.

Dasberg, S. and F. N. Dalton (1985). Time domain reflectometry field measurements of soil water content and electrical conductivity. *Soil Sci. Soc. Am. J.* 54, 293-297.

Epstein, S. and T. Mayeda (1953). The variation of ^{18}O content of water from natural sources. *Geochimica et Cosmochimica Acta* 4, 213-224.

Ershov, E. D. (1989). Geocryological conditions of the Taymyr region. In: *Geocryology of the USSR* (ed. D. Ershov). Moscow, Nedra, 140-163, (in Russian).

Ershov, E. D. (1995). *Physical and chemical basics of geocryology*, Moscow University press, Moscow, Russia, 369 pp, (in Russian).

Farouki, O. T. (1981). Thermal properties of soils. Cold Regions Research and Engineering Laboratory, Hanover, N.H., *Monograph 81-1*, 136 pp.

Gat, J. R. (1980). The isotopes of hydrogen and oxygen in precipitation, 21-44. In *Handbook of environmental isotope geochemistry* 1 (eds. P. Fritz and J.C. Fontes), Elsevier Scientific Publishing Company, Amsterdam.

Gat, J. R. (1995). Stable isotopes of fresh and saline lakes, 139-165. In *Physics and chemistry of lakes* (eds. A. Lerman and J. Gat), 2nd edition, Springer Verlag.

Gavrilova, M. K. (1981) *Recent climate and permafrost in continents.* Novosibirsk, Nauka, (in Russian), 112 pp.

Gibson, J. J., T. W. D. Edwards and G. G. Bursey (1993). Estimating evaporation using stable isotopes. *Nordic Hydrology* 24, 79-94.

Guymon, G. L. and J. N. Luthin (1974). A coupled heat and moisture transport model for arctic soils. *Water Res. Res.* 10 (5), 995-1001.

Hallet, B. (1978). Solute redistribution in freezing ground, 86-91. In *Permafrost, Proc. Third Int. Conf. 1,* National Research Council of Canada, Ottawa, Canada.

Halliwel, D. H. and W. R. Rouse (1987). Soil heat flux in permafrost: Characteristics and accuracy of measurement. *Journal of Climatology* 7, 571-584.

Harris, S. A., H. M. French, J. A. Heginbottom, G. H. Johnston, B. Ladanyi, D. C. Sego and R. O. van Everdingen (1988). *Glossary of Permafrost and Related Ground-Ice Terms, Tech. Memo.*142, National Research Council of Canada, Ottawa.

Hayhoe, H. N. and D. Balchin (1988). Time domain reflectometry and electrical conductance measurements during seasonal frost. *Cold Regions Science and Technology* 15, 195-200.

Heimovaara, T. J. (1993). Design of triple-wire time domain reflectometry probes in practice and theory. *Soil Sci. Soc. Am. J.* 57, 1410-1417.

Heimovaara, T. J. and E. de Water (1993). A computer controlled TDR system for measuring water content and bulk electrical conductivity, *Report 41*, Laboratory of Physical Geography and Soil Science, University of Amsterdam, 27 pp.

Heimovaara, T. J., A. C. Focke, W. Bouten and J. M. Verstraaten (1995). Assessing temporal variations in the soil water composition with time domain reflectometry, *Soil Sci. Soc. Am. J.* 59, 689-698.

Herkelrath, W. N., S. P. Hamburg and F. Murphy (1991). Automatic, real-time monitoring of soil moisture in a remote field area with time domain reflectometry. *Water Res. Res.* 27 (5), 857-864.

Hinkel, K. M. and S. I. Outcalt (1994). Identification of heat transfer processes during soil cooling, freezing, and thaw in central Alaska. *Permafrost and Periglacial Proc.* 5, 217-235.

Hinkel, K. M., S. I. Outcalt and F. E. Nelson (1993). Near surface heat-transfer regimes at adjacent permafrost and non-permafrost sites in Central Alaska. *Proc. Sixth Int. Conf. on Permafrost*, July 1993, Beijing, China, 261-266.

Hinzman, L. D. and D. L. Kane (1992). Potential response of an Arctic watershed during a period of global warming. *Journal of Geophysical Res.* 97 (B3), 2811-2820.

Hinzmann, L. D., D. L. Kane, C. S. Benson and K. R. Everett (1996). Energy balance and hydrological processes in an arctic watershed. In *Landscape functions and disturbance in Arctic Tundra* (eds. J. F. Reynolds and J. D. Tenhunen), *Ecological Studies* 120, Springer Verlag, Berlin-Heidelberg, 437 pp.

Hinzmann, L. D., D. L. Kane, R. E. Gieck and K. R. Everett (1991). Hydrologic and thermal properties of the active layer of the Alaskan Arctic. *Cold Regions Science and Technology* 19, 95-110.

Hromadka, T. V., G. L. Guymon and R. L. Berg (1981). Some approaches to modeling phase change in freezing soils. *Cold Regions Science and Technology* 4, 137-145.

International Atomic Energy Agency (1983). Isotope techniques in the hydrogeological assessment of potential sites for the disposal of high level radioactive wastes. *Technical report series* 228, IAEA Vienna, 147 pp.

Jackson, J. D. (1975). *Classical Electrodynamics*. John Wiley & Sons (ed.), New York, 2nd edition.

Kane, D. L. , L. D. Hinzman and J. P. Zarling (1991). Thermal response of the active layer to climatic warming in a permafrost environment. *Cold Regions Science and Technology* 19, 111-122.

Kane, D. L., R. E. Gieck and L. D. Hinzmann (1990). Evapotranspiration from a small Alaskan Arctic watershed. *Nordic Hydroloy* 21, 253-272.

Kennedy, G. F. and J. Lielmezs (1973). Heat and mass transfer of freezing water-soil system. *Water Res. Res.* 9(2), 395-400.

Klute, A. (ed.) (1986). *Methods of soil analysis, 1: Physical and mineralogical methods. Agronomy Series* 9. American Society of Agronomy, Madison, WI, 2nd edition.

Lachenbruch, A. H. and B. V. Marshall (1986). Changing climate: Geothermal evidence from permafrost in the Alaskan Arctic. *Science 234*, 689-696.

Lachenbruch, A. H., T. T. Cladouhos and R. W. Saltus (1988). Permafrost temperature and the changing climate, *Proc. Fifth Int. Conf. on Permafrost 3*, August 1988, Trondheim, Norway, 9-17.

Lee, D. R. and J. A. Cherry (1978). A field exercise on groundwater flow using seepage meters and mini-piezometers. *J. of Geological Education* 27, 6-10.

Lunardini, V. J. (1993). Permafrost formation time. In *Proc. Sixth Int. Conf. on Permafrost* 1, July 1993, Beijing, China, South China University of Technology Press, 420-425.

Lundin, L. C. and H. Johnsson (1994). Ion dynamics of a freezing soil monitored *in situ* by time domain reflectometry. *Water Res. Res.*, 30 (12), 3471-3478.

Mackay, J. R. (1983). Downward water movement into frozen ground, western arctic coast, Canada. *Can. J. Earth Sci.* 20, 120-134.

Mackay, J. R. (1983). Oxygen isotope variations in permafrost, Tuktoyaktuk Peninsula area, Northwest Territories. In *Current Res., Part B*, Geological Survey of Canada, Paper 83-1B, 67-74.

Marsh, P. and M. K. Woo (1993). Infiltration of meltwater into frozen soil in a continuous permafrost environment. *Proc. Sixth Int. Conf. on Permafrost*, July 1993, Beijing, China, 443-448.

Melles, M. (1994). The expeditions Norilsk/Taymyr 1993 and Bunger Oasis 1993/94 of the AWI research unit Potsdam. *Reports on Polar Research* 148, 80 pp.

Melles, M., C. Siegert, J. Hahne and H. W. Hubberten (1996). Climatic and environmental history of north-central Siberia during the late quaternary period-first results. *Geowissenschaften* 14 (9), 376-380, (in German).

Merlivat, L. and J. Jouzel (1979). Global climatic interpretation of the deuterium-oxygen 18 relationship for precipitation. *J. of Geophys. Res.* 84, 5029-3033.

Michel, F. A. (1982). Isotope investigations of permafrost waters in northern Canada. *Unpubl. Ph.D. thesis*, Dept. of Earth Sciences, Univ. of Waterloo, Waterloo, Ontario, Canada, 227 pp.

Mikhalev, D. V. (1989). The formation of the Oxygen isotopic composition of the segregated ice in the active layer. In *Conditions and processes of cryogenic migration of solutes* (ed. V. P. Romanov), Institute of Cryology, the USSR Academy of Sciences, Yakutsk, 162-169. (in Russian).

Mualem, Y. (1976). A new model for predicting the hydraulic conductivity of unsaturated porous media. *Water Res. Res.* 12, 593-622.

Mualem, Y. and S. P. Friedman (1991). Theoretical prediction of electrical conductivity in saturated and unsaturated soil. *Water Res. Res.* 27 (10), 2771-2777.

Murray, R. J. and I. Simmonds (1995). Response of climate and cyclones to reductions in arctic winter sea ice. *J. of Geophys. Res.* 100 (C3), 4791-4806.

Nadler, A., S. Dasberg and I. Lapid (1991). Time domain reflectometry measurements of water content and electrical conductivity of layered soil columns. *Soil Sci. Soc. Am. J.* 55, 938-943.

National Research Council of Canada (1988). *Glossary of permafrost and related ground ice terms.* Technical Memorandum No. 142. Permafrost Subcommittee, Associate Committee on Geotechnical Research, National Research Council of Canada (NRCC 27952), Ottawa, Ontario, 156 pp.

Nersesova, Z. A and N. A. Tsytovich (1963). Unfrozen water in frozen soils. *Proc. First Int. Conf. on Permafrost*, Lafayette, Indiana, November 1963, National Academy of Sciences-National Research Council, Washington, D.C., 230-234.

Nikolayev, V. I. and D. V. Mikhalev (1995). An oxygen-isotope paleothermometer from ice in Siberian permafrost. *Quaternary Res.* 43, 14-21.

Nixon, J. F. (1975). The role of convective heat transport in the thawing of frozen soil. *Can. Geotech. J.* 12, 425-429.

Ohmura, A. (1982). Climate and energy balance of the arctic tundra. *J. of Climatology* 2, 65-84.

Outcalt, S. I., F. E. Nelson and K. M. Hinkel (1990). The zero-curtain effect: heat and mass transfer across an isothermal region in freezing soil. *Water Res. Res.* 26 (7), 1509-1516.

Panday, S. P. and M. Y. Corapcioglu (1991). Solute rejection in freezing soils. *Water Res. Res.* 27 (1), 99-108.

Parmuzina, O. Y. (1978). Cryogenic texture and some characteristics of ice formation in the active layer (in Russian), 141-164. In *Problems of Cryolithology* 7 (ed. A. I. Popov), Moscow University Press, 1980, translated in *Polar Geography and Geology* IV (3), 131-152.

Patterson, D. E. and M. W. Smith. (1980). The use of time domain reflectometry for the measurement of unfrozen water content in frozen soils. *Cold Regions Science and Technology* 3, 205-210.

Pfeiffer, E.-M., A. Gundelwein, T. Nöthen, H. Becker and G. Guggenberger (1996). Characterization of the organic matter in permafrost soils and sediments of the Taymyr Peninsula/Siberia and Severnaya Zemlya/Arctic Region, 46-63. *In* Russian German Cooperation: The expedition Taymyr 1995 and the expedition Kolyma 1995 of the ISSP Pushino group, (eds. D. Y. Bolshiyanov and H.-W. Hubberten), *Reports on Polar Res.* 211.

Press, W. H., S. A. Teukolsky, W. T. Vetterling and B. P. Flannery (1992). *Numerical Recipes in C. The Art of Scientific Computing,* Cambridge University Press, Cambridge, 2nd edition.

Priestley, C. H. B. and R. T. Taylor (1972). On the assessment of surface heat flux and evaporation using large-scale parameters. *Mon. Weather Rev.* 100, 81-92.

Ray, R. J., W. B. Krantz, T. N. Caine and R. D. Gunn (1983). A model for sorted patterned-ground regularity. *J. Glaciol.* 29, 317-337.

Rhoades, J. D., N. A. Monteghi, P. J. Shouse and W. J. Alves (1989). Soil electrical conductivity, water content and surface conductivity on bulk electrical conductivity. *Soil Sci. Soc. Am. J.* 53, 433-439.

Rhoades, J. D., P. A. C. Raats and R. J. Prather (1976). Effects of liquid-phase electrical conductivity, water content, and surface conductivity on bulk electrical conductivity. *Soil Sci. Soc. Am. J.* 40, 651-655.

Roth, K., R., Schulin, H. Flühler and W. Attinger (1990). Calibration of Time Domain Reflectometry for water content measurement using a composite dielectric approach. *Water Res. Res.* 26 (10), 2267-2273.

Rouse, W. R. (1984). Microclimate at arctic tree line, 2. Soil microclimate of tundra and forest, *Water Res. Res. 20* (1), 67-73.

Rouse, W. R., P. F. Mills and R. B. Stewart (1977). Evaporation in high latitudes. *Water Res. Res. 13* (6), 909-914.

Santeford, H. S. (1978). Snow soil in interaction in interior Alaska. In *Modeling of snow cover runoff*, (eds. S. C. Colbeck and M. Ray), Cold Regions Research and Engineering Laboratory, Hanover, N.H., 311-318.

Shaver, G. R. (1996). Integrated ecosystem research in Northern Alaska, 1947-1994, 19-34. In *Landscape function and disturbance in Arctic tundra* (eds. J. F. Reynolds and J. D. Tenhunen). *Ecological studies* 120. New York, Springer Verlag.

Sheppard, S. M. F. (1986). Characterization and isotopic variations in natural waters. *In* Stable isotopes in high temperature geological processes (eds. J. W. Valley, H. P. Taylor and J. R. O'Neil), *Reviews in Mineralogy* 16, 165-180.

Siegert, C. and Bolshiyanov, D. Y. (1995). Russian-German Cooperation: The Expedition Taymyr 1994. Reports on Polar Res. 175, 91 pp.

Smith, M. W. and A. R. Tice. (1988). Measurement of the unfrozen water content of soils: a comparison of NMR and TDR methods, *Proc. Fifth Int. Conf. on Permafrost* 1, August 1988, Trondheim, Norway, 473-477.

Smith, M. W. and C. R. Burn (1987). Outward flux of vapour from frozen soils at Mayo, Yukon, Canada: results and interpretations. *Cold Regions Science and Technology* 13, 143-152.

Spaans, E. J. A. and J. M. Baker. (1995). Examining the use of time domain reflectometry for measuring liquid water content in frozen soil. *Water Res. Res.* 31 (12), 2917-2925.

Stähli, M. and D. C. Stadler (1996). Water and solute dynamics in freezing soil columns, 31-48. In *Water and solute dynamics in frozen forest soils, measurements and modeling*, (D. C Stadler), Diss. ETH No. 11574, Zürich, Switzerland.

Stein, J. and D. Kane. (1983). Monitoring the unfrozen water content of soil and snow using time domain reflectometry. Water Res. Res. 19 (6), 1573-1584.

Taylor, G. S. and J. N. Luthin (1978). A model for coupled heat and moisture transfer during soil freezing. *Can. Geotechn. J.* 15, 548-555.

Tektronix (1988). 1502B metallic time domain reflectometer, operator manual. Tektronix, Beaverton, Oregon.

Topp, G. C., J. L. Davis and A. P. Annan (1980). Electromagnetic determination of soil water content: Measurements in coaxial transmission lines. *Water Res. Res.* 16 (3), 574-582.

Vaikmäe, R. (1991). Oxygen-18 in permafrost ice. *Proc. Int. Symp. on the use of isotope technique in water resources development*, Vienna, March 1991. Int. atomic energy agency, paper IAEA-SM-319/34, 29 pp.

van Loon, W. K. P., P. H. Perfect, P. H. Groenevelt and B. D. Kay. (1990). Application of time domain reflectometry to measure solute redistribution during soil freezing. *Proc. Int. Frozen Soil Symp.*, CRREL Report 90-1, Hanover, NH, USA, 186-194.

van Loon, W. K. P., P. H. Perfect, P. H. Groenevelt and B. D. Kay (1991). Application of dispersion theory to time domain reflectometry in soils. *Transp. Porous Media* 6, 391-406.

Weller, G. and B. Holmgren (1974). The microclimates of the arctic tundra. *J. of Appl. Meteorology 13*, 854-862.

William, P. J. and M. W. Smith (1989). *The frozen earth: fundamentals of geocryology.* Cambridge University Press, Cambridge, U.K.

Woo, M. K, R. Heron and P. Marsh (1982). Basal ice in high arctic snowpacks. *Arctic and Alpine Res.* 14 (3), 251-260.

Woo, M. K. and P.Marsh (1990). Response of soil moisture change to hydrological processes in a continuous permafrost environment. *Nordic Hydrology* 21, 235-252.

Zegelin, S.J., I. White and D. R. Jenkins (1992). Improved field probes for soil water content and electrical conductivity measurement using time-domain reflectometry. *Water Res. Res.* 25, 2367-2376.

Appendix

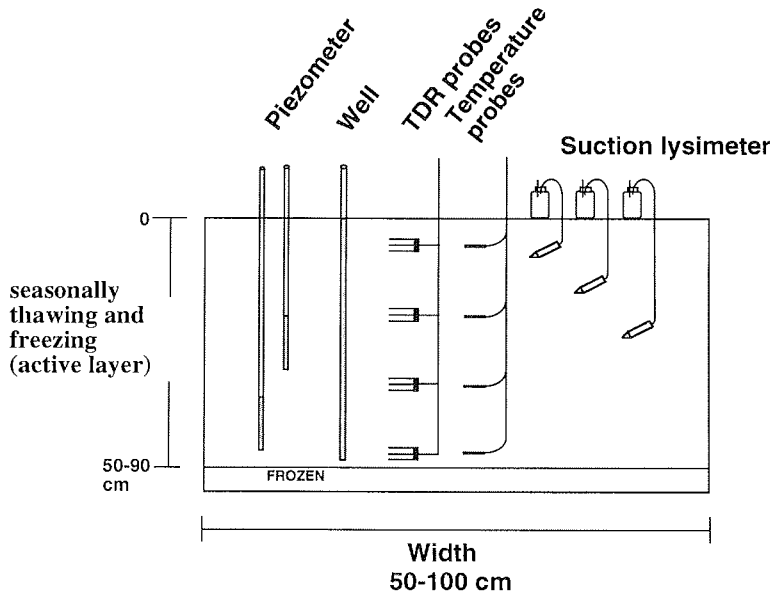

Figure A.1. Scheme of instrumented soil pit.

Table A.1. Input parameters for the calculation of σ_w from TDR determined σ_b for slopes 1, 2, 3. θ_{sat} determined from TDR probes under saturation.

Slope 1

Date	Site	Depth	θ_{sat}	θ	Soil tempe-rature	σ_b TDR	σ_w Suction lysimeter
		[cm]	[$m^3 m^{-3}$]	[$m^3 m^{-3}$]	[°C]	[mS m^{-1}]	[mS m^{-1}]
17. Aug 94	1x	53	0.31	0.29	0.0	13.64	23.50
20. Aug 94	1x	53	0.31	0.29	-0.1	14.12	25.70
22. Aug 94	1x	53	0.31	0.30	0.0	16.48	27.10
24. Aug 94	1x	53	0.31	0.30	-0.1	15.99	28.40
26. Aug 94	1x	53	0.31	0.29	-0.1	15.97	26.80
28. Aug 94	1x	53	0.31	0.29	-0.2	16.35	24.30
24. Aug 94	1x	39	0.33	0.31	0.1	13.15	26.90
28. Aug 94	1x	39	0.33	0.31	0.1	13.69	22.20
22. Aug 94	1x	23	0.48	0.52	0.9	31.49	21.10
24. Aug 94	1x	23	0.48	0.53	0.5	34.37	18.90
26. Aug 94	1x	23	0.48	0.52	0.3	35.41	19.44
28. Aug 94	1x	23	0.48	0.47	0.4	34.80	18.20
09. Aug 94	1a	36	0.30	0.17	1.4	6.13	16.10
15. Aug 94	1a	36	0.30	0.16	0.2	6.34	15.61
24. Aug 94	1a	36	0.30	0.17	0.2	6.50	17.03
28. Aug 94	1a	36	0.30	0.17	0.5	6.44	16.39
09. Aug 94	1a	21	0.30	0.10	2.6	3.75	32.10
15. Aug 94	1a	21	0.30	0.10	0.5	3.72	11.95
22. Aug 94	1a	21	0.30	0.12	2.2	4.06	10.20
24. Aug 94	1a	21	0.30	0.11	0.8	3.98	11.00
28. Aug 94	1a	21	0.30	0.10	1.2	3.91	11.42
03. Aug 94	1b	57	0.40	0.40	1.5	35.13	24.40
07. Aug 94	1b	57	0.40	0.39	0.4	37.28	24.20
09. Aug 94	1b	57	0.40	0.39	0.6	36.06	24.40
12. Aug 94	1b	57	0.40	0.39	0.7	34.37	24.10
17. Aug 94	1b	57	0.40	0.39	0.6	35.39	21.60
20. Aug 94	1b	57	0.40	0.39	0.5	36.26	22.50
22. Aug 94	1b	57	0.40	0.40	0.6	45.28	23.90
24. Aug 94	1b	57	0.40	0.41	0.3	46.80	25.40
28. Aug 94	1b	57	0.40	0.41	0.2	43.74	24.80
07. Aug 94	1b	35	0.35	0.31	2.0	13.69	22.40
09. Aug 94	1b	35	0.35	0.31	2.1	13.79	22.70
12. Aug 94	1b	35	0.35	0.31	2.3	13.92	22.20
17. Aug 94	1b	35	0.35	0.31	2.0	13.87	20.10
20. Aug 94	1b	35	0.35	0.30	1.7	13.72	20.80
22. Aug 94	1b	35	0.35	0.32	1.9	14.35	22.90
24. Aug 94	1b	35	0.35	0.32	0.9	14.22	24.50
28. Aug 94	1b	35	0.35	0.32	1.0	14.44	24.20
03. Aug 94	1b	20	0.35	0.26	4.0	10.74	27.40
07. Aug 94	1b	20	0.35	0.24	3.7	10.44	24.60
09. Aug 94	1b	20	0.35	0.24	3.7	10.22	23.30
17. Aug 94	1b	20	0.35	0.24	3.2	9.62	19.00
15. Aug 94	1c	60	0.40	0.40	0.3	30.78	38.10
22. Aug 94	1c	60	0.40	0.40	0.8	30.24	40.10

28. Aug 94	1c	60	0.40	0.40	0.4	30.77	38.70
03. Aug 94	1c	40	0.42	0.42	2.7	36.32	25.50
07. Aug 94	1c	40	0.42	0.42	1.5	29.35	25.80
09. Aug 94	1c	40	0.42	0.42	1.8	27.92	25.80
12. Aug 94	1c	40	0.42	0.42	2.1	25.00	25.20
15. Aug 94	1c	40	0.42	0.41	0.9	20.51	25.90
17. Aug 94	1c	40	0.42	0.42	1.8	20.12	23.10
20. Aug 94	1c	40	0.42	0.43	1.5	19.75	23.80
22. Aug 94	1c	40	0.42	0.43	1.7	19.85	25.90
24. Aug 94	1c	40	0.42	0.43	1.0	19.70	27.40
28. Aug 94	1c	40	0.42	0.43	1.1	19.82	26.40
03. Aug 94	1c	27	0.45	0.45	3.6	19.51	23.40
07. Aug 94	1c	27	0.45	0.46	2.5	20.47	23.60
09. Aug 94	1c	27	0.45	0.46	2.7	20.60	23.80
12. Aug 94	1c	27	0.45	0.46	3.1	20.68	23.30
17. Aug 94	1c	27	0.45	0.47	2.8	20.90	21.40
20. Aug 94	1c	27	0.45	0.47	2.4	20.69	23.30
22. Aug 94	1c	27	0.45	0.47	2.4	20.65	24.30
24. Aug 94	1c	27	0.45	0.47	1.3	20.74	26.40
28. Aug 94	1c	27	0.45	0.47	1.5	21.02	24.80
07. Aug 94	1c	9	0.40	0.34	2.5	19.97	22.80
09. Aug 94	1c	9	0.40	0.34	2.7	18.97	23.50
12. Aug 94	1c	9	0.40	0.34	3.1	17.65	23.30
15. Aug 94	1c	9	0.40	0.35	1.2	16.92	24.10
17. Aug 94	1c	9	0.40	0.35	2.8	17.82	22.10
20. Aug 94	1c	9	0.40	0.35	2.4	18.40	23.90
22. Aug 94	1c	9	0.40	0.41	2.4	21.13	25.30
24. Aug 94	1c	9	0.40	0.41	1.3	21.77	26.60
28. Aug 94	1c	9	0.40	0.40	1.5	20.95	26.10

Slope 2

Date	Site	Depth	θ_{sat}	θ	Soil tempe-rature	σ_b TDR	σ_w Suction lysimeter
		[cm]	[$m^3\ m^{-3}$]	[$m^3\ m^{-3}$]	[°C]	[$mS\ m^{-1}$]	[$mS\ m^{-1}$]
22. Aug 94	2x	52	0.37	0.37	1.3	28.45	107.00
24. Aug 94	2x	52	0.37	0.37	0.6	28.40	107.70
22. Aug 94	2x	47	0.40	0.41	1.5	28.68	74.00
24. Aug 94	2x	47	0.40	0.41	0.7	28.39	79.60
26. Aug 94	2x	47	0.40	0.41	0.4	27.34	78.80
28. Aug 94	2x	47	0.40	0.41	0.7	26.59	77.50
24. Aug 94	2x	34	0.36	0.35	0.8	14.19	63.40
26. Aug 94	2x	34	0.36	0.35	0.7	12.98	62.90
28. Aug 94	2x	34	0.36	0.35	1.1	12.22	61.30
03. Jul 95	2x	34	0.34	0.23		7.32	59.10
08. Aug 95	2x	34	0.34	0.34		17.92	67.20
01. Jul 95	2x	34	0.34	0.21		6.81	58.20
22. Aug 94	2x	23	0.38	0.38	3.1	15.14	59.30
24. Aug 94	2x	23	0.38	0.38	0.9	15.32	58.70
26. Aug 94	2x	23	0.38	0.38	1.4	14.88	53.60
28. Aug 94	2x	23	0.38	0.38	1.5	14.35	48.10

22. Jun 95	2x	23	0.41	0.36		9.77	48.50
03. Jul 95	2x	23	0.41	0.33		9.67	50.10
13. Jul 95	2x	23	0.41	0.31		9.56	56.80
22. Aug 95	2x	23	0.41	0.41		20.10	56.00
22. Aug 94	2x	65	0.34	0.33	0.8	27.32	106.50
26. Aug 94	2x	65	0.34	0.33	0.1	25.60	111.00
28. Aug 94	2x	65	0.34	0.33	0.3	25.62	108.90
08. Aug 95	2x	65	0.35	0.34		20.23	118.80
12. Aug 94	2a	78	0.30	0.28	0.1	6.51	34.30
15. Aug 94	2a	78	0.30	0.28	-0.1	6.60	34.80
17. Aug 94	2a	78	0.30	0.28	0.0	6.41	29.80
20. Aug 94	2a	78	0.30	0.28	-0.1	6.55	31.60
22. Aug 94	2a	78	0.30	0.28	0.1	6.36	33.40
24. Aug 94	2a	78	0.30	0.28	0.0	6.77	35.70
28. Aug 94	2a	78	0.30	0.28	-0.7	6.60	32.90
28. Aug 94	2a	41	0.30	0.20	0.9	3.54	29.20
30. Jul 94	2a	15	0.30	0.11	10.2	2.09	33.60
09. Aug 94	2a	15	0.30	0.11	4.3	2.36	34.20
15. Aug 94	2a	15	0.30	0.11	1.1	2.56	29.90
22. Aug 94	2a	15	0.30	0.12	3.3	2.48	29.50
24. Aug 94	2a	15	0.30	0.11	1.9	2.42	31.30
28. Aug 94	2a	15	0.30	0.11	2.1	2.45	28.80
07. Aug 94	2b	54	0.32	0.29	0.7	11.55	43.20
12. Aug 94	2b	54	0.32	0.29	1.1	11.39	42.60
03. Aug 94	2b	37	0.30	0.26	2.6	9.85	36.70
07. Aug 94	2b	37	0.30	0.25	1.6	14.76	35.70
12. Aug 94	2b	37	0.30	0.25	2.1	14.58	35.50
20. Aug 94	2b	37	0.30	0.25	1.6	14.58	33.80
26. Aug 94	2b	37	0.30	0.28	0.6	14.01	36.00
28. Aug 94	2b	37	0.30	0.28	0.9	13.90	35.70
28. Aug 94	2b	17	0.30	0.21	2.1	9.31	33.00
03. Aug 94	2c	52	0.30	0.28	2.2	9.37	47.30
07. Aug 94	2c	52	0.30	0.28	1.0	10.96	44.50
09. Aug 94	2c	52	0.30	0.28	1.3	10.69	44.90
12. Aug 94	2c	52	0.30	0.27	1.5	10.69	43.90
15. Aug 94	2c	52	0.30	0.27	0.5	10.86	44.40
17. Aug 94	2c	52	0.30	0.27	1.3	10.61	39.40
20. Aug 94	2c	52	0.30	0.27	1.0	10.97	37.80
21. Aug 94	2c	52	0.30	0.29	1.3	11.35	42.20
24. Aug 94	2c	52	0.30	0.29	0.8	11.42	43.40
26. Aug 94	2c	52	0.30	0.29	0.4	11.44	43.60
28. Aug 94	2c	52	0.30	0.28	0.7	11.39	49.30
07. Aug 94	2c	30	0.36	0.14	2.9	4.95	40.00
09. Aug 94	2c	30	0.36	0.14	2.9	4.82	40.50
12. Aug 94	2c	30	0.36	0.14	3.2	4.90	40.00
15. Aug 94	2c	30	0.36	0.13	1.0	4.81	40.30
17. Aug 94	2c	30	0.36	0.14	3.1	4.81	35.60
21. Aug 94	2c	30	0.36	0.19	3.3	6.12	38.60
24. Aug 94	2c	30	0.36	0.36	1.1	11.72	40.00
26. Aug 94	2c	30	0.36	0.36	1.1	11.81	43.50
28. Aug 94	2c	30	0.36	0.17	1.5	5.28	39.40
03. Aug 94	2c	13	0.30	0.20	8.9	5.01	40.20
07. Aug 94	2c	13	0.30	0.16	9.2	3.82	38.50
09. Aug 94	2c	13	0.30	0.16	8.7	3.63	38.80

15. Aug 94	2c	13	0.30	0.15	5.5	3.72	37.80
17. Aug 94	2c	13	0.30	0.15	8.1	3.37	33.70
20. Aug 94	2c	13	0.30	0.15	8.0	3.50	34.90
24. Aug 94	2c	13	0.30	0.20	5.5	4.94	38.20
26. Aug 94	2c	13	0.30	0.19	6.7	4.50	38.70
28. Aug 94	2c	13	0.30	0.18	6.3	4.11	39.10
03. Aug 94	2d	46	0.44	0.46	1.6	19.72	46.80
07. Aug 94	2d	46	0.44	0.46	0.7	20.51	46.70
09. Aug 94	2d	46	0.44	0.46	0.8	20.75	46.90
12. Aug 94	2d	46	0.44	0.46	0.4	21.18	46.10
15. Aug 94	2d	46	0.44	0.46	1.0	20.18	46.40
17. Aug 94	2d	46	0.44	0.46	0.9	20.55	40.90
20. Aug 94	2d	46	0.44	0.46	0.9	20.44	43.80
22. Aug 94	2d	46	0.44	0.46	1.0	20.52	44.30
24. Aug 94	2d	46	0.44	0.46	0.7	20.49	46.10
26. Aug 94	2d	46	0.44	0.46	-0.1	21.18	45.50
28. Aug 94	2d	46	0.44	0.46	0.8	20.64	45.90
07. Aug 94	2d	26	0.44	0.45	1.9	29.58	63.20
09. Aug 94	2d	26	0.44	0.46	2.1	29.03	64.10
12. Aug 94	2d	26	0.44	0.45	2.6	20.02	62.70
15. Aug 94	2d	26	0.44	0.45	1.1	17.39	62.90
17. Aug 94	2d	26	0.44	0.45	2.5	17.40	54.50
22. Aug 94	2d	26	0.44	0.45	2.3	17.33	55.10
26. Aug 94	2d	26	0.44	0.46	0.4	17.44	58.90
28. Aug 94	2d	26	0.44	0.46	1.6	16.84	58.10
03. Aug 94	2d	6	0.42	0.42	5.3	20.36	66.20
07. Aug 94	2d	6	0.42	0.42	5.6	21.77	66.40
09. Aug 94	2d	6	0.42	0.42	5.4	22.40	67.20
12. Aug 94	2d	6	0.42	0.42	5.5	22.73	65.70
15. Aug 94	2d	6	0.42	0.43	1.9	23.38	67.50
17. Aug 94	2d	6	0.42	0.43	4.9	23.40	59.50
20. Aug 94	2d	6	0.42	0.43	4.4	24.15	64.00
22. Aug 94	2d	6	0.42	0.43	4.0	24.40	65.50
24. Aug 94	2d	6	0.42	0.44	2.1	24.29	66.50
28. Aug 94	2d	6	0.42	0.44	2.7	24.50	64.80

Slope 3

Date	Site	Depth	θ_{sat}	θ	Soil temperature	σ_b TDR	σ_w Suction lysimeter
		[cm]	[$m^3 m^{-3}$]	[$m^3 m^{-3}$]	[°C]	[$mS m^{-1}$]	[$mS m^{-1}$]
07. Aug 94	3a	45	0.53	0.56	-0.1	32.32	115.00
10. Aug 94	3a	45	0.53	0.56	0.0	34.30	121.80
13. Aug 94	3a	45	0.53	0.58	0.1	36.28	125.90
15. Aug 94	3a	45	0.53	0.58	0.0	32.23	121.20
21. Aug 94	3a	45	0.53	0.58	0.2	33.46	126.90
25. Aug 94	3a	45	0.53	0.60	0.1	37.33	135.80
27. Aug 94	3a	45	0.53	0.59	0.1	38.15	137.40
29. Aug 94	3a	45	0.53	0.58	0.1	41.39	143.20
07. Aug 94	3a	24	0.49	0.52	1.6	19.31	73.00
10. Aug 94	3a	24	0.49	0.52	1.6	20.04	75.70

13. Aug 94	3a	24	0.49	0.53	1.8	20.77	75.60
15. Aug 94	3a	24	0.49	0.54	1.0	19.61	75.20
21. Aug 94	3a	24	0.49	0.54	1.5	17.55	78.90
25. Aug 94	3a	24	0.49	0.54	1.0	17.69	83.60
27. Aug 94	3a	24	0.49	0.54	1.2	18.11	78.10
29. Aug 94	3a	24	0.49	0.53	1.1	22.22	73.80
07. Aug 94	3b	32	0.47	0.50	0.1	18.53	216.00
10. Aug 94	3b	32	0.47	0.50	0.1	18.75	241.00
13. Aug 94	3b	32	0.47	0.51	0.1	19.43	218.00
15. Aug 94	3b	32	0.47	0.51	0.0	20.37	203.00
21. Aug 94	3b	32	0.47	0.51	0.1	20.98	186.40
25. Aug 94	3b	32	0.47	0.51	0.1	21.56	185.90
27. Aug 94	3b	32	0.47	0.51	0.1	21.95	206.00
29. Aug 94	3b	32	0.47	0.50	0.0	21.76	225.00
07. Aug 94	3b	20	0.40	0.41	1.3	13.72	128.00
10. Aug 94	3b	20	0.40	0.41	0.9	13.65	137.70
13. Aug 94	3b	20	0.40	0.41	0.8	13.67	137.30
15. Aug 94	3b	20	0.40	0.41	0.5	13.92	127.00
21. Aug 94	3b	20	0.40	0.41	0.9	13.99	132.00
25. Aug 94	3b	20	0.40	0.41	0.8	14.22	155.50
27. Aug 94	3b	20	0.40	0.40	0.9	13.34	170.90
29. Aug 94	3b	20	0.40	0.39	0.5	13.28	163.00
07. Aug 94	3c	30	0.46	0.45	-0.1	13.28	118.00
13. Aug 94	3c	30	0.46	0.49	-0.1	14.65	130.60
15. Aug 94	3c	30	0.46	0.48	-0.1	14.81	125.50
21. Aug 94	3c	30	0.46	0.49	0.0	15.55	139.60
25. Aug 94	3c	30	0.46	0.49	0.0	15.94	136.50
27. Aug 94	3c	30	0.46	0.49	0.0	16.28	144.30
29. Aug 94	3c	30	0.46	0.48	-0.1	16.43	139.00
07. Aug 94	3c	19	0.49	0.53	1.3	11.68	130.00
10. Aug 94	3c	19	0.49	0.53	0.8	11.73	135.10
13. Aug 94	3c	19	0.49	0.54	0.7	12.20	133.40
15. Aug 94	3c	19	0.49	0.54	0.4	12.96	124.60
21. Aug 94	3c	19	0.49	0.54	1.0	13.00	133.60
27. Aug 94	3c	19	0.49	0.55	0.9	14.55	143.60
29. Aug 94	3c	19	0.49	0.54	0.5	14.58	137.00
07. Aug 94	3e	28	0.54	0.55	0.0	11.36	93.00
10. Aug 94	3e	28	0.54	0.55	0.1	11.26	106.10
13. Aug 94	3e	28	0.54	0.55	0.2	11.20	106.00
15. Aug 94	3e	28	0.54	0.55	0.0	11.79	106.80
21. Aug 94	3e	28	0.54	0.55	0.3	11.14	110.20
29. Aug 94	3e	28	0.54	0.55	0.1	10.72	106.00
07. Aug 94	3f	26	0.50	0.49	0.0	10.02	80.00
13. Aug 94	3f	26	0.50	0.49	0.0	9.95	93.60
15. Aug 94	3f	26	0.50	0.49	-0.1	9.84	95.90
21. Aug 94	3f	26	0.50	0.49	0.1	10.36	110.90
27. Aug 94	3f	26	0.50	0.49	0.1	10.55	112.30
29. Aug 94	3f	26	0.50	0.49	-0.1	10.01	117.00

Table A.2. Grain size distribution of sites in the Levinson-Lessing lake catchment expressed as percent weight.

Site	Sampling depth	Grain size [mm] >8	>4	>2	>1	>0.5	>0.25	>0.125	>0.063	>0.002	<0.002
		Percent weight [%]									
1a	int	54.4	9.5	7.0	4.8	3.3	2.9	2.8	2.9	10.0	2.3
1a	bot	62.3	8.3	5.1	3.8	3.2	2.7	2.4	2.9	7.8	1.6
1b	top	53.1	5.5	4.2	3.5	3.4	3.6	3.8	4.4	15.1	3.4
1b	bot	47.7	4.9	4.4	3.9	4.0	3.8	4.2	3.9	17.7	5.4
1c	top	15.1	12.5	6.8	4.2	3.4	3.5	4.6	5.2	30.0	14.8
1c	bot	42.1	8.4	5.0	3.0	2.3	2.1	3.1	3.1	19.7	11.0
1x	int	31.9	14.3	10.1	6.6	2.9	4.2	4.0	3.7	16.9	5.4
2a	int	28.7	16.5	11.5	9.8	8.8	4.6	6.3	4.3	8.9	0.6
2b	int	12.7	7.5	7.9	7.1	7.9	7.2	7.5	7.9	27.3	7.0
2c	int	33.2	7.5	6.2	4.8	5.1	5.9	6.7	7.3	19.6	3.8
2d	int	0.9	2.5	1.9	2.1	5.5	16.6	25.3	19.6	24.8	0.7
2x	top	26.8	10.9	6.3	4.0	4.5	8.0	10.9	8.8	17.8	2.0
3a	int	18.4	0.3	0.2	0.2	0.8	5.7	14.5	26.4	28.5	5.1
3b	int	12.1	9.6	5.4	4.1	4.9	7.1	9.4	9.6	27.8	9.9
3c	int	6.7	2.9	3.6	3.5	4.8	8.2	13.2	13.7	31.9	11.7
3x	top	0.0	0.0	0.1	0.4	3.3	13.3	27.2	22.2	26.5	7.1
3x	bot	4.1	2.3	2.1	1.7	3.3	9.1	17.0	17.2	32.1	11.2

Sampling depth: int = sample integrated across soil column, bot = sample taken from bottom of soil pit, top = sample taken from top of soil pit

Table A.3. Daily average, minimum and maximum data of the KRASNAJA weather station. 360° = North.

Date 1995	Air temp. [°C]	Min. air temp. [°C]	Max. air temp. [°C]	Rel. humidity [%]	Min. rel. humid. [%]	Max. rel. humid. [%]	Solar radiation [W m^{-2}]	Net radiation [W m^{-2}]	Wind speed [m s^{-1}]	Wind direction degree	Wind direct. Std. dev.	Soil temp. (15cm depth) [°C]
08. Jun	0.4	-0.6	2.2	88.6	73.8	95.1	156.3		13.0	100.3	11.3	-0.3
09. Jun	1.8	0.0	4.1	88.5	75.0	91.5	119.1		4.2	5.5	20.1	-0.3
10. Jun	1.0	-0.5	2.3	91.7	83.1	94.5	64.1	75.97	4.0	334.7	6.8	-0.2
11. Jun	-0.1	-0.7	1.1	90.6	83.2	95.0	117.8	55.87	6.5	340.8	5.7	-0.2
12. Jun	0.6	-0.7	1.8	93.9	72.1	95.1	184.4	89.44	3.5	355.8	7.2	-0.1
13. Jun	0.1	-1.4	1.3	85.7	76.4	94.4	124.3	94.04	4.3	148.5	12.6	-0.1
14. Jun	1.2	0.0	2.6	90.4	84.3	93.6	116.7	83.61	6.6	4.4	13.0	0.0
15. Jun	0.7	-0.1	1.8	92.1	89.7	95.6	70.9	69.51	5.9	335.4	6.9	0.0
16. Jun	2.5	0.3	5.2	83.3	73.1	95.2	131.4	58.41	2.5	244.4	10.4	0.2
17. Jun	1.9	-0.2	3.6	84.7	65.4	94.3	162.6	81.44	5.1	79.1	7.8	0.5
18. Jun	2.5	0.5	4.6	89.1	63.6	94.4	117.1	66.17	2.9	118.5	15.3	0.7
19. Jun	3.7	0.8	8.5	96.8	67.9	96.8	87.6	60.70	5.7	3.7	14.7	1.0
20. Jun	1.7	0.8	2.5	92.9	81.9	94.7	140.8	68.52	3.4	168.0	11.1	1.4
21. Jun	1.3	-0.3	3.4	86.8	77.1	96.3	143.1	76.95	5.7	337.7	6.8	1.3
22. Jun	-0.6	-2.1	1.8	78.2	69.0	91.5	205.3	73.94	6.8	334.0	7.6	0.8

23. Jun	0.3	-2.9	4.0	67.3	62.5	91.4	253.6	57.98	5.4	315.8	9.8	1.0
24. Jun	3.9	0.6	6.9	55.9	49.5	81.1	218.3	66.42	6.3	289.8	16.4	1.4
25. Jun	7.6	3.1	11.3	69.1	54.3	78.0	296.8	96.38	2.7	196.7	17.6	3.2
26. Jun	8.3	2.6	12.4	84.3	59.2	88.7	268.9	48.80	3.4	216.1	7.5	4.3
27. Jun	7.1	1.3	14.1	78.4	59.3	88.3	173.7	74.41	7.3	215.6	9.1	4.5
28. Jun	4.5	1.1	7.9	61.8	49.8	80.1	259.1	53.22	5.2	225.3	12.9	3.2
29. Jun	5.2	1.5	7.7	97.2	61.3	97.2	113.6	54.01	8.5	139.6	6.6	3.8
30. Jun	8.0	2.3	13.1	81.6	51.2	97.2	245.6	61.25	3.0	223.5	11.0	4.7
01. Jul	3.6	0.2	8.9	88.1	78.6	93.9	32.8	49.13	4.9	335.5	9.7	3.9
02. Jul	2.6	-0.1	6.2	84.5	74.4	91.3	108.2		5.5	346.5	8.3	1.9
03. Jul	4.9	2.4	7.3	87.7	67.7	90.5	224.5		4.3	349.1	9.0	3.9
04. Jul	4.0	2.0	6.7	82.6	76.0	94.5	137.8		6.0	351.3	8.7	3.5
05. Jul	4.0	0.1	7.3	82.1	66.2	90.4	113.3		4.8	353.8	7.6	3.2
06. Jul	6.6	2.5	11.6	74.0	53.0	92.6	230.3		2.3	341.5	17.2	5.0
07. Jul	11.3	7.0	16.0	78.0	45.9	80.2	302.5		2.5	316.9	16.6	7.2
08. Jul	9.3	6.2	14.5	80.4	61.5	87.6	240.0		2.9	211.0	9.1	7.3
09. Jul	8.7	4.8	13.4	82.4	58.7	90.3	194.4		3.0	208.0	6.7	6.8
10. Jul	12.1	6.3	16.1	67.7	48.8	88.1	213.8		2.7	276.3	10.5	7.2
04. Aug	6.7	5.2	9.0	90.3	77.3	93.0	59.8		3.4	333.3	13.9	4.9
05. Aug	5.4	3.4	8.4	81.0	59.2	94.7	121.1	67.65	3.2	286.3	11.3	4.4
06. Aug	6.7	2.5	10.6	79.1	58.6	87.2	138.3	45.46	6.1	185.3	10.3	4.1
07. Aug	8.5	6.3	12.1	72.6	52.7	94.7	147.8	27.18	6.4	237.4	18.0	5.1
08. Aug	7.4	4.4	11.3	92.7	53.3	93.5	109.3	25.74	4.9	211.6	14.8	4.4
09. Aug	6.1	3.3	9.6	83.3	60.4	95.0	113.5	34.89	5.0	316.3	8.5	4.6
10. Aug	6.4	2.2	10.9	83.4	57.6	87.7	205.5	48.49	3.4	163.8	13.5	4.3
11. Aug	9.4	3.3	15.0	73.9	64.0	91.3	102.1	40.64	5.2	178.8	12.9	4.9
12. Aug	11.2	4.4	19.1	87.7	73.0	93.6	56.7	34.77	5.1	325.9	11.1	6.9
13. Aug	5.4	0.9	8.8	87.9	82.3	97.1	58.0	22.47	2.6	239.2	9.3	4.4
14. Aug	4.6	0.1	8.5	86.5	71.6	92.1	96.5	39.99	4.7	347.8	8.9	4.0
15. Aug	0.7	-0.8	3.2	77.9	66.5	90.4	116.4	43.63	4.7	354.0	9.0	2.0
16. Aug	3.9	1.0	5.7	92.3	68.5	94.0	66.5	37.50	3.2	320.1	11.1	2.3
17. Aug	5.2	1.7	10.8	89.6	64.6	96.2	82.7	45.29	2.2	347.5	10.7	3.4
18. Aug	8.2	2.4	14.3	83.6	58.0	97.6	179.0	37.15	4.9	176.0	7.4	4.2
19. Aug	7.9	2.9	12.7	96.3	81.7	97.2	113.2	24.84	4.2	199.1	12.7	4.9
20. Aug	12.1	5.2	19.3	96.4	65.6	98.4	151.4	51.71	4.0	179.9	12.6	6.4
21. Aug	10.4	5.0	17.3	96.9	56.7	98.9	144.0	43.73	2.5	207.8	12.9	6.9
22. Aug	9.2	5.1	13.1	93.6			52.9	37.20	1.0	160.7	12.9	6.1
23. Aug	11.8	7.2	18.4	96.0			109.9	35.47	1.4	188.0	12.6	7.1
24. Aug	8.7	4.9	13.7	98.5			133.8	23.08	2.6	165.8	9.0	5.8
25. Aug	11.2	8.9	14.7	81.6			90.5	55.56	5.1	156.8	11.2	6.5
26. Aug	8.5	6.3	10.9	82.7			69.9	23.23	5.0	179.5	7.6	5.5
27. Aug	8.4	6.2	11.7	84.1			70.4	18.09	4.9	210.6	8.8	5.2
28. Aug	6.2	4.4	7.9	86.2			37.0	34.08	2.6	309.5	7.2	4.5
29. Aug	6.4	2.9	9.9	91.0			59.8	25.86	2.4	224.0	9.1	4.1
30. Aug	5.1	1.7	8.0	90.6			55.9	25.32	2.8	226.2	6.5	3.6
31. Aug	7.1	5.2	8.6	89.6			11.9	25.81	5.0	201.2	8.9	4.3
01. Sep	6.2	4.4	9.6	71.8			39.3	10.47	4.3	214.4	11.8	4.0
02. Sep	3.3	2.1	5.5	85.3			47.3	21.56	8.4	281.8	9.4	2.9
03. Sep	2.2	1.3	3.2	82.6			43.6	26.88	5.4	279.8	12.1	2.1
04. Sep	1.7	0.8	3.5	88.8			51.6	27.47	4.7	293.4	9.1	1.8

05. Sep	1.8	0.3	4.3	93.7			73.0	31.63	4.7	303.2	7.8	1.7
06. Sep	2.2	0.8	4.3	89.8			46.0	24.03	4.5	319.0	7.3	1.9
07. Sep	-0.3	-1.2	1.1	82.6			40.7	27.42	3.7	310.3	9.1	1.1
08. Sep	1.4	-0.6	3.3	88.8			63.9	21.47	2.6	194.2	11.3	0.8
09. Sep	0.0	-1.8	1.2	76.2			55.5	33.38	5.2	133.9	13.1	0.9
10. Sep	-2.0	-5.2	-0.3	82.2			72.0	29.54	5.9	329.3	8.6	0.2
11. Sep	-3.9	-5.0	-1.7	83.5			54.5	6.27	7.7	305.7	7.5	0.0
12. Sep	-2.8	-4.3	-0.8	84.2			75.0	10.11	7.0	280.2	8.8	0.0
13. Sep	-3.6	-4.6	-2.5	85.8			45.2	33.31	3.8	257.0	9.1	0.0
14. Sep	-3.8	-5.1	-2.2	86.8			48.2	20.18	5.7	251.5	11.2	0.0
15. Sep	-3.8	-9.2	-1.4	87.6			75.5	7.08	5.0	104.0	8.8	0.0
16. Sep	-2.5	-6.0	-0.3	88.2			44.4		3.3	311.0	8.3	0.0
17. Sep	-2.8	-4.7	-0.7	84.6			45.6	5.58	1.7	210.0	14.3	0.0
18. Sep	-3.4	-6.1	-1.2	79.7			68.1	5.45	3.2	179.7	13.4	0.0
19. Sep	-4.7	-6.8	-2.1	77.0			39.3	2.46	3.0	298.1	9.5	0.0
20. Sep	-0.7	-3.4	0.8	93.7			48.0	7.87	4.3	230.4	10.1	0.0
21. Sep	-0.6	-3.8	1.2	84.1	81.1	95.5	35.3	21.81	7.4	294.4	8.9	0.0
22. Sep	-2.7	-3.7	-1.6	89.9	72.4	90.4	33.5	4.52	5.0	304.2	7.3	0.0
23. Sep	-1.7	-3.6	-0.5	92.4	83.0	93.6	28.1	9.78	2.0	163.7	7.8	0.0
24. Sep	-1.8	-2.8	-0.9	92.6	83.8	94.9	44.2	14.43	4.6	185.8	6.6	0.0
25. Sep	-3.1	-5.1	-1.7	85.9	74.8	94.1	37.8		3.3	170.1	19.0	0.0
26. Sep	-4.0	-9.0	-2.2	86.4	77.1	90.2	39.2		6.5	90.4	13.9	0.0
27. Sep	-3.7	-4.6	-2.6	84.7	74.5	89.6	39.3		4.2	122.7	9.2	0.0
28. Sep	-6.4	-8.6	-3.3	93.7	79.8	94.1	33.4	3.49	4.4	349.3	9.7	-0.1
29. Sep	-4.4	-8.4	-1.1	88.1	81.1	93.9	22.8	8.76	3.2	349.1	19.7	-0.2
30. Sep	-2.3	-4.1	-1.2	86.4	75.4	91.4	21.5	1.45	3.4	76.2	12.3	-0.1
01. Oct	-3.7	-4.8	-2.3	88.0	73.0	90.6	25.8		3.1	16.2	13.3	-0.1
02. Oct	-5.0	-7.8	-4.0	85.4	74.9	90.3	26.5		3.1	339.0	15.9	-0.2
03. Oct	-5.1	-10.0	-3.2	92.9	83.3	94.6	28.1		2.4	353.0	10.8	-0.2
04. Oct	-8.4	-11.4	-5.6	85.9	81.2	94.7	33.0		3.9	157.2	7.1	-0.5
05. Oct	-9.6	-11.1	-7.9	91.4	80.7	92.5	22.1		4.8	130.4	7.4	-0.9
06. Oct	-12.1	-16.5	-9.4	83.8	79.4	92.5	22.6		3.7	165.0	11.1	-1.4
07. Oct	-17.8	-21.1	-10.2	83.9	77.2	89.0	33.3		2.2	7.0	14.6	-2.3
08. Oct	-13.4	-18.2	-7.1	83.4	80.6	88.2	15.5		4.3	352.8	13.0	-3.6
09. Oct	-5.2	-7.4	-3.5	85.1	80.7	89.3	12.8		4.3	344.8	9.4	-2.7
10. Oct	-4.5	-6.3	-3.4	85.7	78.1	88.3	6.7		4.1	69.7	10.4	-2.3
11. Oct	-5.7	-6.5	-4.8	85.5	77.6	88.8	10.7		5.0	120.2	7.2	-2.4
12. Oct	-10.0	-12.9	-6.5	89.5	76.8	91.2	10.1		3.9	156.6	10.3	-3.0
13. Oct	-13.4	-15.9	-11.9	83.7	74.7	90.2	11.1		4.6	181.4	7.6	-3.9

Table A.4. Daily average, minimum and maximum data of the climate station at site 2x. 360° = North.

Date	Relative humidity [%]	Air tempe-rature [°C]	Net radiation [W m^{-2}]	Wind speed [m s^{-1}]	Wind direction degree	Wind direct. Std. dev.	Rain [mm]	Min. air temp. [°C]	Max. air temp. [°C]
23. May 95	90.8	-0.5	84.18	5.3	143.6	53.9	0.0	-2.8	1.2
24. May 95	87.1	-1.0	114.29	9.3	305.5	15.3	0.0	-3.4	1.5
25. May 95	88.6	-2.9	36.05	6.9	320	13.6	0.0	-3.7	-1.9
26. May 95	86.4	-1.1	23.04	4.2	142.1	21.2	0.0	-4.2	0.9
27. May 95	86.5	-3.5	44.97	8.1	337.3	25.6	0.0	-7.2	0.4
28. May 95	78.9	-5.0	60.17	5.4	288.5	26.5	0.0	-10.2	-2.2
29. May 95	76.5	-2.8	108.56	5.1	163.1	28.4	0.0	-4.9	-1.0
30. May 95	81.1	-3.8	69.88	7.4	106.6	39.6	0.0	-5.3	-1.3
31. May 95	80.5	-3.2	112.64	7.7	236.6	44.6	0.0	-4.9	-1.1
01. Jun 95	79.4	-2.8	123.08	3.9	350.1	85.3	0.0	-3.7	-1.5
02. Jun 95	90.1	-2.6	29.82	6.6	338.7	14.8	0.0	-5.0	0.2
03. Jun 95	87.6	-0.7	66.86	3.5	60.01	95.7	0.0	-2.8	0.8
04. Jun 95	89.5	0.8	154.84	6.5	330.7	17.3	0.0	-1.1	2.6
05. Jun 95	83.4	1.9	187.45	3.7	312.9	86.5	0.0	-0.7	4.8
06. Jun 95	87.9	1.4	93.80	2.9	83.8	70.7	0.0	0.3	2.5
07. Jun 95							0.0		
08. Jun 95							5.0		
09. Jun 95							0.0		
10. Jun 95							2.3		
11. Jun 95							0.1		
12. Jun 95							0.0		
13. Jun 95							0.1		
14. Jun 95							0.5		
15. Jun 95	94.5	1.6	60.69	5.4	332.2	20.0	7.0	1.0	2.5
16. Jun 95	75.9	5.2	54.56	2.7	31.5	29.9	1.2	0.0	6.0
17. Jun 95	80.8	3.1	139.68	4.9	72	16.8	0.2	1.1	4.9
18. Jun 95	82.9	3.6	111.91	3.2	86.6	63.0	1.6	1.6	5.5
19. Jun 95	89.8	4.6	75.72	5.3	0.997	63.1	5.7	1.7	8.9
20. Jun 95	91	2.4	85.11	3.8	110.3	58.5	0.4	1.0	3.4
21. Jun 95	90.4	2.2	115.11	5.4	324.3	14.3	0.0	1.0	4.2
22. Jun 95	81.4	0.3	141.05	6.6	322.5	13.0	0.0	-1.1	1.9
23. Jun 95	75.4	1.2	171.31	4.9	311.7	28.2	0.0	-1.6	5.1
24. Jun 95	61.85	5.0	135.53	5.2	297.4	44.2	0.0	1.6	8.2
25. Jun 95	59.48	9.4	181.46	2.9	181.3	84.0	0.0	5.0	13.0
26. Jun 95	60.08	11.9	165.63	3.0	158.9	47.8	0.0	7.5	15.5
27. Jun 95	72.5	9.3	129.93	6.0	164	70.5	0.0	2.3	15.9
28. Jun 95	62.87	5.7	168.83	4.7	217	57.4	0.0	2.1	9.3
29. Jun 95	77.4	6.7	106.48	7.8	111.6	18.5	0.8	5.6	8.5
30. Jun 95	69.76	9.9	160.78	2.8	202.6	84.6	0.2	3.5	14.8
01. Jul 95	90.5	4.9	29.56	5.0	336.1	38.6	8.5	1.0	11.9
02. Jul 95	86.9	3.3	78.15	5.3	342.2	13.3	0.4	0.6	6.9
03. Jul 95	81.6	5.8	158.86	3.9	340	19.9	0.0	3.2	7.5
04. Jul 95	86.7	5.0	105.77	5.7	340.7	16.7	0.0	2.8	7.0
05. Jul 95	80	5.0	92.77	4.6	342.8	14.2	0.0	1.0	7.9
06. Jul 95	73.2	7.5	140.10	2.2	317.6	42.1	0.0	3.7	11.9
07. Jul 95	61.9	12.6	182.91	2.3	313.7	53.9	0.0	7.7	16.6
08. Jul 95	70.1	13.1	150.68	2.4	172.8	66.6	0.0	9.9	16.5
09. Jul 95	70.2	11.9	129.96	2.7	161.6	40.3	0.0	8.0	14.6
10. Jul 95	63.73	14.1	116.11	2.4	349.3	75.5	0.0	10.8	16.6
11. Jul 95	61.77	14.0	178.61	4.4	345.5	21.6	0.0	11.4	16.4

12. Jul 95	64.58	12.2	144.90	5.4	0.363	23.9	0.0	9.5	15.1
13. Jul 95	67.96	10.8	91.74	2.5	307.3	76.4	0.6	8.9	13.1
14. Jul 95	67.85	8.5	143.90	3.0	339.6	72.0	0.0	3.9	13.2
15. Jul 95	65.76	12.2	112.33	3.5	127.5	26.6	2.0	9.3	15.8
16. Jul 95	78.3	12.6	132.72	5.5	99.2	17.2	12.5	8.7	17.1
17. Jul 95	87.7	13.0	49.96	7.5	104	30.2	31.7	11.1	14.4
18. Jul 95	90.6	8.7	47.12	3.0	300.9	85.6	1.0	6.0	12.6
19. Jul 95	93	6.7	57.42	2.4	290.8	69.7	16.4	4.8	8.7
20. Jul 95	93.3	7.3	91.91	4.7	323.8	16.4	1.2	4.7	10.5
21. Jul 95	87	6.7	80.10	4.5	319.5	19.2	0.0	3.5	8.4
22. Jul 95	88	5.8	57.17	6.4	341.4	13.4	0.0	3.7	7.3
23. Jul 95	78.4	11.5	179.39	5.5	78.3	67.6	0.0	5.9	16.1
24. Jul 95	82.8	10.5	140.03	8.5	111.6	10.5	0.0	7.8	12.3
25. Jul 95	86.9	11.1	103.45	4.3	129.9	20.6	0.0	9.8	12.0
26. Jul 95	81.3	12.5	132.84	4.3	164.9	74.0	1.2	7.7	18.3
27. Jul 95	74.4	10.9	162.38	4.4	350.9	28.4	0.0	6.9	15.1
28. Jul 95	71.2	13.6	146.10	2.0	197.4	68.2	0.0	8.8	18.0
29. Jul 95	78.4	13.3	59.45	3.1	146.9	35.0	3.6	10.6	15.9
30. Jul 95	85.5	10.9	73.35	3.5	307	44.0	0.6	8.0	13.0
31. Jul 95	87.3	6.9	69.78	4.2	333.9	45.8	6.5	4.3	11.4
01. Aug 95	82.8	6.7	85.60	1.8	175	47.7	1.8	4.4	8.5
02. Aug 95	82.9	8.0	96.49	2.3	124.4	50.4	0.6	6.0	10.4
03. Aug 95	81	9.0	84.25	3.5	111.6	39.2	2.4	6.8	11.3
04. Aug 95	87.9	7.6	52.49	3.3	329.2	51.9	7.9	6.0	8.8
05. Aug 95	79.2	6.4	89.77	3.1	272.7	38.0	0.0	4.3	8.8
06. Aug 95	71.8	7.9	86.80	5.5	163	28.3	0.6	4.2	11.3
07. Aug 95	71.9	9.2	89.14	5.5	219.7	54.9	3.6	7.2	12.2
08. Aug 95	75.4	8.5	55.87	5.1	199.6	32.8	1.6	5.9	11.4
09. Aug 95	80.9	6.9	74.12	4.7	305.6	40.4	0.8	4.4	10.4
10. Aug 95	73.9	7.3	111.14	3.1	132	93.2	0.0	3.0	11.7
11. Aug 95	73	11.3	61.11	5.8	144.7	16.1	0.0	7.2	16.4
12. Aug 95	85.8	12.3	38.49	4.6	322.3	59.8	4.8	5.8	19.4
13. Aug 95	90.5	7.2	44.10	2.5	132.2	89.7	0.0	4.0	9.6
14. Aug 95	85	5.4	66.79	4.5	340.6	21.1	0.0	1.1	8.8
15. Aug 95	76.4	1.5	66.51	4.5	342.9	22.6	0.0	0.0	3.9
16. Aug 95	79.9	4.8	45.26	3.1	316.5	37.7	0.0	2.3	6.4
17. Aug 95	86	6.3	46.75	2.1	355.8	66.5	0.0	2.6	10.7
18. Aug 95	73.5	10.3	86.46	4.2	130.3	31.4	0.0	3.9	14.9
19. Aug 95	85.4	11.2	69.43	3.3	168.7	54.1	0.0	5.2	16.8
20. Aug 95	84.9	14.6	86.55	3.8	136.1	52.0	0.0	8.9	19.6
21. Aug 95	83	13.4	87.21	2.1	146	65.8	0.0	7.5	17.7
22. Aug 95	84.1	13.5	55.13	1.0	69.18	82.2	0.0	8.3	18.1
23. Aug 95	85	14.4	50.12	1.3	90	100.2	0.0	10.6	19.1
24. Aug 95	89.6	12.0	81.42	1.9	137	80.7	0.0	8.0	16.1
25. Aug 95	80.3	12.9	46.88	5.9	121.2	34.9	4.2	10.3	15.8
26. Aug 95	82	10.2	17.59	5.2	163.7	22.1	0.0	8.5	12.6
27. Aug 95	84.6	9.3	44.92	4.9	193.9	61.3	0.2	7.1	11.9
28. Aug 95	85.1	7.1	22.85	2.5	317.3	46.5	0.0	5.4	8.5
29. Aug 95	85.1	7.9	28.22	2.7	123.7	94.4	0.2	5.1	10.3
30. Aug 95	86	6.2	27.94	2.5	145.6	77.0	5.0	3.1	8.9
31. Aug 95	92.1	8.4	10.20	5.0	158.5	67.3	18.2	6.3	9.7
01. Sep 95	84.7	7.2	24.86	4.7	201.6	58.8	1.0	6.0	10.1
02. Sep 95	83.2	4.2	26.86	8.0	271.3	14.7	0.6	3.2	6.2
03. Sep 95	87	3.2	22.05	4.5	274.4	27.4	1.4	2.2	4.1
04. Sep 95	87.7	2.7	35.91	4.5	287.2	23.4	0.8	1.8	4.3
05. Sep 95	88.1	2.6	44.98	4.3	297.9	13.8	0.0	1.3	4.6
06. Sep 95	89.3	3.0	29.14	4.2	316.4	18.2	0.0	1.6	5.1
07. Sep 95	80.4	0.6	19.43	3.6	315.4	36.2	0.0	0.0	2.2
08. Sep 95	79.7	2.3	34.42	2.7	165.8	47.1	0.2	0.3	3.9

09. Sep 95	85.6	0.8	30.70	5.2	12.19	47.0	0.2	-0.8	1.8
10. Sep 95	81	-1.2	19.68	5.7	323.1	17.3	0.0	-4.4	0.2
11. Sep 95	77.5	-3.0	11.52	7.6	296.6	12.3	0.2	-4.1	-1.5
12. Sep 95	78.5	-1.9	40.57	6.0	274.8	25.3	0.0	-3.3	-0.5
13. Sep 95	86.2	-2.6	18.54	3.9	344.8	25.1	0.0	-3.3	-1.7
14. Sep 95	81.6	-2.8	9.35	4.6	255.8	67.0	0.0	-4.1	-1.4
15. Sep 95							0.0		
16. Sep 95							0.0		
17. Sep 95							0.0		
18. Sep 95							0.0		
19. Sep 95							0.0		
20. Sep 95							0.0		
21. Sep 95							2.0		
22. Sep 95							0.0		
23. Sep 95							0.0		
24. Sep 95							0.0		
25. Sep 95							0.0		
26. Sep 95							0.0		
27. Sep 95	86.7	-3.1	-18.01	3.2	98.5	16.2	0.0	-3.6	0.0
28. Sep 95	88.1	-5.4	6.93	4.1	345.3	46.2	0.0	-7.6	-2.4
29. Sep 95	91.2	-3.6	-2.85	3.4	2.183	47.9	0.0	-7.4	0.0
30. Sep 95	87.2	-1.4	-2.66	3.4	62.64	55.1	0.0	-2.8	-0.5
1. Oct 95	86.5	-2.8	-3.03	2.6	35.66	75.6	0.0	-4.2	-1.8
2. Oct 95	84.7	-4.2	-6.94	2.9	4.141	22.5	0.0	-5.8	-3.3
3. Oct 95	91.6	-3.9	-5.17	2.0	10.72	30.8	0.0	-7.2	-2.5
4. Oct 95	87.8	-7.2	-11.13	4.1	125.3	29.7	0.0	-10.4	-4.5
5. Oct 95	85.2	-8.6	-17.44	5.1	106.3	37.5	0.0	-9.8	-7.1
6. Oct 95	87.9	-10.9	-7.95	2.6	95.1	82.7	0.0	-14.5	-8.5
7. Oct 95	83.2	-15.1	-15.18	1.2	39.64	57.6	0.0	-17.9	-9.4
8. Oct 95	83.8	-12.6	-1.44	3.3	6.605	21.4	0.0	-15.9	-6.9
9. Oct 95	86.3	-4.3	-4.20	3.6	359	42.6	0.0	-6.9	-2.7
10. Oct 95	87.3	-3.6	-4.98	4.2	53.61	53.5	0.0	-5.5	-2.7
11. Oct 95	86	-4.8	-9.14	5.5	94.7	13.8	0.0	-5.7	-4.0
12. Oct 95	86.1	-9.1	-26.01	4.2	123.7	44.5	0.0	-11.9	-5.7
13. Oct 95	85	-12.7	-10.60	4.0	160.1	37.9	0.0	-14.4	-11.2
14. Oct 95							0.0		
15. Oct 95							0.0		

Table A.5. Depth [cm] of installed instruments on slopes 1, 2 and 3.

Site	TDR/Temperature Probes							Suction lysimeters*					Piezometers#			Wells	
	1	2	3	4	5	6	7	1	2	3	4	5	1	2	3	1	2
1A	51	36	21	7				45	30	15			20	29		50	58
1B	57	35	20	7				45	30	13			59	29		57	57
1C	60	40	27	9				45	30	15	60		28	55		69	57
1X	53	39	23	8				45	30	15			49	27		54	
2A	78	60	41	15				74	45	17			54	22		78	
2B	75	54	37	17				50	30	15			65	26		71	
2C	77	52	30	13				52	35	15			78	39		79	
2D	46	26	6					47	26	12			35	19		46	
2X	78	65	52	47	34	23	11	61	50	40	30	20	73	37		77	
3A	45	24	9					35	15				24	27		47	
3B	32	20	11					30	15				28	15		30	
3C	30	19	9					30	15				29	13		29	
3D	31	10						15	30				40	27	16	33	
3E	28	13						15	30				21	14		22	

3F	26	16	9		25		17			24
3G							52	27	17	
3H							40	15		36
3J							43	17		40
3X	21	15	7		30	15	21	12		22

* suction lysimeter length 5 cm

depth of bottom of screened intervall [10 cm]

Table A.6. Depth of upper and lower frozen ground determined by permafrost probe and TDR measurements. Groundwater level below surface was derived from wells.

Site 2x					
Date	Groundwater level below surface	Depth of lower frozen ground		Depth of upper frozen ground	
		Permafrost probe	TDR	Permafrost probe	TDR
	[cm]	[cm]	[cm]	[cm]	[cm]
12. Jun 95	0	14			
17. Jun 95	0	20			
19. Jun 95	3				
21. Jun 95	30	33			
23. Jun 95			34		
26. Jun 95		35			
28. Jun 95	47				
30. Jun 95			52		
03. Jul 95	52				
05. Jul 95		45			
07. Jul 95			65		
08. Jul 95	65				
12. Jul 95		59			
15. Jul 95	68				
21. Jul 95	21	85			
25. Jul 95	15	84	78		
30. Jul 95	11				
07. Aug 95	11	87			
14. Aug 95	9				
21. Aug 95	14	89			
27. Aug 95	8			0	
11. Sep 95		96		8	
15. Sep 95		100		7	
20. Sep 95		95		20	11
27. Sep 95		86			
29. Sep 95				23	23
03. Oct 95					34
09. Oct 95					47

Table A.7. Stable isotope ratios of water samples taken in 1994 and 1995 in the Levinson-Lessing lake watershed. Values for σ_w and pH are given in Bolshiyanov and Hubberten (1996) and Siegert and Bolshiyanov (1995).

Sample no.	Date	Sample site	$\delta^{18}O$	δD
245	26. Aug 94	1 A SOIL 1	-17.56	-132
25	29. Jul 94	1 A SOIL 2	-18.33	-136
28	30. Jul 94	1 A SOIL 2	-18.36	-138
32	03. Aug 94	1 A SOIL 2	-18.27	-137
52	07. Aug 94	1 A SOIL 2	-18.07	-135
93	12. Aug 94	1 A SOIL 2	-18.32	-138
151	20. Aug 94	1 A SOIL 2	-18.44	-139
26	29. Jul 94	1 A SOIL 3	-15.37	-117
30	30. Jul 94	1 A SOIL 3	-15.45	-118
33	03. Aug 94	1 A SOIL 3	-15.62	-118
53	07. Aug 94	1 A SOIL 3	-15.28	-115
94	12. Aug 94	1 A SOIL 3	-15.19	-116
152	20. Aug 94	1 A SOIL 3	-14.99	-114
1	27. Jul 94	1 B SOIL 1	-18.69	-141
2	29. Jul 94	1 B SOIL 1	-18.78	-131
3	30. Jul 94	1 B SOIL 1	-18.76	-141
34	03. Aug 94	1 B SOIL 1	-18.74	-142
54	07. Aug 94	1 B SOIL 1	-18.71	-140
96	12. Aug 94	1 B SOIL 1	-18.78	-143
157	20. Aug 94	1 B SOIL 1	-18.75	-141
239	26. Aug 94	1 B SOIL 1	-18.27	-127
17	27. Jul 94	1 B SOIL 2	-18.78	-143
4	29. Jul 94	1 B SOIL 2	-18.81	-142
5	30. Jul 94	1 B SOIL 2	-18.84	-142
55	07. Aug 94	1 B SOIL 2	-18.71	-143
97	12. Aug 94	1 B SOIL 2	-18.78	-142
158	20. Aug 94	1 B SOIL 2	-18.30	-138
240	26. Aug 94	1 B SOIL 2	-18.28	-138
6	27. Jul 94	1 B SOIL 3	-17.74	-136
7	29. Jul 94	1 B SOIL 3	-17.74	-135
8	30. Jul 94	1 B SOIL 3	-17.86	-135
35	03. Aug 94	1 B SOIL 3	-18.11	-136
56	07. Aug 94	1 B SOIL 3	-18.32	-138
98	12. Aug 94	1 B SOIL 3	-18.43	-140
241	26. Aug 94	1 B SOIL 3	-18.06	-137
242	26. Aug 94	1 B PIEZO 2	-16.80	-126
57	07. Aug 94	1 B WELL	-18.66	-128
9	30. Jul 94	1 B WELL 2	-16.98	-129
156	20. Aug 94	1 B WELL 2	-14.66	-109
244	26. Aug 94	1 B WELL 2	-16.83	-129
99	12. Aug 94	1 C SOIL 0	-18.03	-136
10	27. Jul 94	1 C SOIL 1	-17.90	-136
11	29. Jul 94	1 C SOIL 1	-17.92	-135
12	30. Jul 94	1 C SOIL 1	-17.92	-136
36	03. Aug 94	1 C SOIL 1	-17.99	-137
58	07. Aug 94	1 C SOIL 1	-17.95	-136
100	12. Aug 94	1 C SOIL 1	-18.02	-137
160	20. Aug 94	1 C SOIL 1	-17.96	-137

246	26. Aug 94	1 C SOIL 1	-17.99	-137
23	29. Jul 94	1 C SOIL 2	-18.19	-138
13	30. Jul 94	1 C SOIL 2	-18.25	-138
37	03. Aug 94	1 C SOIL 2	-18.40	-140
59	07. Aug 94	1 C SOIL 2	-18.27	-138
101	12. Aug 94	1 C SOIL 2	-18.34	-140
161	20. Aug 94	1 C SOIL 2	-18.26	-139
247	26. Aug 94	1 C SOIL 2	-18.17	-139
14	29. Jul 94	1 C SOIL 3	-17.19	-132
15	30. Jul 94	1 C SOIL 3	-17.44	-133
38	03. Aug 94	1 C SOIL 3	-17.60	-136
60	07. Aug 94	1 C SOIL 3	-17.73	-133
102	12. Aug 94	1 C SOIL 3	-17.94	-138
162	20. Aug 94	1 C SOIL 3	-17.61	-135
248	26. Aug 94	1 C SOIL 3	-17.53	-136
249	26. Aug 94	1 C PIEZO 1	-16.80	-130
250	26. Aug 94	1 C PIEZO 2	-18.36	-140
29	30. Jul 94	1 C WELL 2	-16.97	-132
61	07. Aug 94	1 C WELL 1	-17.90	-136
103	12. Aug 94	1 C WELL 1	-16.53	-130
159	20. Aug 94	1 C WELL 1	-17.63	-134
251	26. Aug 94	1 C WELL 1	-16.97	-130
154	20. Aug 94	1 X SOIL 1	-18.84	-140
253	26. Aug 94	1 X SOIL 1	-18.43	-139
155	20. Aug 94	1 X SOIL 3	-17.81	-134
254	26. Aug 94	1 X SOIL 3	-17.79	-134
255	26. Aug 94	1 X PIEZO 1	-18.21	-135
256	26. Aug 94	1 X PIEZO 2	-17.94	-134
257	28. Aug 89	1 X WELL	-17.88	-133
153	20. Aug 94	1 X WELL	-18.10	-135
62	07. Aug 94	2 A SOIL 1	-17.71	-126
105	12. Aug 94	2 A SOIL 1	-17.75	-135
164	20. Aug 94	2 A SOIL 1	-17.57	-133
198	23. Aug 94	2 A SOIL 1	-17.66	-134
219	26. Aug 94	2 A SOIL 1	-17.62	-132
24	30. Jul 94	2 A SOIL 2	-17.49	-131
39	03. Aug 94	2 A SOIL 2	-17.61	-134
63	07. Aug 94	2 A SOIL 2	-17.46	-131
106	12. Aug 94	2 A SOIL 2	-17.46	-132
165	20. Aug 94	2 A SOIL 2	-17.47	-132
16	30. Jul 94	2 A SOIL 3	-17.80	-132
64	07. Aug 94	2 A SOIL 3	-17.26	-130
218	26. Aug 94	2 A SOIL 3	-16.39	-121
65	07. Aug 94	2 A WELL	-17.47	-131
107	12. Aug 94	2 A WELL	-17.52	-132
163	20. Aug 94	2 A WELL	-17.54	-130
217	26. Aug 94	2 A WELL	-17.21	-128
40	03. Aug 94	2 B SOIL 1	-17.41	-131
66	07. Aug 94	2 B SOIL 1	-17.41	-129
109	12. Aug 94	2 B SOIL 1	-17.41	-131
167	20. Aug 94	2 B SOIL 1	-17.47	-131
220	26. Aug 94	2 B SOIL 1	-17.44	-130
41	03. Aug 94	2 B SOIL 2	-17.29	-131
67	07. Aug 94	2 B SOIL 2	-17.37	-128

110	12. Aug 94	2 B SOIL 2	-17.26	-129
168	20. Aug 94	2 B SOIL 2	-17.26	-131
221	26. Aug 94	2 B SOIL 2	-17.38	-129
224	26. Aug 94	2 B PIEZO 1	-17.39	-130
223	26. Aug 94	2 B PIEZO 2	-17.26	-128
68	07. Aug 94	2 B WELL	-17.49	-129
108	12. Aug 94	2 B WELL	-17.43	-131
166	20. Aug 94	2 B WELL	-16.71	-126
222	26. Aug 94	2 B WELL	-16.84	-124
42	03. Aug 94	2 C SOIL 1	-17.52	-133
69	07. Aug 94	2 C SOIL 1	-17.21	-130
112	12. Aug 94	2 C SOIL 1	-16.82	-127
170	20. Aug 94	2 C SOIL 1	-16.25	-125
195	21. Aug 94	2 C SOIL 1	-16.90	-128
203	23. Aug 94	2 C SOIL 1	-16.90	-130
206	23. Aug 94	2 C SOIL 1	-16.79	-129
225	26. Aug 94	2 C SOIL 1	-16.54	-124
175	20. Aug 94	2 C SOIL 1	-16.81	-125
70	07. Aug 94	2 C SOIL 2	-16.09	-122
113	12. Aug 94	2 C SOIL 2	-16.03	-123
204	23. Aug 94	2 C SOIL 2	-16.33	-126
207	23. Aug 94	2 C SOIL 2	-16.31	-125
226	26. Aug 94	2 C SOIL 2	-16.36	-119
176	20. Aug 94	2 C SOIL 2	-16.25	-122
43	03. Aug 94	2 C SOIL 3	-15.30	-120
71	07. Aug 94	2 C SOIL 3	-15.46	-117
205	23. Aug 94	2 C SOIL 3	-15.48	-119
227	26. Aug 94	2 C SOIL 3	-15.85	-129
171	20. Aug 94	2 C SOIL 3	-15.38	-118
196	21. Aug 94	2 C SOIL2	-16.33	-124
197	22. Aug 94	2 C SOIL3	-15.23	-117
229	26. Aug 94	2 C PIEZO 1	-17.30	-122
230	26. Aug 94	2 C PIEZO 2	-15.44	-116
72	07. Aug 94	2 C WELL	-17.05	-127
111	12. Aug 94	2 C WELL	-17.12	-129
228	26. Aug 94	2 C WELL	-16.47	-129
44	03. Aug 94	2 D SOIL 1	-17.06	-128
73	07. Aug 94	2 D SOIL 1	-16.99	-126
115	12. Aug 94	2 D SOIL 1	-18.38	-126
173	20. Aug 94	2 D SOIL 1	-16.55	-119
208	23. Aug 94	2 D SOIL 1	-16.37	-125
211	26. Aug 94	2 D SOIL 1	-16.31	-124
178	20. Aug 94	2 D SOIL 1	-16.76	-122
74	07. Aug 94	2 D SOIL 2	-17.09	-127
116	12. Aug 94	2 D SOIL 2	-16.89	-128
209	23. Aug 94	2 D SOIL 2	-16.95	-127
212	26. Aug 94	2 D SOIL 2	-16.88	-125
45	03. Aug 94	2 D SOIL 3	-16.92	-127
75	07. Aug 94	2 D SOIL 3	-16.60	-121
174	20. Aug 94	2 D SOIL 3	-15.88	-121
210	23. Aug 94	2 D SOIL 3	-15.76	-121
213	26. Aug 94	2 D SOIL 3	-16.09	-123
117	12. Aug 94	2 D SOIL 3	-16.07	-124
179	20. Aug 94	2 D SOIL 3	-15.82	-119

214	26. Aug 94	2 D PIEZO	-16.50	-124
215	26. Aug 94	2 D PIEZO	-15.34	-118
118	12. Aug 94	2 D PIEZO 1	-16.94	-128
172	20. Aug 94	2 D WELL	-16.32	-123
89	07. Aug 94	2 D WELL	-17.05	-127
114	12. Aug 94	2 D WELL	-16.74	-127
216	26. Aug 94	2 D WELL	-16.20	-119
191	21. Aug 94	2 E SOIL 1	-18.17	-137
199	23. Aug 94	2 X SOIL 1	-19.27	-145
231	26. Aug 94	2 X SOIL 1	-19.41	-144
200	23. Aug 94	2 X SOIL 2	-19.05	-144
232	26. Aug 94	2 X SOIL 2	-19.09	-141
201	23. Aug 94	2 X SOIL 3	-18.14	-137
233	26. Aug 94	2 X SOIL 3	-18.37	-137
234	26. Aug 94	2 X SOIL 4	-17.87	-135
202	23. Aug 94	2 X SOIL 5	-18.36	-138
235	26. Aug 94	2 X SOIL 5	-18.40	-137
237	26. Aug 94	2 X PIEZO 2	-18.64	-140
236	26. Aug 94	2 X PIEZO 1	-19.08	-143
238	26. Aug 94	2 X WELL	-17.16	-128
76	07. Aug 94	3 A SOIL 1	-19.93	-151
132	13. Aug 94	3 A SOIL 1	-19.94	-150
180	21. Aug 94	3 A SOIL 1	-20.39	-152
77	07. Aug 94	3 A SOIL 2	-19.68	-149
133	13. Aug 94	3 A SOIL 2	-19.78	-150
181	21. Aug 94	3 A SOIL 2	-20.86	-157
261	27. Aug 94	3 A SOIL 2	-18.15	-140
271	27. Aug 94	3 A PIEZO 1	-19.06	-146
131	13. Aug 94	3 A PIEZO 2	-20.14	-152
259	27. Aug 94	3 A PIEZO 2	-20.41	-152
78	07. Aug 94	3 A WELL	-20.16	-153
129	13. Aug 94	3 A WELL	-19.67	-148
182	21. Aug 94	3 A WELL	-19.90	-148
258	27. Aug 94	3 A WELL	-20.54	-154
79	07. Aug 94	3 B SOIL 1	-18.57	-139
135	13. Aug 94	3 B SOIL 1	-18.59	-138
185	21. Aug 94	3 B SOIL 1	-18.62	-140
265	27. Aug 94	3 B SOIL 1	-18.91	-144
136	13. Aug 94	3 B SOIL 2	-18.82	-141
184	21. Aug 94	3 B SOIL 2	-18.65	-138
266	27. Aug 94	3 B SOIL 2	-18.57	-140
264	27. Aug 94	3 B PIEZO 2	-17.82	-132
263	27. Aug 94	3 B PIEZO 1	-18.47	-138
81	07. Aug 94	3 B WELL	-18.65	-141
134	13. Aug 94	3 B WELL	-18.55	-139
183	21. Aug 94	3 B WELL	-18.27	-135
262	27. Aug 94	3 B WELL	-18.14	-135
82	07. Aug 94	3 C SOIL 1	-19.29	-145
138	13. Aug 94	3 C SOIL 1	-19.10	-143
187	21. Aug 94	3 C SOIL 1	-19.00	-141
269	27. Aug 94	3 C SOIL 1	-18.90	-140
83	07. Aug 94	3 C SOIL 2	-19.05	-143
139	13. Aug 94	3 C SOIL 2	-19.03	-142
188	21. Aug 94	3 C SOIL 2	-18.82	-141

270	27. Aug 94	3 C SOIL 2	-18.42	-137
268	27. Aug 94	3 C PIEZO 1	-18.89	-141
84	07. Aug 94	3 C WELL	-18.73	-141
137	13. Aug 94	3 C WELL	-18.60	-139
186	21. Aug 94	3 C WELL	-17.88	-134
267	27. Aug 94	3 C WELL	-18.20	-137
85	07. Aug 94	3 D SOIL 1	-17.44	-132
142	13. Aug 94	3 D SOIL 1	-17.23	-127
274	27. Aug 94	3 D SOIL 1	-15.96	-121
190	21. Aug 94	3 D SOIL 3	-16.41	-126
273	27. Aug 94	3 D PIEZO 1	-16.52	-124
86	07. Aug 94	3 D WELL	-18.20	-137
189	21. Aug 94	3 D WELL	-16.79	-124
272	27. Aug 94	3 D WELL	-17.24	-130
88	07. Aug 94	3 E SOIL 1	-18.34	-139
143	13. Aug 94	3 E SOIL 1	-18.23	-136
277	27. Aug 94	3 E SOIL 1	-17.71	-134
87	07. Aug 94	3 F SOIL 1	-18.24	-137
144	13. Aug 94	3 F SOIL 1	-18.18	-137
192	21. Aug 94	3 F SOIL 1	-18.16	-137
278	27. Aug 94	3 F SOIL 1	-17.88	-135
276	27. Aug 94	3 E PIEZO 1	-17.80	-134
280	27. Aug 94	3 H PIEZO 1	-18.01	-139
281	27. Aug 94	3 H PIEZO 2	-17.43	-135
146	13. Aug 94	3 H WELL	-17.67	-134
193	21. Aug 94	3 H WELL	-17.18	-132
279	27. Aug 94	3 H WELL	-17.55	-132
283	27. Aug 94	3 J PIEZO 1	-17.66	-137
284	27. Aug 94	3 J PIEZO 2	-17.68	-136
282	27. Aug 94	3 J WELL	-17.74	-137
21	21. Jun 94	Snow	-24.83	-179
18	29. Jun 94	Snow	-23.45	-177
20	29. Jun 94	Snow	-26.04	-196
19	29. Jun 94	Snow	-26.25	-198
1	05. Jun 95	Snow	-27.53	-202
5	05. Jun 95	Snow	-31.10	-232
2	05. Jun 95	Snow	-29.90	-221
10	05. Jun 95	Snow	-22.67	-166
3	05. Jun 95	Snow	-32.38	-245
4	05. Jun 95	Snow	-28.92	-217
6	05. Jun 95	Snow	-26.56	-201
7	07. Jun 95	Snow	-31.34	-235
654	14. Sep 95	Snow	-30.48	-237
659	14. Sep 95	Snow	-29.47	-229
660	15. Sep 95	Snow	-22.07	-164
695	25. Sep 95	Snow/Rain ?	-14.85	-114
27	30. Jul 94	Rain	-9.35	-88
31	02. Aug 94	Rain	-10.50	-86
46	04. Aug 94	Rain	-11.02	-93
51	07. Aug 94	Rain	-17.27	-136
120	12. Aug 94	Rain	-14.67	-110
121	13. Aug 94	Rain	-15.30	-119
149	15. Aug 94	Rain	-16.81	-127
150	20. Aug 94	Rain	-12.94	-105

194	22. Aug 94	Rain	-17.56	-137
359	29. Aug 94	Rain	-16.00	-127
8	10. Jun 95	Rain	-18.58	-137
17	13. Jun 95	Rain	-17.94	-140
23	15. Jun 95	Rain	-22.75	-173
24	16. Jun 95	Rain	-19.88	-152
37	18. Jun 95	Rain	-18.72	-149
41	20. Jun 95	Rain	-22.67	-172
58	23. Jun 95	Rain	-12.77	-102
109	01. Jul 95	Rain	-18.01	-136
240	16. Jul 95	Rain	-17.99	-142
241	18. Jul 95	Rain	-11.75	-90
242	19. Jul 95	Rain		
243	20. Jul 95	Rain	-11.64	-89
389	02. Aug 95	Rain		
593	02. Aug 95	Rain	-12.20	-94
388	02. Aug 95	Rain	-15.04	-117
401	03. Aug 95	Rain	-15.71	-133
402	04. Aug 95	Rain	-25.46	-200
403	05. Aug 95	Rain	-22.05	-176
518	12. Aug 95	Rain		
579	25. Aug 95	Rain		
591	31. Aug 95	Rain		
682	21. Sep 95	Rain	-9.14	-79

Table A.8. Soil temperatures from site 2x in 1995.

Date, time	Soil temperature at depth [°C]						
1995	78cm	65cm	52cm	47cm	34cm	23cm	11cm
22.05., 17:22	-12.3	-11.5	-10.9	-10.7	-9.5	-8.3	-7.0
22.05., 17:26	-12.3	-11.5	-11.4	-10.7	-9.5	-8.2	-7.0
22.05., 17:31	-12.2	-11.5	-10.9	-10.7	-9.5	-8.2	-7.0
22.05., 17:36	-12.3	-11.5	-10.9	-10.6	-9.5	-8.3	-7.0
22.05., 17:41	-12.3	-11.5	-10.9	-10.7	-9.5	-8.2	-7.0
22.05., 17:46	-12.3	-11.5	-11.4	-10.6	-9.5	-8.2	-7.1
22.05., 17:51	-12.3	-11.5		-10.6	-9.5	-8.2	-7.1
22.05., 17:56	-12.3	-11.5		-10.7	-9.5	-8.2	-7.0
23.05., 03:04	-12.2	-11.4	-10.8	-10.5	-9.3	-8.1	-6.9
23.05., 06:01	-12.1	-11.2		-10.3	-9.2	-8.0	-6.9
23.05., 09:01	-12.0	-11.1		-10.2	-9.1	-7.9	-6.8
23.05., 12:01	-11.9	-11.0		-10.2	-8.9	-7.7	-6.4
23.05., 15:01	-11.8			-10.0	-8.8	-7.3	-6.0
23.05., 18:01	-11.8			-9.9	-8.6	-7.0	-5.5
23.05., 21:01	-11.7			-9.7	-8.3	-6.7	-5.3
24.05., 00:01	-11.6			-9.5	-8.1	-6.6	-5.2
24.05., 03:01	-11.5			-9.3	-7.9	-6.5	-5.2
24.05., 06:01	-11.3			-9.2	-7.8	-6.4	-5.2
24.05., 09:01	-11.3			-9.1	-7.8	-6.4	-5.2
24.05., 12:01	-11.2	-10.1		-9.0	-7.6	-6.3	-5.0
24.05., 15:01	-11.1			-8.9	-7.5	-6.0	-4.7
24.05., 18:01	-11.1			-8.7	-7.4	-5.8	-4.4

25.05., 03:01	-10.7			-8.5	-7.0	-5.6	-4.7
25.05., 06:01	-10.6			-8.4	-7.0	-5.8	-5.1
25.05., 09:01	-10.6			-8.3	-7.1	-6.0	-5.1
25.05., 12:01	-10.5			-8.4	-7.1	-6.0	-5.0
25.05., 15:01	-10.5			-8.3	-7.1	-5.9	-4.9
25.05., 18:01	-10.4			-8.3	-7.0	-5.8	-4.8
25.05., 21:01	-10.3			-8.3	-6.9	-5.7	-4.8
26.05., 00:01	-10.3			-8.2	-6.9	-5.7	-4.8
26.05., 03:01	-10.2	-9.1		-8.1	-6.9	-5.9	-5.3
26.05., 06:01	-10.2	-9.1		-8.1	-7.0	-6.1	-5.5
26.05., 09:01	-10.1	-9.1		-8.1	-7.0	-6.2	-5.4
26.05., 12:01	-10.1	-9.0		-8.1	-7.1	-6.1	-5.2
26.05., 15:01	-10.0	-9.1	-8.3	-8.1	-7.0	-5.9	-4.8
26.05., 18:01	-10.0	-9.0		-8.1	-6.9	-5.7	-4.5
27.05., 00:01	-10.0	-8.9	-8.5	-7.9	-6.7	-5.3	-4.3
27.05., 03:01	-9.9	-8.9		-7.8	-6.5	-5.3	-4.4
27.05., 06:01	-9.9	-8.7		-7.8	-6.5	-5.4	-4.5
27.05., 09:01	-9.7	-8.7		-7.7	-6.5	-5.4	-4.5
27.05., 12:01	-9.7	-8.6		-7.7	-6.5	-5.4	-4.5
27.05., 15:01	-9.7	-8.6	-7.9	-7.7	-6.5	-5.3	-4.3
27.05., 18:01	-9.7	-8.6	-7.9	-7.6	-6.4	-5.2	-4.3
27.05., 21:01	-9.6	-8.6		-7.5	-6.4	-5.3	-4.5
28.05., 00:01	-9.5			-7.6	-6.4	-5.4	-4.9
28.05., 03:01	-9.6			-7.5	-6.6	-5.7	-5.5
28.05., 06:01	-9.5			-7.6	-6.7	-6.1	-6.0
28.05., 09:01	-9.5	-8.5		-7.7	-6.9	-6.4	-6.1
28.05., 12:01	-9.4	-8.6	-8.1	-7.8	-7.0	-6.4	-5.7
28.05., 15:01	-9.5	-8.5		-7.8	-7.0	-6.2	-5.2
28.05., 18:01	-9.5	-8.6		-7.8	-6.9	-5.9	-4.8
30.05., 06:01	-9.2	-8.2		-7.3	-6.2	-5.3	-4.8
30.05., 09:01	-9.2	-8.2		-7.3	-6.3	-5.5	-4.9
30.05., 12:01	-9.1	-8.1		-7.3	-6.4	-5.5	-4.7
30.05., 15:01	-9.1	-8.2		-7.3	-6.3	-5.4	-4.5
30.05., 18:01	-9.0	-8.1	-7.5	-7.3	-6.3	-5.3	-4.4
30.05., 21:01	-9.0	-8.1	-7.5	-7.3	-6.3	-5.2	-4.5
31.05., 00:01	-9.0	-8.1	-7.5	-7.3	-6.2	-5.3	-4.6
31.05., 03:01	-9.0	-8.0		-7.2	-6.3	-5.4	-4.8
31.05., 06:01	-9.0	-8.0	-7.5	-7.2	-6.3	-5.5	-5.0
31.05., 09:01	-8.9	-8.0	-7.5	-7.2	-6.4	-5.6	-5.0
31.05., 12:01	-8.9	-8.0	-7.5	-7.2	-6.5	-5.6	-4.9
31.05., 15:01	-9.0	-8.0	-7.5	-7.3	-6.4	-5.5	-4.5
31.05., 18:01	-8.9	-8.0	-7.5	-7.3	-6.3	-5.2	-4.1
31.05., 21:01		-8.0	-7.4	-7.2	-6.1	-4.9	-3.8
01.06., 00:01	-8.9	-8.0	-7.4	-7.1	-6.0	-4.7	-3.7
01.06., 03:01	-8.9	-8.0	-7.3	-7.1	-5.9	-4.8	-4.0
01.06., 06:01	-8.8	-7.9	-7.3	-7.0	-5.9	-4.9	-4.3
01.06., 09:01	-8.8	-7.8		-7.0	-5.9	-5.0	-4.3
01.06., 12:01	-8.8	-7.8	-7.3	-7.0	-5.9	-4.9	-3.9
01.06., 15:01	-8.7	-7.8	-7.2	-7.0	-5.8	-4.7	-3.5
01.06., 18:01	-8.7	-7.7		-7.0	-5.8	-4.5	-3.4
01.06., 21:01	-8.7	-7.7	-7.1	-6.8	-5.6	-4.4	-3.4
02.06., 00:01	-8.6	-7.6	-7.0	-6.7	-5.5	-4.4	-3.7
02.06., 03:01	-8.6	-7.5		-6.7	-5.6	-4.5	-4.0
02.06., 06:01	-8.6	-7.5	-7.0	-6.7	-5.6	-4.8	-4.3
02.06., 09:01	-8.5	-7.5	-7.3	-6.7	-5.7	-4.9	-4.3
02.06., 12:01	-8.5	-7.6	-6.9	-6.8	-5.7	-4.8	-4.1
02.06., 15:01	-8.5	-7.5	-7.0	-6.7	-5.7	-4.7	-3.9
02.06., 18:01	-8.4	-7.5	-6.9	-6.7	-5.6	-4.6	-3.8
04.06., 00:01	-8.2	-7.2	-6.6	-6.3	-5.1	-4.0	-3.2

04.06., 03:01	-8.2	-7.1	-6.5	-6.2	-5.1	-4.1	-3.3
04.06., 06:01	-8.1	-7.1	-6.5	-6.2	-5.1	-4.1	-3.4
04.06., 09:01	-8.0	-7.1	-6.4	-6.2	-5.1	-4.1	-3.2
04.06., 12:01	-8.0	-7.1	-6.4	-6.1	-5.1	-4.0	-3.0
04.06., 15:01	-8.0	-7.1		-6.1	-5.0	-3.7	-2.5
04.06., 18:01	-8.0	-7.0		-6.1	-4.8	-3.4	-1.8
04.06., 21:01	-7.9	-6.9		-6.0	-4.6	-3.2	-1.6
05.06., 00:01	-7.9	-6.8	-6.1	-5.9	-4.5	-3.0	-1.5
05.06., 03:01	-7.9	-6.7	-6.0	-5.8	-4.3	-2.8	-1.4
05.06., 06:01	-7.8	-6.7	-6.0	-5.6	-4.2	-2.7	-1.4
05.06., 09:01	-7.7	-6.6	-5.9	-5.5	-4.2	-2.6	-1.4
05.06., 12:01	-7.7	-6.6		-5.4	-4.0	-2.6	-1.3
05.06., 15:01	-7.6	-6.5		-5.4	-4.0	-2.5	-1.1
05.06., 20:04	-7.5	-6.3	-5.6	-5.2	-3.8	-2.2	-0.7
06.06., 00:01	-7.4	-6.2	-5.4	-5.1	-3.6	-2.0	-0.6
06.06., 05:01	-7.3	-6.1	-5.3	-4.9	-3.4	-1.9	-0.5
06.06., 10:01	-7.3	-6.0	-5.2	-4.9	-3.4	-1.8	-0.5
06.06., 15:01	-7.2	-5.9	-5.1	-4.7	-3.3	-1.7	-0.5
06.06., 20:01	-7.1	-5.8	-5.0	-4.6	-3.2	-1.6	-0.4
07.06., 00:01	-7.0	-5.8	-4.9	-4.6	-3.1	-1.6	-0.4
07.06., 05:01	-6.9	-5.7	-4.8	-4.5	-3.0	-1.5	-0.4
07.06., 10:01	-6.8	-5.6	-4.8	-4.5	-3.0	-1.5	-0.4
07.06., 15:01	-6.8	-5.5	-4.7	-4.4	-2.9	-1.5	-0.3
08.06., 00:46	-6.7	-5.4	-4.6	-4.3	-2.8	-1.4	-0.2
08.06., 00:54	-6.7	-5.4	-4.6	-4.3	-2.8	-1.4	-0.3
08.06., 05:06	-6.7	-5.4	-4.5	-4.2	-2.8	-1.3	-0.3
08.06., 10:04	-6.6	-5.3	-4.5	-4.2	-2.7	-1.3	-0.3
08.06., 15:04	-6.4	-5.3	-4.5	-4.1	-2.7	-1.3	-0.3
08.06., 20:04	-6.4	-5.2	-4.4	-4.1	-2.7	-1.3	-0.3
09.06., 00:04	-6.4	-5.2	-4.4	-4.0	-2.6	-1.3	-0.3
09.06., 05:04	-6.3	-5.1	-4.3	-4.0	-2.6	-1.3	-0.3
09.06., 10:04	-6.3	-4.9	-4.3	-4.0	-2.6	-1.4	-0.3
09.06., 15:04	-6.2	-5.0	-4.2	-4.0	-2.6	-1.3	-0.2
09.06., 20:04	-6.2	-4.9	-4.2	-3.9	-2.5	-1.2	-0.2
10.06., 00:04	-6.1	-4.9	-4.1	-3.9	-2.5	-1.2	-0.2
10.06., 05:04	-6.1	-4.9	-4.0	-3.8	-2.5	-1.2	-0.2
10.06., 10:04	-6.1	-4.8	-4.0	-3.8	-2.4	-1.2	-0.2
10.06., 15:04	-6.0	-4.8	-4.0	-3.8	-2.4	-1.1	-0.1
10.06., 20:04	-5.9	-4.7	-4.0	-3.8	-2.4	-1.2	-0.1
11.06., 00:04	-5.9	-4.7	-3.9	-3.7	-2.3	-1.1	-0.1
11.06., 05:04	-5.9	-4.6	-3.9	-3.7	-2.3	-1.1	-0.2
11.06., 10:04	-5.9	-4.6	-3.9	-3.6	-2.3	-1.0	-0.2
11.06., 15:04	-5.7	-4.6	-3.9	-3.6	-2.3	-1.0	-0.1
11.06., 20:04	-5.8	-4.5	-3.8	-3.6	-2.2	-1.0	-0.1
12.06., 00:06	-5.7	-4.5	-3.8	-3.5	-2.3	-1.0	-0.1
12.06., 02:04	-5.7	-4.5	-3.8	-3.5	-2.2	-1.0	-0.1
12.06., 04:04	-5.7	-4.5	-3.8	-3.6	-2.3	-1.0	-0.1
12.06., 06:04	-4.4	-4.5	-3.8	-3.5	-2.2	-1.0	-0.1
12.06., 08:04		-4.5	-3.7	-3.5	-2.2	-1.0	-0.1
12.06., 10:04	-5.6	-4.4	-3.7	-3.5	-2.2	-1.0	0.0
12.06., 12:04	-5.7	-4.4	-3.7	-3.5	-2.3	-1.0	0.0
12.06., 14:04		-4.5	-3.7	-3.5	-2.2	-1.0	0.0
12.06., 16:04	-5.6	-4.4	-3.7	-3.4	-2.2	-1.0	0.0
12.06., 18:04	-5.6	-4.4	-3.7	-3.5		-0.9	0.1
12.06., 20:04		-4.4	-3.7	-3.4	-2.2	-0.9	0.2
12.06., 22:04	-5.6	-4.4	-3.7	-3.4	-2.1	-0.9	0.1
13.06., 00:04	-5.6	-4.4	-3.7	-3.4		-0.9	0.1
13.06., 02:04	-5.5	-4.3	-3.6	-3.4	-2.1	-0.9	0.1
13.06., 04:04	-5.5	-4.3	-3.6	-3.4	-2.1	-0.9	0.0

13.06., 06:04	-5.5	-4.3	-3.6	-3.4	-2.0	-0.8	0.1
13.06., 08:04	-5.5	-4.3	-3.6	-3.3	-2.0	-0.8	0.2
13.06., 10:04	-5.5	-4.3	-3.6	-3.3	-2.0	-0.8	0.3
13.06., 12:04	-5.4	-4.3	-3.6	-3.3	-2.0	-0.8	0.4
13.06., 14:04	-5.4	-4.3	-3.6	-3.3	-2.0	-0.8	0.4
13.06., 16:04	-5.4	-4.3	-3.6	-3.3	-2.0	-0.8	0.4
13.06., 18:04	-5.4	-4.3	-3.5	-3.2	-2.0	-0.7	0.3
13.06., 20:04	-5.4	-4.3	-3.5	-3.3	-2.0	-0.8	0.2
14.06., 14:04		-4.1	-3.4	-3.1	-1.8	-0.6	0.7
14.06., 16:04	-5.2	-4.1	-3.4	-3.1	-1.9	-0.7	0.9
14.06., 18:04		-4.1	-3.4	-3.1		-0.6	0.8
14.06., 20:04		-4.0	-3.3	-3.1	-1.9	-0.6	0.5
14.06., 22:04	-3.8	-4.0	-3.3	-3.1	-1.8	-0.6	0.3
15.06., 00:04	-5.2	-4.0	-3.3	-3.1	-1.8	-0.6	0.2
15.06., 02:04	-5.1	-4.0	-3.3	-3.0	-1.8	-0.6	0.1
15.06., 04:04	-5.1	-4.0	-3.2	-3.1	-1.8	-0.6	0.1
15.06., 06:04	-5.1	-4.0	-3.2	-3.0	-1.8	-0.5	0.1
15.06., 08:04		-3.9	-3.2	-3.0	-1.8	-0.6	0.2
15.06., 10:04		-3.9	-3.2	-2.9	-1.7	-0.5	0.3
15.06., 12:04		-4.0	-3.2	-3.0	-1.7	-0.5	0.5
15.06., 14:04	-5.0	-3.9	-3.2	-3.0	-1.7	-0.6	0.6
15.06., 16:04		-3.9	-3.2	-3.0		-0.5	0.8
15.06., 18:06	-5.0	-3.9	-3.2	-2.9	-1.7	-0.5	0.7
15.06., 21:04		-3.9	-3.2	-2.9	-1.6	-0.5	0.5
16.06., 00:04		-3.9	-3.2	-2.8	-1.6	-0.5	0.3
16.06., 03:04		-3.8	-3.2	-2.9	-1.6	-0.5	0.2
16.06., 06:04	-5.0	-3.8	-3.2	-2.8		-0.5	0.4
16.06., 09:04	-4.9	-3.8	-3.1	-2.9	-1.6	-0.5	0.9
16.06., 12:04		-3.8	-3.1	-2.8	-1.6	-0.4	1.4
16.06., 15:04		-3.7	-3.0	-2.8	-1.6	-0.4	1.7
16.06., 18:04		-3.7	-3.0	-2.8	-1.6	-0.4	1.9
17.06., 21:06	-4.7	-3.5	-2.8	-2.5		0.0	1.7
18.06., 00:04	-4.7	-3.5	-2.8	-2.5	-1.3	0.0	1.4
18.06., 03:04	-4.7	-3.5	-2.7	-2.5	-1.2	0.0	0.9
18.06., 06:04	-4.6	-3.5	-2.7	-2.5	-1.2	0.0	0.8
18.06., 09:04	-4.6	-3.4	-2.6	-2.4	-1.2	0.0	1.1
18.06., 12:04	-4.6	-3.4	-2.6	-2.4	-1.2	0.1	2.3
18.06., 15:04		-3.4	-2.6	-2.4	-1.2	0.3	3.4
18.06., 18:04	-4.5	-3.3	-2.6	-2.3	-1.1	0.2	2.9
18.06., 21:04	-4.5	-3.3		-2.3		0.4	2.9
19.06., 00:04	-4.4	-3.3	-2.5	-2.2	-1.0	0.4	2.0
19.06., 03:04	-4.4	-3.3	-2.5	-2.2	-1.0	0.3	1.2
19.06., 06:04	-4.3	-3.2	-2.6	-2.2	-1.0	0.1	0.9
19.06., 09:04		-3.2		-2.2	-0.9	0.2	1.3
19.06., 12:04		-3.1		-2.2	-0.9	0.4	2.4
19.06., 15:06		-3.2	-2.4	-2.1	-1.0	0.7	3.5
19.06., 12:04		-3.1		-2.2	-0.9	0.4	2.4
19.06., 15:06		-3.2	-2.4	-2.1	-1.0	0.7	3.5
19.06., 18:06	-4.4	-3.2		-2.1	-0.9	0.9	3.6
19.06., 20:04	-4.3	-3.1		-2.1	-0.9	0.9	3.2
19.06., 22:04	-4.3	-3.1		-2.1	-0.9	0.8	2.7
20.06., 00:04	-4.3	-3.1		-2.1	-0.9	0.8	2.2
20.06., 02:04	-4.2	-3.0		-2.1	-0.8	0.6	1.7
20.06., 04:04	-4.2	-3.0		-2.1	-0.8	0.5	1.4
20.06., 06:04	-4.2	-3.0		-2.0	-0.8	0.4	1.2
20.06., 08:04	-4.2	-2.9		-2.0	-0.8	0.4	1.1
20.06., 10:04	-4.1	-2.9		-2.0		0.4	1.2
20.06., 12:04		-2.9		-2.0	-0.7	0.4	1.4
20.06., 14:04		-2.9		-1.9	-0.7	0.6	2.1

20.06., 16:04		-2.9	-1.9	-0.7	0.8	2.4
20.06., 18:04	-4.1	-2.9	-1.9	-0.7	1.0	2.7
20.06., 20:04		-2.9	-1.9	-0.6	1.0	2.7
20.06., 22:04		-2.8	-1.9		1.0	2.6
21.06., 00:04	-4.0	-2.8	-1.8	-0.7	1.0	2.4
21.06., 02:04	-4.0	-2.8	-1.8	-0.6	0.9	2.2
21.06., 04:04	-4.1	-2.8	-1.8	-0.6	0.8	1.9
21.06., 06:04	-3.9	-2.8	-1.8	-0.6	0.7	1.6
21.06., 08:04	-3.9	-2.7	-1.8	-0.6	0.6	1.4
21.06., 10:04	-3.8	-2.8	-1.7	-0.6	0.6	1.4
21.06., 12:04	-3.9	-2.7	-1.8	-0.6	0.6	1.9
21.06., 14:04	-3.9	-2.7	-1.7	-0.5	0.9	2.4
21.06., 16:04		-2.7	-1.7	-0.6	1.1	3.0
21.06., 18:04	-3.9	-2.7	-1.8	-0.5	1.3	3.2
21.06., 21:06	-3.8	-2.7	-1.6	-0.5	1.1	2.3
22.06., 00:04	-3.8	-2.7	-1.7	-0.5	0.8	1.5
22.06., 03:04	-3.7	-2.6	-1.7	-0.5	0.5	0.9
22.06., 06:04	-3.8	-2.6	-1.7	-0.4	0.3	0.6
22.06., 09:04	-3.7	-2.6	-1.6	-0.5	0.2	0.4
22.06., 12:04	-3.7	-2.6	-1.6	-0.5	0.2	0.8
22.06., 15:04		-2.5	-1.6		0.5	1.6
22.06., 18:04	-3.7	-2.5	-1.6	-0.5	0.8	2.1
22.06., 21:04	-3.7	-2.5	-1.6	-0.4	1.0	2.1
23.06., 00:04	-3.7	-2.5	-1.6	-0.4	0.7	1.2
23.06., 03:04	-3.7	-2.5	-1.6	-0.4	0.3	0.5
23.06., 06:04	-3.7	-2.4	-1.6	-0.5	0.1	0.2
23.06., 09:04	-3.7	-2.5	-1.6	-0.4	0.0	0.1
23.06., 12:04	-3.6	-2.4	-1.6	-0.5	0.2	0.9
29.06., 16:04	-2.2	-0.8	0.3	2.0	4.1	5.7
29.06., 18:04	-2.1	-0.8	0.3	2.0	4.3	5.7
29.06., 20:04	-2.1	-0.8	0.3	2.2	4.2	5.4
29.06., 22:04	-2.1	-0.8	0.3	2.2	4.1	5.2
30.06., 10:04	-2.0	-0.7	0.3	1.7	3.1	4.3
30.06., 12:04		-0.7	0.3	1.7	3.6	5.6
30.06., 14:04	-1.9	-0.6	0.3	1.9	4.3	6.8
30.06., 16:04	-1.9	-0.6	0.4	2.1	5.0	8.0
30.06., 18:04	-1.9	-0.6	0.5	2.5	5.8	8.8
30.06., 20:04	-1.9	-0.7	0.5	2.9	6.2	8.8
30.06., 22:04	-1.8	-0.5	0.6	3.1	6.4	8.6
01.07., 00:04	-1.9	-0.6	0.8	3.3	6.3	8.1
01.07., 02:04	-1.9	-0.6	0.8	3.4	6.1	7.6
01.07., 04:04	-1.8	-0.5	0.9	3.4	5.9	7.2
01.07., 06:04	-1.9	-0.5	0.9	3.3	5.6	6.8
01.07., 08:04	-1.8	-0.5	1.0	3.2	5.4	6.4
01.07., 10:04	-1.8	-0.5	1.0	3.1	5.1	5.9
01.07., 12:04	-1.8	-0.5	1.0	3.0	4.8	5.4
01.07., 13:39	-1.7	-0.5	1.0	2.9	4.5	5.0
01.07., 13:44	-1.8	-0.5	0.9	2.9	4.5	4.9
01.07., 13:49	-1.8	-0.5	0.9	2.9	4.5	4.9
01.07., 13:54	-1.8	-0.5	0.9	2.9	4.5	4.9
01.07., 13:59	-1.8	-0.5	1.0	2.9	4.4	4.9
01.07., 14:04	-1.8	-0.5	0.9	2.9	4.4	4.9
01.07., 14:09	-1.8	-0.5	0.9	2.8	4.4	4.9
01.07., 14:14	-1.8	-0.5	0.9	2.9	4.4	4.8
01.07., 14:19	-1.7	-0.5	0.9	2.9	4.4	4.8
01.07., 14:24	-1.8	-0.5	1.0	2.8	4.4	4.8
01.07., 14:29	-1.8	-0.5	0.9	2.8	4.4	4.8
01.07., 14:34	-1.8	-0.5	1.0	2.8	4.4	4.8
01.07., 14:39	-1.8	-0.5	1.0	2.8	4.4	4.7

01.07., 14:44	-1.7	-0.5	0.9	2.8	4.3	4.7
01.07., 15:29	-1.7	-0.5	1.0	2.7	4.2	4.5
01.07., 15:34	-1.7	-0.5	0.9	2.7	4.1	4.5
01.07., 15:39	-1.7	-0.5	0.9	2.7	4.1	4.5
01.07., 15:44	-1.7	-0.4	0.9	2.7	4.2	4.5
01.07., 15:49	-1.8	-0.5	0.9	2.7	4.1	4.5
01.07., 15:54	-1.7	-0.4	0.9	2.7	4.1	4.4
01.07., 15:59	-1.7	-0.5	0.9	2.7	4.1	4.5
01.07., 16:04	-1.8	-0.5	0.9	2.7	4.1	4.4
01.07., 16:09	-1.8	-0.5	0.9	2.7	4.0	4.4
01.07., 16:14	-1.7	-0.5	0.9	2.7	4.1	4.4
01.07., 16:19	-1.7	-0.5	0.9	2.7	4.1	4.4
01.07., 16:24	-1.7	-0.4	0.9	2.6	4.0	4.4
01.07., 16:29	-1.7	-0.4	1.0	2.7	4.0	4.4
01.07., 16:34	-1.8	-0.5	0.9	2.6	4.0	4.4
01.07., 16:44	-1.7	-0.4	0.9	2.6	4.0	4.4
01.07., 16:49	-1.7	-0.5	0.9	2.6	3.9	4.4
01.07., 16:54	-1.8	-0.5	0.9	2.6	4.0	4.3
01.07., 16:59	-1.8	-0.5	0.9	2.6	3.9	4.3
01.07., 17:04	-1.7	-0.5	0.9	2.6	3.9	4.3
01.07., 17:09	-1.7	-0.5	0.8	2.6	3.9	4.3
01.07., 17:14	-1.7	-0.5	0.9	2.6	3.9	4.3
01.07., 17:19	-1.8	-0.4	0.9	2.6	3.9	4.3
01.07., 17:24	-1.7	-0.4	0.9	2.6	3.9	4.2
01.07., 17:29	-1.8	-0.4	0.8	2.5	3.8	4.2
01.07., 17:34	-1.7	-0.4	0.9	2.6	3.8	4.2
01.07., 17:39	-1.8	-0.5	0.9	2.5	3.8	4.2
01.07., 17:44	-1.7	-0.5	0.9	2.6	3.8	4.2
01.07., 17:49	-1.7	-0.4	0.8	2.5	3.8	4.1
01.07., 17:19	-1.8	-0.4	0.9	2.6	3.9	4.3
01.07., 17:24	-1.7	-0.4	0.9	2.6	3.9	4.2
01.07., 17:29	-1.8	-0.4	0.8	2.5	3.8	4.2
01.07., 17:34	-1.7	-0.4	0.9	2.6	3.8	4.2
01.07., 17:39	-1.8	-0.5	0.9	2.5	3.8	4.2
01.07., 17:44	-1.7	-0.5	0.9	2.6	3.8	4.2
01.07., 17:49	-1.7	-0.4	0.8	2.5	3.8	4.1
01.07., 17:54	-1.7	-0.5	0.9	2.5	3.8	4.1
01.07., 17:59	-1.8	-0.5	0.9	2.5	3.7	4.1
01.07., 18:04	-1.7	-0.5	0.9	2.5	3.7	4.1
01.07., 18:09	-1.7	-0.5	0.9	2.5	3.8	4.0
01.07., 18:14	-1.7	-0.5	0.8	2.4	3.7	4.0
01.07., 18:19	-1.7	-0.5	0.9	2.5	3.7	4.0
01.07., 18:24	-1.7	-0.5	0.9	2.5	3.7	4.0
01.07., 18:59	-1.8	-0.4	0.9	2.4	3.7	3.9
01.07., 19:04	-1.7	-0.5	0.8	2.4	3.6	3.8
01.07., 19:09	-1.7	-0.5	0.8	2.4	3.6	3.8
01.07., 19:14	-1.7	-0.5	0.9	2.4	3.6	3.8
01.07., 19:19	-1.7	-0.4	0.8	2.4	3.6	3.8
01.07., 19:24	-1.7	-0.5	0.8	2.3	3.5	3.8
01.07., 19:29	-1.7	-0.4	0.8	2.4	3.5	3.8
01.07., 19:34	-1.7	-0.4	0.8	2.3	3.5	3.7
01.07., 19:39	-1.7	-0.5	0.8	2.3	3.5	3.6
01.07., 19:44	-1.7	-0.4	0.8	2.4	3.4	3.7
01.07., 19:49	-1.7	-0.4	0.9	2.3	3.4	3.7
01.07., 19:54	-1.7	-0.5	0.8	2.3	3.4	3.6
01.07., 19:59	-1.7	-0.5	0.9	2.3	3.4	3.6
01.07., 20:04	-1.7	-0.5	0.8	2.3	3.4	3.6
01.07., 22:49	-1.7	-0.4	0.8	2.1	2.9	2.8
01.07., 23:04	-1.6	-0.4	0.8	2.0	2.9	2.7

01.07., 23:19	-1.7	-0.4		0.8	2.0	2.8	2.7
01.07., 23:34	-1.7	-0.4		0.8	2.0	2.7	2.6
01.07., 23:49	-1.7	-0.4		0.8	2.0	2.7	2.6
02.07., 00:04	-1.7	-0.4		0.7	1.9	2.6	2.6
02.07., 00:19	-1.6	-0.4		0.7	1.9	2.6	2.5
02.07., 00:34	-1.7	-0.4		0.7	1.9	2.5	2.4
02.07., 00:49	-1.6	-0.4		0.7	1.8	2.5	2.4
02.07., 01:04	-1.7	-0.4		0.7	1.8	2.5	2.3
02.07., 01:19	-1.6	-0.4		0.7	1.8	2.4	2.3
02.07., 01:34	-1.7	-0.4		0.7	1.8	2.4	2.3
02.07., 01:49	-1.6	-0.4		0.7	1.8	2.3	2.2
02.07., 02:04	-1.7	-0.4		0.7	1.7	2.3	2.1
02.07., 02:19	-1.6	-0.4		0.7	1.7	2.3	2.1
02.07., 02:34	-1.7	-0.4		0.7	1.7	2.2	2.1
02.07., 02:49	-1.6	-0.4		0.6	1.6	2.1	2.1
02.07., 03:04	-1.6	-0.4		0.6	1.6	2.1	2.0
02.07., 03:19	-1.6	-0.4		0.7	1.6	2.1	2.0
02.07., 03:34	-1.7	-0.4		0.6	1.6	2.1	1.9
02.07., 03:49	-1.6	-0.4		0.7	1.6	2.0	1.9
02.07., 04:04	-1.6	-0.4		0.6	1.5	1.9	1.9
02.07., 04:19	-1.6	-0.4		0.6	1.5	2.0	1.8
02.07., 22:04	-1.5	-0.3		0.3	1.2	2.7	4.1
03.07., 00:08	-1.6	-0.4		0.4	1.4	2.9	3.9
03.07., 03:04	-1.5	-0.3		0.5	1.5	2.8	3.6
03.07., 06:04		-0.3		0.5	1.6	2.9	3.9
03.07., 09:04	-1.5	-0.3		0.4	1.6	3.2	4.5
03.07., 12:04	-1.5	-0.3		0.6	1.8	3.6	5.4
03.07., 15:04	-1.5	-0.3		0.6	2.1	4.4	6.4
03.07., 18:04	-1.5	-0.3		0.7	2.4	4.7	6.1
03.07., 21:04	-1.4	-0.3		0.8	2.5	4.5	5.6
04.07., 00:04	-1.5	-0.3		0.9	2.6	4.2	4.8
04.07., 03:04	-1.4	-0.4		0.9	2.4	3.7	4.1
04.07., 06:04	-1.4	-0.4		0.8	2.2	3.2	3.6
04.07., 09:04	-1.4	-0.2		0.7	2.0	3.0	3.6
04.07., 12:04	-1.4	-0.3		0.7	1.8	3.1	4.2
04.07., 21:04	-1.4	-0.3		0.7	2.2	4.1	5.3
05.07., 00:04	-1.4	-0.3		0.8	2.3	3.9	4.5
05.07., 03:04	-1.4	-0.3	0.3	0.8	2.2	3.4	3.9
05.07., 06:04	-1.4	-0.3		0.8	2.0	3.1	3.3
05.07., 09:04	-1.4	-0.3		0.7	1.8	2.6	3.1
05.07., 12:04	-1.4	-0.3		0.6	1.7	2.8	3.9
05.07., 15:04	-1.3	-0.3		0.6	1.7	3.2	4.4
05.07., 18:04	-1.3	-0.2		0.6	1.9	3.6	5.1
05.07., 21:04	-1.3	-0.2		0.7	2.1	3.8	5.0
06.07., 00:04	-1.3	-0.2		0.7	2.2	3.7	4.7
06.07., 03:04	-1.3	-0.3	0.2	0.8	2.1	3.6	4.2
06.07., 06:04	-1.3	-0.2		0.8	2.1	3.2	3.8
06.07., 09:04	-1.3	-0.2		0.7	2.0	3.2	4.1
06.07., 12:04	-1.3	-0.3		0.8	2.0	3.4	4.9
06.07., 15:03	-1.3	-0.3		0.8	2.1	4.3	6.6
06.07., 15:13	-1.3	-0.3		0.8	2.1	4.3	6.7
06.07., 18:08		-0.2		0.8	2.5	5.5	8.8
06.07., 21:04	-1.3	-0.3	0.3	1.1	3.1	6.6	9.5
07.07., 00:04	-1.3	-0.2	0.4	1.3	3.6	6.8	9.0
07.07., 03:04	-1.3	-0.2	0.6	1.4	3.8	6.5	8.0
07.07., 06:04	-1.3	-0.2	0.7	1.4	3.8	6.0	7.2
07.07., 09:04	-1.3	-0.2	0.7	1.5	3.7	5.8	7.2
07.07., 12:04	-1.3	-0.2	0.7	1.5	3.6	6.1	8.2
07.07., 14:43		-0.2	0.7	1.4	3.8	6.8	9.7

07.07., 14:53	-1.3	-0.2	1.0	1.5	3.8	6.8	9.8
09.07., 19:04	-0.9	0.7		2.7	5.3	8.7	10.5
09.07., 19:19	-1.0	0.7		2.7	5.3	8.8	11.3
09.07., 19:34	-0.9	0.7	1.8	2.8	5.4	8.8	11.4
09.07., 19:49	-1.0	0.7	2.0	2.8	5.4	8.8	
09.07., 20:04	-0.9	0.6	2.0	2.8	5.4	8.9	11.4
09.07., 20:19	-0.9	0.7	2.0	2.8	5.4	8.8	11.3
09.07., 20:34	-0.9	0.7	2.0	2.8	5.4	8.9	11.3
09.07., 20:49	-0.9	0.7	2.1	2.8	5.5	8.9	11.3
09.07., 21:04	-0.9	0.7	2.0	2.8	5.5	8.9	11.2
09.07., 21:19	-0.9	0.7	1.9	2.8	5.5	8.9	11.2
09.07., 21:34	-0.9	0.7	2.0	2.9	5.6	8.9	11.0
09.07., 21:49	-0.9	0.7		2.8	5.5	8.9	11.0
09.07., 22:04	-0.9	0.8	2.1	2.9	5.5	8.9	10.9
09.07., 22:19	-1.0	0.7	2.0	2.9	5.6	8.9	10.7
08.07., 00:04	-1.2	-0.1	1.2	2.0	5.0	8.6	10.7
08.07., 03:04	-1.2	0.0	1.3	2.2	5.1	8.3	9.9
08.07., 06:04	-1.2	-0.1	1.3	2.2	5.0	7.8	9.1
08.07., 09:04	-1.2	0.0	0.3	2.3	4.9	7.5	9.0
08.07., 12:04	-1.2	0.0	1.4	2.3	4.8	7.7	9.9
08.07., 15:04	-1.2	0.1		2.3	4.9	8.3	
08.07., 18:04	-1.1	0.1	1.5	2.4	5.2	8.9	
08.07., 21:04		0.2	0.3	2.6	5.5	9.1	
09.07., 00:04	-1.1	0.3	1.8	2.7	5.6	8.9	10.7
09.07., 03:04	-1.1	0.3	1.9	2.9	5.6	8.4	9.6
09.07., 06:04	-1.1	0.5	1.9	2.9	5.4	7.8	8.8
09.07., 09:04	-1.1	0.5	1.9	2.8	5.2	7.3	8.5
09.07., 12:04	-1.0	0.6	1.9	2.7	5.0	7.5	9.3
09.07., 15:04	-1.0	0.7		2.6	5.0	7.8	10.2
11.07., 03:04	-0.7	1.1	2.8	3.4	6.0	8.8	10.2
11.07., 06:04	-0.7	1.2	2.8	3.4	5.9	8.3	9.5
11.07., 09:04	-0.7	1.3	2.8	3.4	5.7	8.0	9.3
11.07., 12:04	-0.6	1.2	2.8	3.4	5.6	8.1	9.8
11.07., 15:04	-0.7	1.3	2.8	3.3	5.7	8.5	
11.07., 18:04	-0.7	1.4		3.4	5.9	9.2	
11.07., 21:04	-0.6	1.3	2.9	3.5	6.2	9.6	12.0
12.07., 00:04	-0.6	1.4	3.0	3.7	6.3	9.5	11.2
12.07., 03:04	-0.6	1.5	3.1	3.8	6.3	8.9	10.0
12.07., 06:04	-0.5	1.6	3.2	3.7	6.0	8.2	9.1
12.07., 09:04	-0.6	1.6	3.1	3.7	5.8	7.8	8.7
12.07., 12:04	-0.5	1.6	3.3	3.6	5.6	7.7	9.1
12.07., 15:04	-0.5	1.6	3.0	3.5		8.1	9.9
12.07., 18:04	-0.4	1.6	3.0	3.5		8.4	10.5
14.07., 00:04	-0.3	1.6	2.9	3.4	5.6	8.3	9.6
14.07., 03:04	-0.3	1.7	3.0	3.5	5.7	7.8	8.4
14.07., 06:04	-0.3	1.7	3.0	3.5	5.4	7.0	7.2
14.07., 09:04	-0.2	1.7	3.0	3.4	5.1	6.4	6.8
14.07., 12:04	-0.2	1.7	2.9	3.3	4.9	6.2	7.0
14.07., 15:04	-0.2	1.7	2.8	3.2	4.7	6.6	11.7
14.07., 18:04	-0.2	1.6	2.7	3.1	4.8	7.5	10.0
14.07., 21:04	-0.2	1.6	2.8	3.2	5.2	8.1	
15.07., 00:04	-0.2	1.6	2.9	3.3	5.5	8.1	9.5
15.07., 03:04	-0.2	1.7	3.0	3.4	5.5	7.6	8.4
15.07., 06:04	-0.2	1.8	3.0	3.4	5.3	7.0	7.7
15.07., 09:04	-0.2	1.8	3.0	3.4	5.2	6.9	7.9
15.07., 12:04	-0.2	1.7	2.9	3.3	5.1	7.1	8.2
15.07., 15:04	-0.2	1.7	2.9	3.3	5.2	7.5	9.0
15.07., 00:04	-0.2	1.6	2.9	3.3	5.5	8.1	9.5
15.07., 03:04	-0.2	1.7	3.0	3.4	5.5	7.6	8.4

15.07., 06:04	-0.2	1.8	3.0	3.4	5.3	7.0	7.7
15.07., 09:04	-0.2	1.8	3.0	3.4	5.2	6.9	7.9
15.07., 12:04	-0.2	1.7	2.9	3.3	5.1	7.1	8.2
15.07., 15:04	-0.2	1.7	2.9	3.3	5.2	7.5	9.0
15.07., 18:08	-0.2	1.7	3.0	3.3	5.4	8.1	10.4
16.07., 00:04	-0.2	1.8	3.1	3.6	5.7	8.0	9.3
16.07., 06:04	-0.1	1.9	3.3	3.8	5.4	7.4	8.2
16.07., 12:04	-0.1	1.6	3.3	3.7	5.2	7.5	9.5
16.07., 18:04	-0.1	1.6	3.3	3.7	5.4	8.4	
17.07., 00:04	-0.1	1.8	3.7	4.0	5.8	8.4	9.9
17.07., 06:04	-0.1	1.9	3.6	4.1	5.7	8.0	9.3
17.07., 12:04	0.0	2.0	3.5	4.1	5.6	7.9	9.5
27.07., 06:04	0.8	2.7	4.1	4.5	5.8	7.3	7.6
27.07., 12:04	0.8	2.6		4.2	5.4	7.0	8.2
27.07., 18:04		2.5	3.7	4.2	5.4	8.0	
28.07., 00:04	0.8	2.6	3.8	4.3	6.0	8.7	10.5
28.07., 06:04	0.9	2.7	4.0	4.5		8.1	8.9
28.07., 12:04	0.8	2.7	4.0	4.5	5.9	7.9	
28.07., 18:04		2.7	4.0	4.5	6.3	9.6	
29.07., 00:04	1.0	2.9	4.4	4.9	7.0	10.1	11.8
29.07., 06:04	1.1	3.1	4.6	5.1		9.0	9.9
29.07., 12:04	1.1	3.1		5.0	6.5	8.6	10.1
29.07., 18:04	1.1	3.1		5.0	6.7	9.3	11.0
30.07., 00:04	1.2	3.1		5.1		9.2	10.4
30.07., 06:04	1.2	3.2		5.1	6.5	8.5	9.4
30.07., 12:04	1.2	3.2		4.9		7.7	8.4
03.08., 06:04	1.0	2.3		3.6	4.5	5.8	6.3
03.08., 12:04	1.0	2.3		3.5	4.3	5.5	6.1
03.08., 18:04	1.0			3.4	4.2	5.8	7.1
03.08., 18:04	1.0			3.4	4.2	5.8	7.1
04.08., 06:04	0.9	2.1	2.4	3.3	4.1	5.1	5.3
04.08., 12:04	0.9	2.0	2.7	3.1	3.7	4.8	5.4
04.08., 18:04				3.0	3.7	5.6	8.1
05.08., 06:04	0.9	2.0		3.3	4.1	5.1	5.0
05.08., 12:04	0.9	2.0		3.1		4.8	5.6
05.08., 18:04	0.9	1.9		3.0		5.6	7.0
06.08., 06:04	0.8	2.0	3.0	3.1	4.0	5.8	7.2
06.08., 12:04	0.9	2.0	2.9	3.2	4.1	5.6	6.4
06.08., 18:04				3.3	4.2	6.1	
07.08., 14:04	0.9	2.0	2.9	3.2		4.9	6.0
08.08., 00:04	1.0	2.2		3.4	4.3	5.8	6.4
08.08., 02:04		1.9	2.9	3.1	4.1	5.7	6.7
08.08., 14:04		2.0	2.9	3.2	3.9	5.2	6.3
09.08., 00:04	0.8	1.9		3.1		6.2	7.3
09.08., 02:04	0.9	2.0	2.8	3.2	3.9	5.0	5.0
09.08., 14:04		1.8	2.5	2.8	3.2	4.7	
10.08., 00:04	0.9	1.9	2.7	3.1	4.1	5.5	6.3
10.08., 02:04	0.9	1.9	2.8	3.3	4.4	6.0	6.4
10.08., 14:04		1.9	2.8	3.2	3.9	5.5	7.0
11.08., 02:04		2.0	3.1	3.5		7.1	
11.08., 14:04	1.2	2.4	3.7	4.2		8.4	9.8
12.08., 02:04	1.4	2.8	3.9	4.5	5.7	7.1	7.0
12.08., 14:04		2.6		3.9		5.9	7.2
13.08., 02:04	1.3	2.4	3.4	3.9	4.8	6.1	6.5
13.08., 14:04		2.3	3.2	3.5	4.2	5.5	6.7
14.08., 02:04	1.1	2.1	2.9	3.3	3.7	4.1	3.4
14.08., 14:04	0.9	1.6	2.2	2.4	2.3	2.5	2.6
15.08., 02:04	0.7	1.2	1.8	2.0	2.3	2.9	2.8
15.08., 14:04		1.0	1.5	1.8	1.9	2.9	3.8

16.08., 02:04	0.6	1.0	1.6	1.9	2.3	3.5	3.9
16.08., 14:04		1.0	1.7	1.9	2.2	3.3	4.5
17.08., 02:04	0.6	1.2	2.0	2.4	3.2	4.8	5.3
17.08., 14:04		1.4		2.4	3.0	4.4	
18.08., 02:04		1.6	2.6	2.9	4.1	6.2	7.1
18.08., 14:04		1.9	2.8	3.1	4.0	5.7	9.5
19.08., 02:04	1.1	2.1	3.3	3.8		7.5	8.5
19.08., 14:04		2.4		4.0	5.1	7.6	10.9
20.08., 02:04	1.4	2.8	4.2	4.8		9.2	10.3
20.08., 14:04			4.3	4.8	6.0	8.2	
21.08., 02:04	1.7	3.3	4.7	5.2	6.9	9.2	9.8
21.08., 14:04			4.5	4.9		7.9	
22.08., 02:04	1.7	3.3	4.6	5.2		9.2	10.2
22.08., 14:04		3.9	4.7	5.2	6.5	8.9	
23.08., 02:04	1.9	3.5	5.0	5.6	7.3	9.6	10.3
23.08., 14:04		3.6	4.8	5.3	6.3	8.2	
24.08., 02:04	2.0	3.6	4.9	5.4	6.8	8.8	9.8
24.08., 14:04			4.8	5.3	6.4	8.1	9.5
25.08., 02:04	2.0	3.5	4.7	5.2	6.5	8.3	8.8
25.08., 14:04	2.0	3.3	4.5	4.9		7.0	7.8
26.08., 02:04	1.9	3.1	4.3	4.6	5.6	7.0	7.3
26.08., 14:04				4.3	5.0	6.4	7.6
03.09., 02:04	1.1	1.6	2.0	2.3	2.5	3.0	2.8
03.09., 14:04	1.0	1.3		1.9	2.0	2.5	2.9
04.09., 02:04	0.8	1.2	1.6	1.9	2.0	2.5	2.4
04.09., 14:04		1.0		1.6	1.5	2.1	2.7
05.09., 02:04	0.7	0.9		1.6	1.7	2.2	2.1
05.09., 14:04		0.8		1.3	1.3	1.9	2.3
06.09., 02:04	1.7	0.7		1.4	1.6	2.2	2.3
06.09., 14:04		0.7		1.3	1.4	2.0	2.5
07.09., 02:04		0.7		1.4	1.5	2.1	2.2
07.09., 14:04	0.5	0.6	0.8	1.2	1.0	1.2	1.2
08.09., 02:04	0.4	0.4	0.5	0.9	0.7	0.8	0.6
08.09., 14:05		0.2		0.6	0.4	0.9	1.4
09.09., 02:04	0.2	0.2		0.7	0.7	1.1	1.0
09.09., 14:05	0.2	0.1		0.6	0.4	0.9	1.2
10.09., 00:04	0.2	0.1	0.1	0.6	0.5	0.7	0.5
10.09., 03:04	0.2	0.1	0.2	0.5	0.3	0.6	0.4
10.09., 06:04	0.2	0.1	0.2	0.4	0.3	0.4	0.3
10.09., 09:04	0.2	0.1	0.0	0.4	0.2	0.4	0.2
10.09., 12:04	0.2	0.0	0.0	0.4	0.2	0.3	0.2
10.09., 15:04	0.1	0.0		0.4	0.1	0.3	0.2
10.09., 18:04	0.1	0.0		0.4	0.1	0.2	0.1
10.09., 21:04	0.1	-0.1	0.0	0.3	0.0	0.2	0.1
11.09., 00:04	0.1	-0.1	-0.1	0.3	0.0	0.1	0.1
11.09., 03:04	0.0	-0.1	-0.1	0.2	0.0	0.1	0.1
11.09., 06:04	0.1	-0.1	-0.2	0.2	-0.1	0.1	0.1
11.09., 09:04	0.0	-0.2	-0.2	0.2	-0.2	0.1	0.0
11.09., 12:05	0.0	-0.2	-0.2	0.1	-0.2	0.0	0.0
11.09., 15:05	0.0	-0.2	-0.2	0.1	-0.2	0.0	-0.1
11.09., 18:08	0.0	-0.2	-0.2	0.0	-0.2	0.0	0.0
11.09., 20:04	0.0	-0.3	-0.2	0.1	-0.2	0.0	0.0
11.09., 22:04	0.0	-0.3	-0.2	0.0	-0.2	0.0	0.0
12.09., 00:04	0.0	-0.3	-0.3	0.0	-0.2	0.0	0.0
12.09., 02:04	-0.1	-0.3	-0.2	0.0	-0.2	0.0	-0.1
12.09., 04:04	-0.1	-0.3	-0.2	0.0	-0.2	-0.1	0.0
12.09., 06:04	-0.1	-0.3	-0.3	0.0	-0.2	0.0	0.0
12.09., 08:04	-0.1	-0.3	-0.3	0.0	-0.2	0.0	-0.1
12.09., 10:04	-0.1	-0.3	-0.3	0.0	-0.3	0.0	0.0

12.09., 12:04	0.0	-0.3	-0.3	0.0	-0.3	-0.1	-0.1
12.09., 14:04	-0.1	-0.3		0.0	-0.3	-0.1	-0.1
12.09., 16:04	0.0	-0.3	0.0	0.0	-0.3	0.0	-0.1
12.09., 20:08	0.0	-0.4	-0.3	-0.1	-0.3	-0.1	-0.1
12.09., 22:04	-0.1	-0.4	-0.3	0.0	-0.2	-0.1	-0.1
13.09., 00:04	-0.1	-0.3	-0.3	0.0	-0.3	0.0	-0.1
13.09., 02:04	-0.1	-0.3	-0.3	-0.1	-0.3	-0.1	0.0
13.09., 04:04	-0.1	-0.3	-0.3	0.0	-0.3	0.0	0.0
13.09., 06:04	-0.1	-0.4	-0.3	-0.1	-0.3	-0.1	0.0
13.09., 08:04	-0.1	-0.4	-0.4	0.0	-0.3	-0.1	-0.1
13.09., 10:04	-0.1	-0.4	-0.3	-0.1	-0.3	-0.1	-0.1
13.09., 12:04	-0.1	-0.3		-0.1	-0.3	-0.1	-0.1
13.09., 14:04	-0.1	-0.4		-0.1	-0.3	-0.1	-0.1
13.09., 16:04	-0.1	-0.4		-0.1	-0.3	-0.1	-0.1
14.09., 12:04	-0.1	-0.4		-0.1	-0.3	-0.1	-0.1
14.09., 14:04	-0.1	-0.4		-0.1	-0.3	-0.1	-0.1
14.09., 16:04	-0.1	-0.4	-0.1	-0.1	-0.3	-0.1	-0.1
14.09., 18:04	-0.1	-0.4		-0.1	-0.3	-0.1	-0.1
14.09., 20:04	-0.1	-0.4		-0.1	-0.3	-0.1	-0.1
14.09., 22:04	-0.1	-0.4	-0.3	-0.1	-0.3	-0.1	-0.1
15.09., 00:04	-0.1	-0.4		-0.1	-0.3	0.0	-0.1
15.09., 02:04	-0.1	-0.4		-0.1	-0.3	-0.1	-0.1
15.09., 04:04	-0.1	-0.4		-0.1	-0.4	-0.1	0.0
15.09., 06:04	-0.1	-0.4		-0.1	-0.3	-0.1	-0.1
15.09., 08:04	-0.2	-0.3		-0.1	-0.3	-0.1	-0.1
15.09., 10:04	-0.1	-0.4		-0.1	-0.3	-0.1	-0.1
15.09., 12:04	-0.1	-0.4		-0.1	-0.3	-0.1	-0.1
15.09., 14:04	-0.1	-0.4		-0.1	-0.3	-0.1	-0.1
16.09., 10:04		-0.4		-0.1	-0.3	-0.1	-0.1
16.09., 10:30	-0.1	-0.4		-0.1	-0.3	0.0	-0.1
16.09., 11:00	-0.1	-0.4		-0.1	-0.3	-0.1	-0.1
16.09., 11:30	-0.1	-0.4	-0.2	-0.1	-0.3	-0.1	-0.1
16.09., 12:04	-0.1	-0.4	-0.3	-0.1	-0.3	-0.1	-0.1
16.09., 12:30		-0.3	-0.3	-0.1	-0.3	-0.1	-0.1
16.09., 13:00		-0.4	-0.3	-0.1	-0.3	-0.1	-0.1
16.09., 13:30		-0.4	-0.3	-0.1	-0.3	-0.1	-0.1
16.09., 14:04		-0.4	-0.3	-0.1	-0.4	-0.1	-0.1
16.09., 14:30	-0.1	-0.4	-0.3	-0.1	-0.3	-0.1	-0.1
16.09., 15:00	-0.1	-0.4	-0.3	-0.1	-0.3	-0.1	-0.1
16.09., 15:30	0.0	-0.4	-0.3	0.0	-0.3	-0.1	-0.1
16.09., 16:04	-0.1	-0.4	-0.3	-0.1	-0.3	-0.1	-0.1
16.09., 16:30	-0.1	-0.4	-0.4	-0.1	-0.3	0.0	-0.1
16.09., 17:00	-0.1	-0.4	-0.3	-0.1	-0.3	0.0	-0.1
16.09., 17:30	-0.1	-0.4	-0.4	-0.1	-0.3	-0.1	-0.1
16.09., 18:04	-0.1	-0.4	-0.3	-0.1	-0.3	-0.1	-0.1
16.09., 18:30	-0.1	-0.4	-0.4	-0.1	-0.3	-0.1	-0.1
16.09., 19:00	-0.1	-0.3	-0.3	-0.1	-0.3	-0.1	-0.1
16.09., 19:30	-0.1	-0.4	-0.3	-0.1	-0.3	-0.1	-0.1
16.09., 20:04	-0.1	-0.4	-0.4	-0.1	-0.3	-0.1	-0.1
16.09., 20:30	-0.1	-0.4	-0.4	0.0	-0.3	-0.1	-0.1
16.09., 21:00	-0.1	-0.4	-0.3	0.0	-0.3	-0.1	0.0
16.09., 21:30	-0.1	-0.4	-0.3	-0.1	-0.3	-0.1	-0.1
16.09., 22:04	-0.1	-0.4	-0.4	-0.1	-0.3	-0.1	-0.1
16.09., 22:30	-0.1	-0.4	-0.3	-0.1	-0.3	-0.1	-0.1
16.09., 23:00	-0.1	-0.4	-0.3	-0.1	-0.3	-0.1	-0.1
16.09., 23:30	-0.1	-0.4	-0.3	-0.1	-0.3	-0.1	-0.1
17.09., 00:04	-0.1	-0.4	-0.4	-0.1	-0.3	-0.1	-0.1
17.09., 00:30	-0.1	-0.4	-0.1	-0.1	-0.3	-0.1	-0.1
17.09., 01:00	-0.1	-0.4	0.0	-0.1	-0.3	-0.1	-0.1

17.09., 01:30	-0.1	-0.4		-0.1	-0.3	-0.1	-0.1
17.09., 02:04	-0.1	-0.4		-0.1	-0.3	-0.1	-0.1
17.09., 02:30	-0.1	-0.4		-0.1	-0.3	-0.1	-0.1
17.09., 03:00	-0.1	-0.4		-0.1	-0.3	-0.1	-0.1
17.09., 03:30	-0.1	-0.4		-0.1	-0.3	-0.1	-0.1
17.09., 04:04	-0.1	-0.4		-0.1	-0.3	-0.1	-0.1
17.09., 04:30	-0.1	-0.4		-0.1	-0.3	-0.1	-0.1
17.09., 05:00	-0.1	-0.4		-0.1	-0.3	-0.1	-0.1
17.09., 05:30	-0.1	-0.4		0.0	-0.3	-0.1	-0.1
17.09., 06:04	-0.1	-0.4		-0.1	-0.3	-0.1	-0.1
17.09., 06:30	-0.1	-0.4		-0.1	-0.3	-0.1	-0.1
17.09., 07:00	-0.1	-0.4		-0.1	-0.3	-0.1	-0.1
17.09., 07:30	0.0	-0.4		0.0	-0.3	-0.1	-0.1
17.09., 08:04	-0.2	-0.4		-0.1	-0.3	-0.1	-0.1
17.09., 08:30	0.0	-0.4		-0.1	-0.3	-0.1	-0.1
17.09., 09:00	-0.1	-0.4		-0.1	-0.3	0.0	-0.1
17.09., 09:30	-0.1	-0.4	-0.3	-0.1	-0.3	-0.1	-0.1
17.09., 10:04	0.0	-0.4	-0.3	-0.1	-0.3	-0.1	-0.1
17.09., 10:30	-0.1	-0.4	-0.5	-0.1	-0.3	-0.1	-0.1
17.09., 11:00	-0.1	-0.4	-0.4	0.0	-0.3	0.0	-0.1
17.09., 11:30	-0.1	-0.4	-0.4	-0.1	-0.3	-0.1	-0.1
17.09., 12:04	-0.1	-0.4		-0.1	-0.3	-0.1	-0.1
17.09., 12:30	-0.1	-0.4		-0.1	-0.3	-0.1	-0.1
17.09., 13:00	-0.1	-0.4		-0.1	-0.3	-0.1	-0.1
17.09., 13:20	-0.1	-0.4		-0.1	-0.3	-0.1	-0.1
17.09., 13:32	-0.1	-0.3		-0.1	-0.3	-0.1	-0.1
17.09., 16:04	-0.1	-0.4		-0.1		-0.1	-0.1
17.09., 16:30	-0.1	-0.4		-0.1		0.0	-0.1
17.09., 17:00	-0.1	-0.4	-0.3	0.0	-0.3	0.0	-0.1
17.09., 17:30	-0.1	-0.4	-0.4	-0.1	-0.3	-0.1	-0.1
19.09., 08:04	-0.1	-0.4		-0.1	-0.3	-0.1	-0.4
19.09., 10:04	-0.1	-0.3	-0.3	-0.1	-0.3	-0.1	-0.4
19.09., 12:04	-0.1	-0.4	-0.3	-0.1	-0.3	-0.1	-0.3
19.09., 14:04		-0.4	-0.3	-0.1	-0.3	-0.1	-0.3
19.09., 16:04	-0.1	-0.4	-0.3	-0.1	-0.3	-0.1	-0.3
19.09., 18:04	-0.1	-0.3		-0.1	-0.3	-0.1	-0.2
19.09., 20:04	0.0	-0.4		0.0	-0.3	-0.1	-0.2
19.09., 22:04	-0.1	-0.4	-0.3	-0.1	-0.3	-0.1	-0.2
20.09., 00:04	-0.1	-0.4	-0.4	-0.1	-0.4	-0.1	-0.3
20.09., 02:04	-0.1	-0.4	-0.4	-0.1	-0.4	-0.1	-0.3
20.09., 04:04	-0.1	-0.4	-0.3	-0.1	-0.3	-0.1	-0.3
20.09., 06:04	-0.1	-0.4	-0.4	-0.1	-0.4	-0.1	-0.3
20.09., 08:04	-0.1	-0.4	-0.3	-0.1	-0.3	-0.1	-0.3
20.09., 10:04	-0.2	-0.4	-0.4	-0.1	-0.3	-0.1	-0.3
20.09., 12:04	-0.1	-0.4	-0.4	-0.1	-0.3	-0.1	-0.2
20.09., 14:04	-0.1	-0.4	-0.3	-0.1	-0.3	-0.1	-0.2
20.09., 16:04	-0.1	-0.4	-0.3	-0.1	-0.4	-0.1	-0.2
20.09., 18:04	-0.1	-0.4	-0.3	-0.1	-0.3	-0.1	-0.2
20.09., 20:04	-0.1	-0.4	-0.4	-0.1	-0.3	-0.1	-0.2
20.09., 22:04	-0.1	-0.4	-0.3	-0.1	-0.3	-0.1	-0.2
21.09., 00:04	-0.1	-0.4	-0.4	-0.1	-0.4	-0.1	-0.2
21.09., 02:04	-0.1	-0.4	-0.4	-0.1	-0.3	-0.1	-0.2
21.09., 04:04	-0.1	-0.4	-0.3	-0.1	-0.3	-0.1	-0.2
21.09., 06:04	-0.1	-0.4	-0.3	-0.1	-0.3	-0.1	-0.2
21.09., 08:04	-0.1	-0.4	-0.3	-0.1	-0.4	-0.1	-0.2
21.09., 10:04	-0.1	-0.4	-0.3	-0.1	-0.3	-0.1	-0.2
21.09., 12:04	-0.1	-0.4	-0.3	-0.1	-0.3	-0.1	-0.1
21.09., 14:04	-0.1	-0.4	-0.3	-0.1	-0.4	-0.1	-0.1
21.09., 16:04	-0.1	-0.4		-0.1	-0.3	0.0	-0.1

21.09., 18:04	-0.1	-0.4		-0.1	-0.3	-0.1	-0.1
21.09., 20:04	-0.2	-0.4	-0.2	-0.1	-0.3	-0.1	-0.2
21.09., 22:04	-0.1	-0.3	-0.3	-0.1	-0.3	-0.1	-0.1
22.09., 00:04	-0.1	-0.4	-0.3	-0.1	-0.3	-0.1	-0.1
22.09., 02:04	-0.1	-0.4	-0.3	-0.1	-0.3	-0.1	-0.2
22.09., 04:04	-0.1	-0.4	-0.3	-0.1	-0.3	-0.1	-0.2
22.09., 06:04	-0.1	-0.4	-0.3	-0.1	-0.4	-0.1	-0.3
22.09., 08:04	-0.1	-0.4	-0.4	-0.1	-0.3	-0.1	-0.4
22.09., 10:04	-0.1	-0.4	-0.4	-0.1	-0.3	-0.1	-0.4
22.09., 12:04	-0.1	-0.4	-0.3	-0.1	-0.3	-0.1	-0.4
22.09., 14:04	-0.1	-0.4	-0.4	-0.1	-0.3	-0.1	-0.4
22.09., 16:04	-0.1	-0.4	-0.3	-0.1	-0.3	-0.1	-0.3
22.09., 18:04	-0.1	-0.4	-0.3	-0.1	-0.3	-0.1	-0.3
22.09., 20:04	-0.1	-0.4		-0.1	-0.3	-0.1	-0.3
22.09., 22:04	-0.1	-0.4		-0.1	-0.3	-0.1	-0.3
23.09., 00:04	-0.1	-0.4		-0.1	-0.3	-0.1	-0.3
23.09., 02:04	-0.1	-0.3	-0.5	-0.1	-0.3	-0.1	-0.4
23.09., 04:04	-0.1	-0.4		-0.1	-0.3	-0.1	-0.4
23.09., 06:04	-0.1	-0.4		-0.1	-0.3	-0.1	-0.4
23.09., 08:04	-0.1	-0.4	-0.4	-0.1	-0.3	-0.1	-0.4
23.09., 10:04	-0.1	-0.4	-0.2	-0.1	-0.4	-0.1	-0.3
23.09., 12:04		-0.3	-0.4	-0.1	-0.3	-0.1	-0.3
23.09., 14:04		-0.4	-0.4	-0.1	-0.3	-0.1	-0.2
23.09., 16:04	-0.1	-0.4	-0.4	-0.1	-0.4	-0.1	-0.2
23.09., 18:04	-0.1	-0.4	-0.4	-0.1	-0.3	-0.1	-0.2
23.09., 20:04	-0.1	-0.4	-0.5	-0.1	-0.3	-0.1	-0.2
23.09., 22:04	-0.2	-0.4	-0.3	-0.1	-0.3	-0.1	-0.2
24.09., 00:04	-0.2	-0.4	-0.3	-0.1	-0.2	-0.1	-0.2
24.09., 02:04	-0.2	-0.4	-0.4	-0.1	-0.1	-0.1	-0.2
24.09., 04:04	-0.2	-0.4	-0.3	-0.1	-0.1	-0.1	-0.2
24.09., 06:04	-0.1	-0.4	-0.4	-0.1	-0.2	-0.1	-0.2
24.09., 08:04	-0.2	-0.4	-0.3	-0.1	-0.1	-0.1	-0.2
24.09., 10:04	-0.1	-0.4	-0.4	-0.1	-0.2	-0.1	-0.2
24.09., 12:04	-0.1	-0.3	-0.4	-0.1	-0.1	-0.1	-0.2
24.09., 14:04		-0.4	-0.3	-0.1	-0.1	-0.1	-0.2
24.09., 16:04	-0.1	-0.4	-0.4	-0.1	-0.2	-0.1	-0.2
25.09., 16:04	-0.1	-0.4	-0.4	-0.1	-0.1	-0.1	-0.2
25.09., 18:04	-0.1	-0.4	-0.4	-0.1	-0.1	-0.1	-0.2
25.09., 20:04	-0.1	-0.4	-0.3	-0.1	-0.1	-0.1	-0.1
25.09., 22:04	-0.1	-0.3	-0.3	-0.1	-0.1	-0.1	-0.2
26.09., 00:04	-0.1	-0.4	-0.3	-0.1	-0.2	-0.1	-0.2
26.09., 02:04	-0.1	-0.4	-0.3	-0.1	-0.1	-0.1	-0.2
26.09., 04:04	-0.1	-0.3	-0.4	-0.1	-0.2	-0.1	-0.2
26.09., 06:04	-0.1	-0.3	-0.4	-0.1	-0.1	-0.1	-0.2
26.09., 08:04	-0.1	-0.4	-0.3	-0.1	-0.1	-0.1	-0.2
26.09., 10:04	-0.1	-0.3	-0.3	-0.1	-0.1	-0.1	-0.3
26.09., 12:04	-0.1	-0.3	-0.4	-0.1	-0.1	-0.1	-0.4
26.09., 14:04		-0.4	-0.2	-0.1	-0.1	-0.1	-0.4
26.09., 16:04	-0.2	-0.4		-0.1	-0.1	-0.1	-0.4
26.09., 18:04	-0.1	-0.4	-0.3	-0.1	-0.1	-0.1	-0.3
26.09., 20:04	-0.1	-0.4	-0.4	-0.1	-0.1	-0.1	-0.4
26.09., 22:04	-0.1	-0.3	-0.4	-0.1	-0.1	-0.1	-0.4
27.09., 00:04	-0.1	-0.4	-0.3	-0.1	-0.2	-0.1	-0.5
27.09., 02:04	-0.1	-0.4	-0.4	-0.1	-0.1	-0.1	-0.6
27.09., 04:04	-0.1	-0.4	-0.4	-0.1	-0.1	-0.1	-0.7
27.09., 06:04	-0.1	-0.4	-0.4	-0.1	-0.1	-0.1	-0.7
27.09., 08:04	-0.1	-0.4	-0.4	-0.1	-0.1	-0.1	-0.7
27.09., 10:04	-0.1	-0.4	-0.4	-0.1	-0.1	-0.1	-0.7
27.09., 12:04	-0.1	-0.3	-0.4	-0.1	-0.1	-0.1	-0.6

27.09., 14:04	-0.1	-0.3		-0.1	-0.1	-0.2	-0.6
27.09., 16:04	-0.1	-0.4		-0.1	-0.1	-0.2	-0.5
27.09., 21:04	-0.1	-0.4		-0.1	-0.1	-0.1	-0.8
28.09., 00:04	-0.2	-0.4		-0.1	-0.1	-0.2	-0.9
28.09., 03:04	-0.2	-0.4		-0.1	-0.1	-0.2	-0.9
28.09., 06:04	-0.1	-0.4		-0.1	-0.1	-0.2	-0.9
28.09., 09:04	-0.1	-0.4		-0.1	-0.1	-0.2	-1.0
28.09., 12:04	-0.1	-0.4		-0.1	-0.1	-0.2	-1.1
28.09., 15:04	-0.1	-0.4		-0.1	-0.1	-0.2	-1.1
28.09., 18:04	-0.1	-0.4		-0.1	-0.1	-0.3	-1.1
28.09., 21:04	-0.1	-0.4		-0.1	-0.1	-0.3	-1.4
29.09., 00:04	-0.1	-0.3		-0.1	-0.1	-0.4	-1.7
29.09., 03:04	-0.1	-0.4		-0.1	-0.1	-0.5	-1.8
29.09., 06:04	-0.1	-0.4		-0.1	-0.2	-0.5	-1.7
29.09., 09:04	-0.2	-0.4		-0.1	-0.2	-0.6	-1.6
29.09., 12:04	-0.1	-0.4		-0.2	-0.1	-0.6	-1.4
30.09., 21:04	-0.2	-0.3		-0.1	-0.1	-0.4	-0.6
01.10., 00:04	-0.2	-0.4		-0.2	-0.1	-0.4	-0.7
01.10., 03:04	-0.2	-0.3		-0.1	-0.2	-0.4	-0.7
01.10., 06:04	-0.2	-0.3		-0.2	-0.1	-0.4	-0.7
01.10., 09:04	-0.2	-0.3		-0.1	-0.1	-0.4	-0.7
01.10., 12:04		-0.3		-0.1	-0.2	-0.4	-0.7
01.10., 15:04	-0.2	-0.3		-0.1	-0.1	-0.4	-0.7
01.10., 18:04	-0.2	-0.3		-0.1	-0.1	-0.4	-0.6
01.10., 21:04	-0.2	-0.4		-0.1	-0.1	-0.4	-0.7
02.10., 00:04	-0.2	-0.3		-0.1	-0.2	-0.3	-0.7
02.10., 03:04	-0.2	-0.3		-0.1	-0.1	-0.4	-0.7
02.10., 06:04	-0.2	-0.4		-0.1	-0.1	-0.4	-0.8
02.10., 09:04	-0.2	-0.3		-0.1	-0.2	-0.4	-1.0
02.10., 12:04	-0.2	-0.4		-0.1	-0.1	-0.6	-1.0
02.10., 15:04	-0.1	-0.4		-0.1	-0.1	-0.6	-1.0
02.10., 18:04	-0.2	-0.3		-0.2	-0.2	-0.6	-1.0
02.10., 21:04	-0.2	-0.3		-0.1	-0.1	-0.6	-1.1
03.10., 00:04	-0.2	-0.4		-0.1	-0.2	-0.6	-1.1
03.10., 03:04	-0.2	-0.3		-0.1	-0.2	-0.7	-1.0
03.10., 06:04	-0.2	-0.3		-0.1	-0.2	-0.6	-1.0
03.10., 09:04	-0.2	-0.3		-0.2	-0.2	-0.6	-0.9
03.10., 12:04	-0.2	-0.3		-0.2	-0.2	-0.6	-0.9
03.10., 15:04	-0.2	-0.3		-0.1		-0.6	-0.8
03.10., 18:04	-0.2	-0.3		-0.2	-0.2	-0.6	-0.8
06.10., 18:08	-0.3	-0.3		-0.2	-1.4	-2.9	-4.2
06.10., 21:04	-0.3	-0.3		-0.3	-1.4	-3.0	-4.2
07.10., 00:04	-0.3	-0.4		-0.2	-1.5	-3.0	-3.9
07.10., 03:04	-0.4	-0.4	-0.5	-0.3	-1.6	-2.9	-3.8
07.10., 06:04	-0.4	-0.2	-0.5	-0.4	-1.6	-2.9	-3.9
07.10., 09:04	-0.3	-0.2	-0.3	-0.5	-1.7	-3.0	-4.1
07.10., 12:04	-0.4	-0.1	-0.4	-0.5	-1.7	-3.1	-4.3
08.10., 20:08	-0.5	-0.8		-1.8	-3.0	-4.2	-4.9
08.10., 22:04	-0.5	-0.9		-1.9	-3.0	-4.1	-4.8
09.10., 00:04	-0.6	-1.0		-1.9	-3.0	-4.1	-4.7
09.10., 02:04	-0.5	-1.1		-2.1	-3.0	-4.0	-4.6
09.10., 04:04	-0.6	-1.1		-2.1	-3.0	-4.0	-4.5
09.10., 06:04	-0.6	-1.2		-2.1	-3.0	-3.9	-4.3
09.10., 08:04	-0.7	-1.3		-2.1	-3.0	-3.8	-4.2
09.10., 10:04	-0.8	-1.4		-2.2	-3.0	-3.8	-4.1
09.10., 12:04	-0.8	-1.4		-2.2	-3.0	-3.7	-4.0
09.10., 14:04	-0.9	-1.5		-2.2	-3.0	-3.6	-3.9
09.10., 16:04	-1.0	-1.5		-2.2	-2.9	-3.5	-3.8
09.10., 18:04	-1.0	-1.6		-2.2	-2.9	-3.5	-3.7

09.10., 20:04	-1.1	-1.6	-2.2	-2.8	-3.4	-3.7
09.10., 22:04	-1.2	-1.6	-2.2	-2.8	-3.4	-3.7
10.10., 00:04	-1.2	-1.6	-2.3	-2.8	-3.4	-3.7
10.10., 02:04	-1.2	-1.7	-2.3	-2.8	-3.3	-3.7
10.10., 04:04	-1.4	-1.7	-2.4	-2.8	-3.3	-3.7
10.10., 06:04	-1.4	-1.8	-2.3	-2.8	-3.3	-3.7
10.10., 08:04	-1.5	-1.8	-2.3	-2.8	-3.3	-3.6
10.10., 10:04	-1.5	-1.9	-2.3	-2.8	-3.4	-3.6
10.10., 12:04	-1.6	-1.9	-2.4	-2.8	-3.3	-3.6

Table A.9. Volumetric water content from site 2x in 1995.

Date, time	Volumetric water content θ at depth [$m^3 m^{-3}$]						
1995	78cm	65cm	52cm	47cm	34cm	23cm	11cm
21.05, 17:22	0.07	0.08	0.06	0.06	0.05	0.08	0.03
21.05, 17:26	0.07	0.08	0.06	0.06	0.05	0.08	0.03
21.05, 17:31	0.07	0.08	0.06	0.06	0.05	0.08	0.03
21.05, 17:36	0.07	0.07	0.06	0.06	0.05	0.08	0.03
21.05, 17:41	0.07	0.07	0.06	0.06	0.05	0.08	0.03
21.05, 17:46	0.07	0.07	0.06	0.06	0.05	0.08	0.03
21.05, 17:51	0.07	0.07	0.06	0.06	0.05	0.08	0.03
22.05, 03:04	0.07	0.07	0.06	0.06	0.05	0.08	0.03
22.05, 06:01	0.07	0.07	0.06	0.06	0.05	0.08	0.03
22.05, 09:01	0.07	0.07	0.06	0.06	0.05	0.08	0.03
22.05, 12:01	0.07	0.07	0.06	0.06	0.04	0.08	0.03
22.05, 15:01	0.07	0.07	0.06	0.06	0.04	0.08	0.03
22.05, 18:01	0.07	0.07	0.06	0.06	0.04	0.08	0.03
22.05, 21:01	0.07	0.08	0.06	0.06	0.05	0.08	0.03
23.05, 00:01	0.07	0.07	0.06	0.06	0.05	0.08	0.03
23.05, 03:01	0.07	0.07	0.06	0.06	0.05	0.08	0.03
23.05, 06:01	0.07	0.08	0.06	0.06	0.05	0.08	0.03
23.05, 09:01	0.07	0.07	0.06	0.06	0.05	0.08	0.03
23.05, 12:01	0.07	0.07	0.06	0.06	0.05	0.08	0.03
23.05, 15:01	0.07	0.07	0.06	0.06	0.05	0.08	0.03
24.05, 03:01	0.07	0.08	0.07	0.07	0.05	0.09	0.03
24.05, 06:01	0.08	0.08	0.07	0.07	0.05	0.08	0.03
24.05, 09:01	0.08	0.08	0.07	0.07	0.05	0.08	0.03
24.05, 12:01	0.07	0.08	0.07	0.06	0.05	0.08	0.03
24.05, 15:01	0.07	0.08	0.06	0.07	0.05	0.08	0.03
24.05, 18:01	0.07	0.08	0.07	0.07	0.05	0.08	0.03
24.05, 21:01	0.07	0.08	0.07	0.07	0.05	0.08	0.03
25.05, 03:01	0.08	0.08	0.07	0.07	0.05	0.09	0.03
25.05, 06:01	0.08	0.08	0.07	0.07	0.05	0.08	0.03
25.05, 09:01	0.07	0.08	0.07	0.07	0.05	0.08	0.03
25.05, 12:01	0.07	0.08	0.06	0.07	0.05	0.08	0.03
25.05, 15:01	0.07	0.08	0.06	0.06	0.05	0.08	0.03
26.05, 03:01	0.08	0.08	0.07	0.07	0.05	0.08	0.03
26.05, 06:01	0.08	0.08	0.07	0.07	0.05	0.08	0.03
26.05, 09:01	0.08	0.08	0.07	0.07	0.05	0.08	0.03
26.05, 12:01	0.08	0.08	0.07	0.07	0.05	0.08	0.03
26.05, 15:01	0.08	0.08	0.07	0.07	0.05	0.09	0.03
26.05, 18:01	0.08	0.08	0.07	0.07	0.05	0.09	0.03
26.05, 21:01	0.08	0.08	0.07	0.07	0.05	0.09	0.03
27.05, 03:01	0.08	0.08	0.07	0.07	0.05	0.09	0.04
27.05, 06:01	0.08	0.08	0.07	0.07	0.05	0.09	0.03
27.05, 09:01	0.08	0.08	0.07	0.07	0.05	0.08	0.03
27.05, 12:01	0.08	0.08	0.07	0.07	0.05	0.08	0.03
27.05, 15:01	0.08	0.07	0.06	0.07	0.05	0.08	0.03

29.05. 09:01	0.08	0.08	0.07	0.07	0.05	0.08	0.03
29.05. 12:01	0.08	0.08	0.07	0.07	0.05	0.08	0.03
29.05. 15:01	0.08	0.08	0.07	0.07	0.05	0.08	0.03
29.05. 18:01	0.08	0.08	0.07	0.07	0.05	0.08	0.03
29.05. 21:01	0.08	0.08	0.07	0.07	0.05	0.08	0.03
30.05. 00:01	0.08	0.08	0.07	0.07	0.05	0.08	0.03
30.05. 03:01	0.08	0.08	0.07	0.07	0.05	0.09	0.03
30.05. 06:01	0.08	0.08	0.07	0.07	0.05	0.09	0.03
30.05. 09:01	0.08	0.08	0.07	0.07	0.05	0.08	0.03
30.05. 12:01	0.08	0.08	0.07	0.07	0.05	0.09	0.03
30.05. 15:01	0.08	0.08	0.07	0.07	0.05	0.08	0.03
30.05. 18:01	0.08	0.08	0.07	0.07	0.05	0.08	0.03
30.05. 21:01	0.08	0.08	0.06	0.07	0.05	0.08	0.03
31.05. 00:01	0.08	0.08	0.07	0.07	0.05	0.09	0.03
31.05. 03:01	0.08	0.08	0.07	0.07	0.05	0.09	0.03
31.05. 06:01	0.08	0.08	0.06	0.07	0.05	0.08	0.03
31.05. 09:01	0.08	0.08	0.06	0.07	0.05	0.08	0.03
31.05. 12:01	0.08	0.08	0.06	0.07	0.05	0.08	0.03
31.05. 15:01	0.08	0.08	0.06	0.07	0.05	0.08	0.03
31.05. 18:01	0.08	0.08	0.06	0.07	0.05	0.08	0.03
31.05. 21:01	0.08	0.08	0.06	0.07	0.05	0.09	0.03
01.06. 00:01	0.08	0.08	0.07	0.07	0.05	0.09	0.03
01.06. 03:01	0.08	0.08	0.07	0.07	0.05	0.09	0.03
01.06. 06:01	0.08	0.08	0.07	0.07	0.05	0.09	0.03
01.06. 09:01	0.08	0.08	0.07	0.07	0.05	0.09	0.03
01.06. 12:01	0.08	0.08	0.07	0.07	0.05	0.08	0.03
01.06. 15:01	0.08	0.08	0.06	0.07	0.05	0.09	0.03
03.06. 00:01	0.08	0.08	0.07	0.07	0.05	0.08	0.03
03.06. 03:01	0.08	0.08	0.07	0.07	0.05	0.09	0.03
03.06. 06:01	0.08	0.08	0.07	0.07	0.05	0.09	0.03
03.06. 09:01	0.08	0.08	0.07	0.07	0.05	0.08	0.03
03.06. 12:01	0.08	0.08	0.06	0.07	0.05	0.08	0.03
03.06. 15:01	0.08	0.07	0.06	0.07	0.05	0.08	0.03
03.06. 18:01	0.07	0.07	0.06	0.07	0.05	0.08	0.03
03.06. 21:01	0.07	0.07	0.06	0.07	0.05	0.08	0.03
04.06. 00:01	0.07	0.07	0.06	0.07	0.05	0.09	0.03
04.06. 03:01	0.08	0.08	0.07	0.07	0.05	0.09	0.03
04.06. 06:01	0.08	0.08	0.07	0.07	0.05	0.09	0.03
04.06. 09:01	0.08	0.08	0.06	0.07	0.05	0.09	0.03
04.06. 12:01	0.07	0.07	0.06	0.06	0.05	0.09	0.03
04.06. 15:01	0.07	0.07	0.06	0.06	0.05	0.09	0.03
04.06. 20:04	0.07	0.07	0.06	0.07	0.05	0.09	0.05
05.06. 00:01	0.08	0.08	0.07	0.07	0.05	0.09	0.05
05.06. 05:01	0.08	0.08	0.07	0.07	0.05	0.10	0.05
05.06. 10:01	0.08	0.08	0.07	0.07	0.05	0.09	0.04
05.06. 15:01	0.08	0.08	0.06	0.07	0.05	0.09	0.04
05.06. 20:01	0.08	0.08	0.07	0.07	0.05	0.10	0.04
06.06. 00:01	0.08	0.08	0.07	0.07	0.05	0.10	0.05
06.06. 05:01	0.07	0.08	0.07	0.07	0.05	0.10	0.04
06.06. 10:01	0.08	0.08	0.07	0.07	0.05	0.10	0.05
06.06. 00:04	0.08	0.08	0.07	0.08	0.05	0.11	0.06
07.06. 00:46	0.08	0.08	0.07	0.08	0.05	0.10	0.06
07.06. 00:54	0.08	0.08	0.07	0.07	0.05	0.10	0.06
07.06. 05:06	0.08	0.08	0.07	0.08	0.05	0.10	0.06
07.06. 10:04	0.08	0.08	0.07	0.07	0.05	0.10	0.06
07.06. 15:04	0.08	0.08	0.07	0.08	0.05	0.10	0.06
07.06. 20:04	0.08	0.08	0.07	0.08	0.05	0.10	0.06
08.06. 05:04	0.08	0.08	0.07	0.08	0.05	0.11	0.05
08.06. 10:04	0.08	0.08	0.07	0.07	0.05	0.10	0.05
08.06. 15:04	0.08	0.08	0.06	0.07	0.05	0.10	0.06
08.06. 20:04	0.08	0.08	0.07	0.08	0.06	0.11	0.07
09.06. 00:04	0.08	0.08	0.07	0.08	0.05	0.11	0.08
09.06. 05:04	0.08	0.08	0.07	0.08	0.06	0.10	0.08
09.06. 10:04	0.08	0.08	0.07	0.08	0.05	0.11	0.07
09.06. 15:04	0.08	0.08	0.07	0.08	0.05	0.10	0.08

09.06, 20:04	0.08	0.08	0.07	0.08	0.05	0.11	0.09
10.06, 00:04	0.08	0.08	0.07	0.08	0.06	0.10	0.09
10.06, 05:04	0.08	0.08	0.07	0.08	0.06	0.11	0.07
10.06, 10:04	0.08	0.08	0.07	0.08	0.06	0.11	
10.06, 15:04	0.08	0.08	0.07	0.08	0.06	0.11	0.07
10.06, 20:04	0.08	0.08	0.07	0.08	0.06	0.10	0.09
11.06, 00:06	0.08	0.08	0.07	0.08	0.06	0.11	0.10
11.06, 02:04	0.08	0.09	0.07	0.08	0.06	0.11	0.09
11.06, 04:04	0.08	0.08	0.07	0.08	0.06	0.11	0.09
11.06, 06:04	0.08	0.08	0.07	0.08	0.06	0.10	0.10
11.06, 08:04	0.08	0.08	0.07	0.08	0.05	0.11	0.10
11.06, 10:04	0.08	0.08	0.07	0.08	0.05	0.11	0.09
11.06, 12:04	0.08	0.08	0.07	0.08	0.05	0.10	0.13
11.06, 14:04	0.08	0.08	0.07	0.08	0.05	0.10	0.18
11.06, 16:04	0.08	0.08	0.07	0.08	0.05	0.10	0.22
11.06, 18:04	0.08	0.08	0.07	0.08	0.05	0.11	0.25
11.06, 20:04	0.08	0.08	0.07	0.08	0.05	0.11	0.28
11.06, 22:04	0.08	0.08	0.07	0.08	0.06	0.11	0.30
12.06, 00:04	0.08	0.08	0.07	0.08	0.06	0.11	0.31
12.06, 02:04	0.08	0.08	0.07	0.08	0.06	0.11	0.32
12.06, 04:04	0.08	0.08	0.07	0.08	0.06	0.11	0.31
12.06, 06:04	0.08	0.08	0.07	0.08	0.06	0.11	0.31
12.06, 08:04	0.08	0.08	0.07	0.08	0.06	0.11	0.31
12.06, 10:04	0.08	0.08	0.07	0.08	0.06	0.11	0.32
12.06, 12:04	0.08	0.08	0.07	0.08	0.06	0.11	0.34
12.06, 14:04	0.08	0.08	0.07	0.08	0.05	0.11	0.35
12.06, 16:04	0.08	0.08	0.07	0.08	0.06	0.10	0.35
12.06, 18:04	0.08	0.08	0.07	0.08	0.06	0.11	0.36
12.06, 20:04	0.08	0.08	0.07	0.08	0.06	0.11	0.36
13.06, 14:04	0.08	0.08	0.07	0.08	0.05	0.11	0.36
13.06, 16:04	0.08	0.08	0.07	0.08	0.05	0.11	0.36
13.06, 18:04	0.08	0.08	0.07	0.08	0.06	0.11	0.36
13.06, 20:04	0.08	0.08	0.07	0.08	0.06	0.11	0.36
13.06, 22:04	0.08	0.08	0.07	0.08	0.06	0.11	0.36
14.06, 00:04	0.08	0.09	0.07	0.08	0.06	0.11	0.36
14.06, 02:04	0.08	0.08	0.07	0.08	0.06	0.11	0.36
14.06, 04:04	0.08	0.08	0.07	0.08	0.06	0.11	0.36
14.06, 06:04	0.08	0.08	0.07	0.08	0.06	0.11	0.36
14.06, 08:04	0.08	0.08	0.07	0.08	0.06	0.11	0.36
14.06, 10:04	0.08	0.09	0.07	0.08	0.06	0.11	0.36
14.06, 12:04	0.08	0.08	0.07	0.08	0.06	0.11	0.36
14.06, 14:04	0.08	0.08	0.07	0.08	0.06	0.11	0.36
14.06, 16:04	0.08	0.08	0.07	0.08	0.06	0.11	0.36
14.06, 18:06	0.08	0.08	0.07	0.08	0.06	0.11	0.36
14.06, 21:04	0.08	0.09	0.08	0.08	0.06	0.11	0.36
15.06, 00:04	0.08	0.08	0.07	0.08	0.06	0.11	0.36
15.06, 03:04	0.08	0.09	0.07	0.08	0.06	0.11	0.36
15.06, 06:04	0.08	0.08	0.07	0.08	0.06	0.11	0.36
15.06, 09:04	0.08	0.08	0.07	0.08	0.05	0.11	0.35
15.06, 12:04	0.08	0.08	0.07	0.08	0.06	0.11	0.36
15.06, 15:04	0.08	0.08	0.07	0.08	0.06	0.11	0.35
15.06, 18:04	0.08	0.08	0.07	0.08	0.06	0.11	0.35
16.06, 21:06	0.08	0.08	0.08	0.08	0.06	0.13	0.35
17.06, 00:04	0.08	0.08	0.08	0.09	0.06	0.13	0.35
17.06, 03:04	0.08	0.08	0.08	0.09	0.06	0.14	0.36
17.06, 06:04	0.08	0.08	0.08	0.09	0.06	0.14	0.35
17.06, 09:04	0.08	0.08	0.08	0.09	0.06	0.13	0.35
17.06, 12:04	0.07	0.08	0.07	0.08	0.06	0.13	0.35
17.06, 15:04	0.08	0.08	0.07	0.09	0.06	0.15	0.35
17.06, 18:04	0.08	0.08	0.07	0.09	0.06	0.16	0.35
17.06, 21:04	0.08	0.08	0.08	0.08	0.06	0.19	0.35
18.06, 00:04	0.08	0.09	0.08	0.09	0.06	0.15	0.35
18.06, 03:04	0.08	0.09	0.08	0.09	0.06	0.15	0.35
18.06, 06:04	0.08	0.08	0.08	0.09	0.06	0.16	0.35
18.06, 09:04	0.08	0.08	0.07	0.09	0.06	0.16	0.35

18.06. 12:04	0.08	0.08	0.07	0.08	0.06	0.17	0.35
18.06. 15:06	0.08	0.08	0.07	0.08	0.06	0.19	0.35
19.06. 00:04	0.08	0.08	0.08	0.09	0.06	0.25	0.35
19.06. 02:04	0.08	0.09	0.08	0.09	0.07	0.26	0.35
19.06. 04:04	0.08	0.09	0.08	0.09	0.06	0.27	0.35
19.06. 06:04	0.08	0.08	0.08	0.09	0.06	0.27	0.35
19.06. 08:04	0.08	0.09	0.08	0.09	0.06	0.28	0.36
19.06. 10:04	0.08	0.09	0.08	0.09	0.06	0.28	0.35
19.06. 12:04	0.08	0.08	0.08	0.08	0.06	0.28	0.35
19.06. 14:04	0.08	0.08	0.08	0.09	0.06	0.28	0.35
19.06. 16:04	0.08	0.08	0.07	0.09	0.06	0.29	0.35
19.06. 18:04	0.08	0.08	0.08	0.09	0.06	0.29	0.35
19.06. 20:04	0.08	0.08	0.08	0.09	0.06	0.30	0.35
19.06. 22:04	0.08	0.09	0.08	0.09	0.07	0.31	0.35
20.06. 02:04	0.08	0.09	0.08	0.09	0.07	0.32	0.35
20.06. 04:04	0.08	0.09	0.08	0.09	0.07	0.33	0.35
20.06. 06:04	0.09	0.09	0.08	0.09	0.07	0.34	0.35
20.06. 08:04	0.08	0.09	0.08	0.09	0.07	0.34	0.35
20.06. 10:04	0.08	0.08	0.08	0.09	0.07	0.34	0.35
20.06. 12:04	0.08	0.09	0.08	0.09	0.07	0.34	0.35
20.06. 14:04	0.08	0.08	0.07	0.09	0.07	0.35	0.35
20.06. 16:04	0.08	0.08	0.07	0.09	0.06	0.35	0.35
20.06. 18:04	0.08	0.09	0.08	0.09	0.07	0.36	0.35
20.06. 21:06	0.08	0.09	0.08	0.09	0.07	0.37	0.35
21.06. 00:04	0.08	0.09	0.08	0.09	0.07	0.37	0.35
21.06. 03:04	0.08	0.09	0.08	0.09	0.07	0.37	0.36
21.06. 06:04	0.09	0.09	0.08	0.09	0.07	0.37	0.35
21.06. 09:04	0.09	0.09	0.08	0.09	0.07	0.37	0.33
21.06. 12:04	0.08	0.09	0.08	0.09	0.07	0.37	0.32
21.06. 15:04	0.08	0.09	0.08	0.09	0.07	0.37	0.32
21.06. 18:04	0.08	0.08	0.07	0.09	0.07	0.37	0.32
21.06. 21:04	0.08	0.09	0.08	0.09	0.07	0.37	0.31
22.06. 00:04	0.09	0.09	0.08	0.09	0.07	0.38	0.31
22.06. 03:04	0.09	0.09	0.08	0.09	0.07	0.38	0.30
22.06. 06:04	0.09	0.09	0.08	0.10	0.07	0.37	0.30
22.06. 09:04	0.08	0.09	0.08	0.09	0.07	0.37	0.29
22.06. 12:04	0.08	0.09	0.08	0.09	0.07	0.36	0.29
25.06. 15:41	0.08	0.08	0.07		0.22	0.34	0.26
29.06. 22:23	0.08	0.09	0.21	0.27	0.21	0.31	0.24
01.07. 22:52	0.09	0.10	0.26	0.32	0.23	0.33	0.25
03.07. 15:09	0.09	0.10	0.27	0.32	0.23	0.32	0.25
11.07. 13:55	0.10	0.27	0.26	0.31	0.22	0.31	0.25
29.07. 16:11	0.39	0.33	0.34	0.38	0.34	0.37	0.33
06.08. 16:43	0.38	0.34	0.37	0.41	0.34	0.40	0.33
13.08. 14:46	0.37	0.34	0.37	0.41	0.33	0.41	0.33
20.08. 17:45	0.36	0.33	0.36	0.41	0.33	0.41	0.32
26.08. 15:27	0.37	0.35	0.37	0.42	0.33	0.40	0.33
08.09. 20:09	0.36	0.35	0.37	0.42	0.33	0.39	0.29
10.09. 16:04	0.35	0.34	0.35	0.40	0.27	0.35	0.27
12.09. 17:30	0.35	0.30	0.32	0.37	0.26	0.33	0.20
14.09. 14:49	0.34	0.28	0.32	0.36	0.25	0.33	0.14
16.09. 13:13	0.32	0.26	0.31	0.35		0.33	0.11
17.09. 12:10	0.31	0.25	0.31	0.34	0.24	0.32	0.09
19.09. 11:59	0.30	0.24	0.30	0.32	0.23	0.31	0.06
20.09. 15:59	0.29	0.23	0.30	0.32	0.23	0.31	0.10
21.09. 11:44	0.29	0.23	0.29	0.31	0.23	0.29	0.07
22.09. 15:08	0.29	0.22	0.29	0.30	0.22	0.30	0.07
23.09. 18:00	0.28	0.22	0.28	0.30	0.22	0.29	0.08
25.09. 19:19	0.27	0.22	0.28	0.29	0.22	0.28	0.06
26.09. 16:53	0.26	0.21	0.27	0.28	0.27	0.22	0.06
28.09. 12:27	0.23	0.20	0.26	0.27	0.21	0.19	0.05
29.09. 16:49	0.22	0.19	0.26	0.27	0.20	0.18	0.05
01.10. 13:47	0.20	0.17	0.25	0.25	0.18	0.17	0.05
02.10. 19:48	0.19	0.16	0.24	0.24	0.16	0.16	0.05
05.10. 16:39	0.17	0.14	0.22	0.20	0.09	0.13	0.05

06.10, 14:20	0.17	0.13	0.15	0.14	0.08	0.12	0.05
07.10, 18:26	0.16	0.10	0.12	0.12	0.08	0.12	0.05
08.10, 17:10	0.13	0.08	0.12	0.12	0.07	0.12	0.04
09.10, 12:46	0.13	0.08	0.11	0.12	0.06	0.12	0.05
12.10, 12:01	0.13	0.08	0.12	0.11	0.08	0.12	0.05